Submitted to ADVANCED MATERIALS

DOI: 10.1002/adma.((please add manuscript number))
Article type: Review

Title **CVD Polymers: A new paradigm for surface modification and device fabrication**

By *Anna Maria Coclite, Rachel M. Howden, David C. Borrelli, Christy D. Petruczok, Rong Yang, Jose Luis Yagüe, Asli Ugur, Nan Chen, Sunghwan Lee, Won Jun Jo, Andong Liu, Xiaoxue Wang,* and *Karen K Gleason* *

[*] Prof. K. K. Gleason, D. Borrelli, Dr. N. Chen, Dr. R. Howden, W. J. Jo, Dr. S. Lee, A. Liu, C. Petruczok, Dr. A. Ugur, X. Wang, Dr. J.L. Yagüe, R. Yang
Department of Chemical Engineering, Massachusetts Institute of Technology,
Cambridge, MA 02139, USA
E-mail: kkg@mit.edu
Prof. A. M. Coclite
Institute of Solid State Physics, Graz University of Technology, Graz, 8010, Austria

Keywords: Chemical Vapor Deposition, Conformality, Functional polymers, Surface modification, Conjugated polymers

Well-adhered, conformal, thin (<100 nm) coatings can easily be obtained by Chemical Vapor Deposition (CVD) for a variety of technological applications. Room temperature modification with functional polymers can be achieved on virtually any substrate: organic, inorganic, rigid, flexible, planar, three-dimensional, dense, or porous. In CVD polymerization, the monomer(s) are delivered to the surface through the vapor phase and then undergo simultaneous polymerization and thin film formation. By eliminating the need to dissolve macromolecules, CVD enables insoluble polymers to be coated and prevents solvent damage to the substrate. CVD film growth proceeds from the substrate up, allowing for interfacial engineering, real-time monitoring, and thickness control. initiated-CVD has shown successful results in terms of rationally designed micro- and nano-engineered materials to control molecular interactions at material surfaces. Oxidative-CVD success was mainly demonstrated for the deposition of organic conducting and semiconducting polymers.

Submitted to ADVANCED MATERIALS

Received: ((will be filled in by the editorial staff))
Revised: ((will be filled in by the editorial staff))
Published online: ((will be filled in by the editorial staff))

1. Introduction

Chemical vapor deposition (CVD) is a powerful technology for engineering surfaces and is typically the method of choice for growing high quality inorganic layers. More recently CVD methods have been invented which fully retain the rich chemistry of organic monomers.[1, 2] The solvent-free deposition of robust thin films with high densities of organic functional groups is an enabling technology for surface modification of, but not limited to, industrial parts, membranes, microfluidic structures, and biomedical devices. In analogy to their inorganic counterparts, CVD polymeric layers can be integrated into device fabrication schemes for optoelectronics and sensors. The desirable attributes of CVD polymers include surface energy modification, environmental protection, mechanical flexibility, conformal coverage, and/or chemical and biological specificity.

Chemical vapor deposition (CVD) expands the application space for polymeric surface modification. Vapor deposition is ideally suited for synthesizing thin films of polymers that are insoluble or infusible. Indeed, fluoropolymers, crosslinked organic materials, and conjugated polymers are three of the most studied categories of CVD polymer films. Additionally, solvent-free processing avoids potential swelling or dissolution of the substrate.

By building the polymeric thin films from the surface up, strategic use of interfacial modification enables covalent chemical bonds to form between the CVD polymer film and substrate. The interfacial grafting results in surface layers, which are robustly adhered to the underlying substrate. CVD provides precise control over film thickness and also yields so-called “conformal coatings”, which uniformly cover complex geometric features, including trenches, microparticles, and nanotubes.[3-5]

Synthesis from vapor phase monomers (also referred in the text as gas phase monomers) obviates the need to remove entrained solvents using a curing step. Lack of residual solvent is favorable for achieving biocompatibility.[6] Further reductions in impurity levels can be achieved through the purification of the low molecular weight monomers before their use as reactants in the CVD polymerization process. Optoelectronic device performance and stability typical improve as impurity levels decrease.

In contrast to solution synthesis methods, the monomeric reactants for CVD do not need to be soluble. However, the monomeric species must be volatile. Vapor phase processes can be classified depending on the deposition mechanism: chain growth (e.g. plasma enhanced chemical vapor deposition, PECVD[7, 8]) and step growth polymerization (e.g. vapor deposition polymerization, VDP[9] or CVD grown parylene[6, 10]). Chain growth and step growth mechanisms have been demonstrated also for initiated CVD (iCVD) and oxidative CVD (oCVD), respectively. The focus of this review will be mainly on the latter two techniques (iCVD and oCVD) to highlight the successful implementation of these techniques in many technological fields. The characteristics of iCVD polymers have been exploited for a wide range of applications, including wettability, sensing, microelectronics, and protein adsorption control applications.[1, 11-13] To date the oCVD method has been applied to the synthesis of organic conducting and semiconducting polymers and have been integrated into photovoltaic cells[14-16] and biosensors.[17, 18]

2. Step Growth Polymerization: oCVD

2.1 Overview

The many advantages of oxidative Chemical Vapor Deposition (oCVD) and the step growth reaction scheme that it follows makes it particularly useful for depositing films of conjugated polymers. During the oCVD process, polymer synthesis and thin film deposition occur in a single step. The monomer and oxidant precursors are both delivered through the vapor phase. As a result, neither the monomers nor the resulting polymer need to be soluble, a

key differentiator from solution-based synthesis approaches. For example, thiophene can be directly oCVD polymerized to form polythiophene films. Thus, there is no need for specialty synthesis to add solubilizing substituents, such as the addition of a hexyl group to thiophene in order to synthesize soluble monomer for poly(3-hexyl thiophene) (P3HT). The highly crystalline nature of many insoluble conjugated polymers may have a positive impact on stability and electrical properties. Additionally, since solvents are not used to deliver the polymer or its precursors, there is no need to consider compatibility of the substrate with solvents, thus making the oCVD process substrate independent. The oCVD method also enables the formation of grafted interfaces for robustly adhered layers.[19] The ability to deposit layers of uniform thickness over non-planar structures, known as conformal coverage, enables devices to be fabricated on rough surfaces, such as ordinary, untreated paper.[20] Furthermore, the resulting polymer properties can easily be tuned by controlling the deposition parameters, such as the stage temperature.[21] The use of a shadow mask during oCVD enables patterning of the polymer films, a technique termed vapor printing.

oCVD follows the same step growth mechanism of oxidative polymerization as in solution. The oxidizing agent reacts with monomers to form cation radicals. Pairs of cation radicals then dimerize and deprotonate. Subsequent stepwise reactions with the oxidizing agent and the cation radicals grow the polymer chain. The typical oCVD setup involves the use of a vacuum chamber with monomer inlet ports on the side and an oxidant source at the bottom (**Figure 1a**). The monomer is heated in a jar outside the chamber and controllably fed in through a heated line. An oxidant that is solid at room temperature, such as iron(III) chloride or copper(II) chloride, is typically used. The oxidant is placed in a crucible at the bottom of the chamber and sublimes upon heating (for example, $FeCl_3$ is heated to ~340 °C). Oxidants that are liquid at room temperature, such as bromine and vanadium oxytrichloride, have also been used.[22, 23] Liquid oxidants can be introduced into the chamber using a method similar to that used for introducing monomer species, which can allow greater flow rate

control. Substrates are placed on the temperature-controlled stage, which is inverted and facing down towards the oxidant source. Modest stage temperatures (25 °C to 150 °C) are used, with the value depending on the polymer being deposited. During a deposition, the pressure is maintained at a value (typically ~100 mTorr) using a butterfly valve.

The first demonstrations of oCVD were utilized for forming conducting films of poly(3,4-ethylenedioxythiophene) (PEDOT).[21, 24] More recently, the oCVD technique has expanded to the deposition of other conjugated polymers, including semiconducting layers and functionalizable conducting copolymers. To date, these oCVD polymers have been applied to fulfill various roles in organic photovoltaics, electrochromic devices, and sensors. A comprehensive review of oCVD and other methods for the vapor deposition of conjugated polymers and their applications has recently been published.[25]

2.2 Substrate Independence

The low deposition temperatures (~20 – 150 °C) enable oCVD polymers to be directly deposited on a wide range of substrates, including paper and plastic, without fear of thermal degradation. Additionally, the oCVD requires no specific process optimization for application to different types of materials. This benefit derives from avoiding surface tension driven phenomena, which lead to dewetting, blanketing, air gap formation, sidewall thinning, and formation of menisci.

The work of Park et al. demonstrates the compatibility of the oCVD process with graphene substrates.[26] The graphene was simply exposed to a vaporized mixture EDOT monomer and the $FeCl_3$ oxidizing agent to form the oCVD polymer layer. The moderate deposition conditions resulted in the direct deposition of a pure PEDOT hole transport layer without damage to the graphene electrode. When integrated into solar cells, the resulting power conversion efficiency was ~94% of the ITO control device. **Figure**s **2a and 2b** compare quartz/graphene substrates coated by oCVD and spin-cast PEDOT:PSS, respectively. In the latter, irregularly shaped dewetting defects are observed, which appear as multiple dark

spots to the human eye. In contrast, the oCVD PEDOT surface is defect-free over the entire area.

Vapor phase reactants are able to diffuse into complex micro- and nano- structured surfaces. Such 3D surface architectures are desired to enhance light absorption in organic photovoltaic devices, where the exciton diffusion length limits active layer thicknesses. Howden et al. showed that oCVD PEDOT is compatible with wide range of nano- to macro-scale textured surfaces,[27] enhancing the light absorption (light trapping) in photovoltaic structures. **Figure 2c** shows the ability of the oCVD PEDOT to precisely follow the geometry the interface. In contrast, voids form when solution-processed PEDOT:PSS (**Figure 2d**) is applied to a similar nanostructured surface. The conformal nature oCVD PEDOT is again demonstrated over a nanowedge pattern (**Figure 2e**), where an ultrathin layer thickness of ~9 nm covers all portions of the features. In contrast, spin-coated PEDOT:PSS (**Figure 2f**) wells up in the bottoms of the features, while thinning at the tops.

The oCVD method is able to penetrate and coat the inner surfaces of porous media, such as foams and membranes. Subsequent dissolution of the membrane leaves behind the oCVD templated features. In the case of membranes with cylindrical pores, nanotubes of conjugated polymers are formed.

When applied to fiber-base substrates, such as paper, electrospun nanofiber mats, or textiles, the oCVD conjugated polymers complete surrounds each fiber.[28] Poly (acrylonitrile) fiber mats conformally coated with oCVD PEDOT (**Figure 2g**) creates a high surface area platform for resistance-based sensing.[29] In contrast, agglomeration occurs in the fibrous substrate after solution application of PEDOT:PSS (**Figure 2h**). In **Figure 2i**, the oCVD PEDOT leaves the rice paper substrate undamaged, while the PEDOT:PSS solution degrades this substrate (**Figure 2j**).

Conformal coating of carbon nanotubes (CNTs) by oCVD PEDOT ~6 nm thick was demonstrated by Vaddiraju et al.[30] By lowering the activation energy required for creation of

mobile carriers, an enhancement in radial conductivity was obtained. This approach can be used to create many functional materials and devices.

2.3 Grafting and Patterning

The vapor phase delivery of oxidants in oCVD builds the film from the surface up and permits covalent bonds to form at the interface between the substrate and the film of the oCVD conjugated polymer. **Figure 3a** shows the successful patterning of grafted PEDOT on silicon. Grafting improves interfacial adhesion, enabling pattern formation. Without grafting, failure due delamination is often observed. Im et al. presents a straightforward one-step process for grafting PEDOT onto flexible polymer substrates containing aromatic bonds, such as polystyrene or polyethylene terephthalate (PET) (**Figure 3b**).[19] Through a Friedel-Craft reaction at the surface, the oCVD oxidant forms radical cations directly on the surface of the substrate material from which the grafted chains grow. Grafting can also be applied to inorganic substrates using silane-coupling agents. For instance, a silicon substrate with a native silicon oxide layer can be treated with oxygen plasma to form hydroxyl groups. The sample is then exposed to trichlorovinylsilane (TCVS) to form a vinyl-terminated surface to which PEDOT can graft.

Excellent interfacial properties are also essential for the fabrication of flexible devices, where adhesion and durability are essential. **Figure 3c** displays patterned, grafted oCVD PEDOT films formed directly on the flexible transparent plastic PET. This fabrication did not require a complex transfer step from another substrate.

Patterns of oCVD PEDOT have been directly formed by vapor printing on paper substrates, including ones already printed with tradition inks. In vapor printing, the synthesis of the polymer chains from vapor phase reactants, thin film formation, and patterning occur in a single step.[20]

The scanning electron micrograph in **Figure 3d** shows the edge of 100 nm thick vapor printed PEDOT electrode on newsprint obtained with shadow masking. The image also shows how well PEDOT conforms to the geometry of the paper fibers. Well-ordered conducting polymer nanostructures (**Figure 3e**) were achieved by colloidal lithography combined with the highly conformal grafted oCVD PEDOT.[31] At the thinnest junction, the PEDOT wall between the nanobowls is only ~25 nm wide.

X-ray diffraction (XRD) reveals the crystallinity and preferential ordering of oCVD PEDOT with respect to a (100)-oriented silicon substrate. For non-grafted samples only (0K0) type reflections are observed while for grafted samples (H00) reflections also appear (**Figure 3f**).

The ability to control the interface of the polymer and the substrate offers the potential to open up new device technologies where the electrical and thermal properties could be tuned independently. Novel nanostructures with organic-inorganic material interfaces could be designed in such a way where charge transport is enhanced and phonon transport is obstructed.

2.4 Conductors and Device Integration

PEDOT is one of the most promising conjugated polymers for flexible organic electronics because of its combination of high electrical conductivity, optical transparency, and mechanical properties.[32] Since oCVD has low substrate temperature requirements, there is no need for elaborate processing strategies, as with microcrystalline silicon or graphene, where the materials are first grown at high temperatures on a handling substrate and then transferred to the surface of less heat resistant materials. Additionally, the conformal coverage oCVD PEDOT layers allows them to be grown directly on top of flexible substrates with rough surfaces, such as ordinary plastic, and even fiber-based papers and textiles. Thus, oCVD PEDOT represents a new fabrication process that is compatible with substrates other

than glass, silicon, and smooth plastics, requires only low-energy input, utilizes only earth-abundant elements (e.g. no indium), and is scalable to large area processing (e.g. roll-to-roll).

The substrate temperature of the oCVD process is a critical parameter for controlling the electrical conductivity of PEDOT thin films. Im et al.[32] reported that increasing substrate temperature from 15 °C to 110 °C while holding all other process conditions constant, resulted in the electrical conductivity of oCVD PEDOT polymer films monotonically increasing from 9.1 x 10^{-4} to 348 S cm^{-1}, a range of more than five orders of magnitude. The improvement in conductivity is attributed to longer conjugation length and higher doping levels.[21, 32] Since higher doping concentration moves the Fermi energy level in the band gap, the work function of PEDOT can also be controlled[32] from ~5.1 to~5.4 eV during oCVD by simply adjusting substrate temperature as shown in **Figure 4a**. The tunability of the work function of oCVD PEDOT films is advantageous for achieving favorable band alignment between dissimilar layers in organic devices, thus lowering the energy barrier to charge transport at the contact interface. More recently, Howden et al.[27] employed diluted acids as post-process rinsing solutions resulting in improved electrical conductivity. Average conductivity increases of 117% and 135% were observed for H_2SO_4 and HBr rinses, respectively, accompanied by dopant exchange. A maximum conductivity of 1620 S cm^{-1} was obtained by rinsing in HBr.

For implementing transparent conducting materials as an electrode or a buffer layer in optoelectronic devices, high optical transparency (T>~85%) in the visible regime is required while maintaining a low sheet resistance (R_{sh}<~100 Ω sq^{-1}). Since there is a trade-off between transparency and electrical conductivity in this class of materials, the thickness has to be controlled to limit losses from optical absorption and, in parallel, to provide sufficiently low sheet resistance for the efficient charge transport or extraction. The sheet resistance and optical transparency can be related by Eq. 1:

$$T = (1 + \frac{Z_0}{2R_{sh}} \frac{\sigma_{op}}{\sigma_{dc}})^{-2} \quad (1)$$

where Z_0 = 377 Ω is the impedance of free space, and σ_{op} and σ_{dc} are the optical and dc conductivities, respectively. [33] **Figure 4b** shows this relation for oCVD PEDOT films deposited on glass substrates at temperatures of 80 °C and a working chamber pressure of 0.1 Torr.[20] The measured data gives the σ_{dc}/σ_{op} ratio of 9, which is comparable to the commercially available solution-processed conducting polymer and is approximately 3-fold lower than the conventional metal oxide (i.e., ITO) of $\sigma_{dc}/\sigma_{op} \approx 35$.[20] With HBr acid rinsing, the σ_{dc}/σ_{op} ratio of oCVD PEDOT improved to 12.[27] Further work to improve σ_{dc}/σ_{op} is currently in progress.

The color-transition properties exhibited by PEDOT have been investigated for electrochromic applications such as smart windows and light management devices. PEDOT displays a transparent light-blue color in the oxidized state and a dark-blue hue in the reduced state. When cycled between oxidized and reduced states, the electrochromic switching of a device fabricated by integrating patterned oCVD PEDOT onto ITO/glass substrates occurs, as can be seen in **Figure 4c**[34] The dark-to-light transition occurs within ~10 s, while a light-to-dark switching requires approximately 1 min.

To demonstrate the utility of the direct fabrication of oCVD layers, PEDOT electrodes have been fabricated on a wide range of flexible, foldable, and non-planar surfaces. The conductivity of oCVD PEDOT electrodes and the performance of full OPV devices with oCVD PEDOT remains unchanged after repeated mechanical deformation tests. In **Figure 5a**, OPV devices with oCVD PEDOT electrodes on polyethylene terephthalate (PET) present no significant change in performance over 100 compressive flexing cycles. In contrast, the electrical conductivity of commercially available ITO on PET substrates deteriorates rapidly and cracks are visible after repeated flexing via optical microscope. Flexibility is essential for implementation of roll-to-roll processing, desired for economical production.

While photovoltaic (PV) devices traditionally utilize illumination through a transparent substrate like glass or plastic, strategies compatible with opaque substrates open up new potential avenues for the use of solar power. Top-illuminated inverted photovoltaic devices on opaque substrates were fabricated[35] using an oCVD PEDOT electrode deposited directly on top the rest of the cell stack (**Figure 5b**). The oCVD PEDOT anode layer is directly deposited on the device stack without any damage to the underlying active layer materials by insertion of a thin buffer layer of molybdenum trioxide (MoO_3).[35, 36] With this inverted device structure, top-illuminated OPV devices were demonstrated on a variety of common opaque substrates such as photo paper, magazine print, and plastic food packaging. Figure 5b shows an OPV fabricated on U.S stamp, having a power conversion efficiencies of 2.0%[35].

Facile monolithic integration of devices into circuits is enabled on paper utilizing substrate-independent vapor-printed oCVD PEDOT electrodes.[20, 26] This approach allows the fabrication and cost-effective prototyping of flexible and foldable organic devices by vapor printing on inexpensive everyday substrates including paper. Large-area PV prototype arrays have been vapor-printed directly on the unmodified surface of fibrous papers, offer a thinner, lighter-weight alternative to plastic substrates (~0.001 g•cm-2, <40 μm thick). The paper PV arrays produce >50V and power common electronic displays in ambient indoor lighting, even after tortuous flexing and folding. **Figure 5c** (top) show a schematic of the process integration flow for fabricating the bottom-illuminated PV device structures using a series of shadow masking steps. For the oCVD step, the mask itself is stencil cut from paper. The completed circuit of individual cells, and printing patterns of each device layer and complete 250-cell series integrated monolithic arrays on tracing paper are shown in Figure 5c (bottom).[20] This same strategy could be utilized to fabricate other types of optoelectronic devices, logic elements, energy storage devices as well as integrated circuits containing mixtures of these discrete devices.

Because oCVD PEDOT films retain their conductivity upon folding, a variety of macro-scale non-planar 3D-structures can be created (**Figure 5d**).[37] These architectures offer the possibility to improve the output power over a given area by more efficiently absorbing and converting the incident light while maintaining a fixed active layer thickness for optimal exciton diffusion. For half-cells fabricated using oCVD PEDOT electrodes and DBP (tetraphenyldibenzoperiflanthene) absorber layers, increased absorption was measured as hinge angle decreased (Figure 5d) for substrates folded into V-shaped configurations.

2.5 oCVD Semiconductors

Semiconducting polymers are of great interest as active layer materials in organic electronic and optoelectronic devices, such as organic photovoltaics (OPVs),[38] organic light emitting diodes,[39] and organic field effect transistors.[40] Researchers have recently employed oCVD for the deposition of several semiconducting polymers. Unsubstituted polythiophene (PT), which is insoluble and typically difficult to process, was easily prepared by oCVD. Using iron(III) chloride as the oxidizing agent, the as-deposited oCVD PT films were blue in appearance.[41] (**Figure 6a**) Excess oxidizing agent present during the oCVD process doped the films, resulting in conductivities up to 20 S/cm. Positions of the mid-gap absorption peaks (0.8 and 1.6 eV) in the doped films demonstrate that the polymer films are heavily doped and bipolarons are present (Figure 6a, middle). Reduction with methanol dedoped the polymer and resulted in neutral, red PT films. Changes in the absorption spectra confirmed the semiconducting nature of the rinsed PT films (Figure 6a, middle). Bilayer heterojunction organic solar cells were then fabricated using semiconducting oCVD PT as the electron donor. The oCVD PT was deposited directly onto ITO-glass substrates. Thermally evaporated C_{60} was used as the electron acceptor layer, and a bathocuproine (BCP) exciton-blocking layer and silver top cathode were used. After optimizing layer thicknesses, power conversion efficiencies up to 0.8% were obtained using 25 nm of PT and 30 nm of C_{60}. To date, this remains the highest efficiency solar cell that utilized a vapor-deposited donor polymer. The

image in the far right of Figure 6a shows the current density-voltage (JV) curve of the PT/C_{60} devices.

Properties of oCVD semiconducting polymers are easily tuned by controlling the deposition parameters. A separate study of oCVD polythiophene demonstrated the use of vanadium oxytrichloride ($VOCl_3$) as the oxidizing agent.[23] Since $VOCl_3$ is a volatile liquid, controlling its flow rate and the stage temperature allowed for control of the surface concentration of $VOCl_3$ on the stage in the reactor chamber. Thus, by controlling those parameters as well as the monomer flow rate, the resulting PT film properties, such as conductivity and absorption maximum, were tuned. Work on oCVD polyisothianaphthene (PITN) has shown the importance of the stage temperature during deposition.[42] PITN is of interest for its various appealing properties, including its low bandgap of 1 eV in the neutral state. In the doped state, PITN should display high optical transmission in the visible part of the spectrum. As shown in **Figure 6b**, the color and transparency of the as-deposited oCVD PITN films greatly depends on the deposition temperature. Higher deposition temperatures were shown to result in greater conjugation and longer polymer chains. The increased conjugation length was manifested in various optical and electronic properties of the oCVD PITN films.

Polyselenophene, an analogue of polythiophene with a slightly lower bandgap, has also been prepared using oCVD.[28] Figure 6c exhibits the ability to conformally deposit the polymer on rough paper substrates.

The versatility of oCVD makes it a promising technique for processing semiconducting polymers with desirable properties for many different organic electronic applications.

2.6 Functional oCVD Copolymers

Various conductive oCVD polymers have been successfully applied in chemiresistive sensors for detecting chemical and biological species. Chemiresistive sensors are an economical sensing technology that operates by measuring changes in the resistance (or conductance) of the sensing element upon exposure.[43] Many conductive polymers are not responsive or selective enough alone to sense low chemical concentrations. However, by covalently bonding a molecule or nanoparticle that is analyte-specific to the conductive polymer backbone, larger changes in the composite resistance will occur upon exposure. To accomplish this, oCVD copolymers have been developed that combine the benefits of both monomer species. For example, copolymers of pyrrole and 3-thiophene acetic acid (TAA) combine the high conductivity and good mechanical properties of pyrrole with the desirable –COOH functional group of TAA.[30] It was then possible to covalently bond silver nanoparticles to the oCVD poly(pyrrole-co-TAA) polymer. This was done using a linker molecule containing a $–NH_2$ group (4-aminothiophenol) that formed an amide bond with the –COOH group of TAA. This approach was then extended to deposit oCVD copolymers of poly(EDOT-co-TAA).[44] The attachment of nickel and palladium nanoparticles allowed for selective detection of toluene and acetone, respectively. Adsorption of vapors of volatile organic compounds onto the metal surfaces caused changes in the charge distribution that resulted in higher resistance (lower conductivity) of the composite films. The resistive response of the hybrid films was found to be proportional to the concentration of analyte present, and thinner films were more responsive due to lower shunt resistances. Detection limits for the composites were estimated as being 10-20 ppm of toluene for Ni/poly(EDOT-co-TAA) and 40-50 ppm of acetone for Pd/poly(EDOT-co-TAA). A significant advantage of this approach of attaching metal nanoparticles to a conductive polymer is its versatility. Instead of needing to develop a completely new chemistry, changes in the chemical being detected can be accomplished by simply changing the metal nanoparticle used.

oCVD copolymers with –COOH and –OH groups have been used for sensing biological agents as well. Copolymers of EDOT and TAA were prepared on glass substrates with bromine as the oxidizing agent.[45] A biomolecule, bovine serum albumin (BSA), was shown to covalently attach to the poly(EDOT-co-TAA) films through carbodiimide chemistry with the –COOH functional group of TAA. This resulted in the sheet resistance of the copolymer more than doubling, thus providing an effective way to detect the presence of BSA. In another study, EDOT was copolymerized with 3-thiopheneethanol (3TE) using $FeCl_3$ as the oxidizing agent on 2 cm x 2 cm electrospun nylon fiber mats (**Figure 6d**).[46] Avidin is a protein with high affinity and specificity towards biotin. By reacting a crosslinker molecule (p-maleimidophenylisocyanate) with the $–NH_2$ group on avidin and the –OH group of 3TE, the avidin biomolecule was covalently attached to the poly(EDOT-co-3TE). Upon exposure of the avidin/copolymer films to solutions of biotin, the biotin quickly attached to the avidin and caused an increase in the resistance of the composite film. The middle image in Figure 6d shows polymer-coated nanofibers that are fluorescing due to the attachment of fluorescently labeled avidin (green) and biotinylated red quantum dots that reacted with the avidin. Exposure of the composite films to 5 nM to 5 μM solutions of biotin showed faster response times and higher steady state responses with higher biotin concentrations (Figure 6d, right). The use of high surface area electrospun fiber mats allowed for significantly improved signal and response time compared to the use of flat substrates. The response of the biosensors on the electrospun fiber mats demonstrated a 6-fold increase in response and a 30% decrease in response time relative to the respective values for sensors on planar substrates. Whereas solution-based methods cannot fully coat such high surface area structures due to wetting effects, oCVD provides conformal coverage that enables the use of these substrates. This approach demonstrates the potential to obtain inexpensive, field-deployable, lightweight, and flexible biosensors that can provide fast detection of various analytes.

3 Chain Growth Polymerization: iCVD

3.1 Overview and mechanism

Initiated CVD (iCVD) is a free-radical polymerization method. The initiator and monomer species enter the iCVD chamber as vapors. In analogy to solution-phase synthesis, the iCVD initiator decomposes to form radical species (**Figure 1b**) that then activate the chain growth polymerization of the monomers. Initiators successful used for iCVD include perfluorooctane sulfonyl fluoride (PFOS)[47], perfluoro-1-butanesulfonyl fluoride (PBSF)[48], triethylamine (TEA)[49], tert-butyl peroxide (TBPO)[50], tert-amyl peroxide (TAPO)[51], and tert-butyl peroxybenzoate (TBPOP)[52]. These initiators contain a labile bond, such as the O-O bond in peroxides, which can be readily cleaved. Ideally, at the relatively mild conditions required to decompose the initiator, the monomers fully retain their pendent functional groups. The result is a surface of well-defined chemical composition having a high density of functionalities. Surface moieties such as perfluoroalkanes and hydroxyl enable systematic adjustment of the surface energy. Reactive groups such as amine, epoxy, carboxylic acid, and propargyl allow for functional attachment of molecules, cells, and nanoparticles to the surface. The full retention of the organic functionality also enables the synthesis of responsive surfaces.

Several options have been demonstrated for inducing initiator decomposition. Using thermal decomposition over heated filament array is denoted as iCVD[53]. Alternatively, the decomposition can be achieved by a low energy plasma discharge, termed, initiated plasma enhanced CVD (iPECVD) [54], or by UV light, termed photo initiated CVD (piCVD)[55]. A variant of piCVD is grafted CVD (gCVD), in which the benzophenone (BP), when photo-decomposed, creates radical sites directly on the surface of the substrate.[56] The reaction of the surface radicals with the monomer species results in covalently tethered chains.

All these processes require only modest energy input and operate at low surface temperatures (~20°C to ~70°C). Keeping the surface at low temperature, promotes the adsorption of the monomers. Even though the gas phase monomer concentration is quite dilute, the liquid-like monomer concentration in the surface layer enables rapid chain growth. Thus, despite the

benign reaction conditions of iCVD, high deposition rates can often be achieved (>200 nm/min). High deposition rates and efficient consumption of the precursors are essential for industrial applications. Understanding the deposition mechanism is therefore needed to predict the deposition conditions which yield high deposition rate and is also useful in optimizing the iCVD process for producing conformal coatings over structured surfaces.

The mechanism of iCVD polymerization has been well documented in literature and it has been demonstrated to follow the same steps of conventional free-radical polymerizations: initiation, propagation, and termination.[51, 57-59] However, while in the liquid phase all of the reaction steps occur at a single temperature, for iCVD some reactions steps take place homogeneously in gas phase at a temperature, which can reach that of the filament, while other reaction steps take place heterogeneously on the much cooler surface of the substrate. The first step involves the thermal fragmentation of the initiator:

$$I_2 \xrightarrow{T_{fil}} 2I^{\cdot} \qquad (2)$$

The fragmentation takes place in the gas phase, at or near the heated filament. The initiator and its fragments are typically quite volatile and therefore have only limited adsorption on the surface. However, the monomers are typically much less volatile and can readily reach concentrations on the surface, which represent significant fraction of a monolayer and in some cases even exceed monolayer coverage.

A radical impinging on the site of absorbed monomer can undergo a heterogeneous reaction to create a surface radical:

$$I^{\cdot}_{gas} + M_{ads} \longrightarrow I - M^{\cdot}_{ads} \qquad (3)$$

The product of reaction (3) readily reacts with other adsorbed monomers via a propagation step:

$$I - M^{\cdot}_{ads} + nM_{ads} \longrightarrow I - M_n{}^{\cdot}_{ads} \qquad (4)$$

When the kinetics of reactions involving the monomer's vinyl bond are the rate-limiting step, the observed iCVD deposition rate increases as substrate temperature increases. Conversely, the iCVD growth decreases when the rate-limiting step is the adsorption of monomer to the surface. This adsorption limited regime is often observed for acrylate monomers, which generally have a high propagation rate constant[58], while the reaction limited regime is typically observed for less reactive vinyl bonds, such as those substituted on to organosilicones[60]. The iCVD polymerization can terminate when the radical ends are capped by reaction with other growing polymeric chains or with initiator radicals.

Numerous studies in literature have demonstrated that substrate temperature[58, 60], monomer flow rate[61], and filament temperature[58] all impact deposition kinetics. However, the ratio between the monomer partial pressure (P_M) and the saturation pressure at the substrate temperature (P_{sat}) is often the dominant parameter.[51, 61] Quartz crystal microbalance studies reveal that P_M/P_{sat} is directly correlated with the concentration of monomer adsorbed on the surface (**Figure 7a**) through the Brunauer-Emmett-Teller adsorption isotherm (Eq.5).[57]

$$V_{ad} = \frac{V_{ml} c (P_M / P_{sat})}{(1 - P_M / P_{sat})[1 - (1 - c)(P_M / P_{sat})]} \quad (5)$$

where $c \approx \exp[(\Delta H_{des} - \Delta H_{vap})/(RT)]$ and $V_{ml} c (P_M / P_{sat}) = [M] \sim V_{ad}\big|_{PM/Psat \to 0}$. V_{ad} is the total adsorbed volume; V_{ml} is the monolayer-adsorbed volume. ΔH_{des} is the enthalpy of desorption and ΔH_{vap} the enthalpy of evaporation.

In iCVD kinetics studies the enthalpy of evaporation, $\Delta H_{vap,}$ determined falls in the range of 20-80 kJ/mol, which is characteristic of physisorption of small molecules on surfaces through van der Waals interactions. The monomer adsorption is promoted by low substrate temperature. Additionally, the surface concentration of monomer determines the sticking probability of the initiator radicals.[61]

The surface polymerization has been proposed to follow the Eley–Rideal mechanism in which the deposition rate depends on the surface coverage of the monomer (θ_M) and the gas-phase

concentration of the radicals, since the radicals have much higher volatility and thus much lower adsorption on the surface.[61]

$$R_{dep} \sim \mathrm{k}_{\mathrm{dep}} \left[I^{\bullet} \right] \theta_M \quad (6)$$

Eq 6 is one of the main kinetic equation describing the radical polymerization growth rate together with the kinetic equations that give the chain length (υ) and molecular weight (M_n):

$$\upsilon = \frac{R_{dep}}{R_i} = \frac{k_{dep}\left[M\right]\left[IM^{\bullet}\right]}{k_i\left[M\right]\left[I^{\bullet}\right]} \quad (7)$$

$$M_n = MW_M X_n \quad (8)$$

where R_i is the initiation rate, characterized by the rate constant k_i. The number-average degree of polymerization, ($X_n=2\upsilon/(2-a)$) is used to calculate the number-average molecular weight, M_n. The parameter *a* reflects the fraction of polymer radicals that terminate by coupling, (1-*a*) being the fraction terminating by disproportionation, while MW_M is the molar mass of the polymer repeat unit.

Trough a multi-response parameter estimation procedure Lau and Gleason[57] developed in 2006 a quantitative model which related the kinetic equations (Eq.6-7) with the P_M/P_{sat}. The model uses the assumptions that the initiator is decomposed in the gas-phase at T_{fil} and the other reactions (initiation (Eq.2), propagation (Eq.3-4) and termination) occur at the surface at T_{sub} (substrate temperature). The termination reactions considered in the model were bimolecular chain termination through coupling or disproportionation, primary radical termination through the attack of a primary radical on a polymer radical or primary radicals recombination:

$$M_n^{\bullet} + M_m^{\bullet} \rightarrow M_{n+m}\ ;\ M_n^{\bullet} + R^{\bullet} \rightarrow M_n\ ;\ \text{or}\ R^{\bullet} + R^{\bullet} \rightarrow R_2\ ; \quad (9)$$

respectively. Chain transfer processes were not considered as termination reaction because under vacuum many of them are either absent or negligible (e.g. there is no transfer to solvent). The modelization of the dependence of the film growth rate and the molecular

weight has been largely used to predict the feasibility of some new process or the scalability in large area reactors.

Also, the filament temperature plays a fundamental role in the process kinetics. While it does not influence the P_M/P_{sat} ratio on the surface, it does influence the concentration of radicals created, and hence the rate at which chains are initiated (Eq.6). **Figure 7b** shows the Arrhenius plot of the deposition rate as a function of the filament temperature.[58] Two regimes can be observed. At low T_{fil}, the film growth rate increases rapidly with increasing filament temperature, characteristic of a reaction-kinetics-limited-process. At high T_{fil}, the deposition rate is less influenced by the changes in the temperatures, which is characteristic of a mass-transfer-limited-regime. In the kinetics-limited regime, the apparent activation energy calculated experimentally from the Arrhenius plot is 166 ± 5 $kJmol^{-1}$, which is in good agreement with the activation energy required to decompose the TBPO molecule (163.6 kJ mol^{-1}). In the mass-transfer-regime, the filament temperature is high enough to efficiently decompose the initiator so the deposition kinetics is instead dominated by the diffusion of the radicals from the gas phase to the substrate surface. Decreasing the mass transfer resistance by increasing the gas flow rate increases the deposition rate in this regime (Figure 7b).

The copolymerization kinetics follows the same rules as in conventional free-radical copolymerization reactions. The copolymer composition will depend on the monomer ratio at the surface. This surface ratio differs from the ratio in the feed gases when the monomers differ in volatility (e.g. have different saturation pressures). Additionally, the tendency of two monomers to copolymerize was quantified through the reactivity ratio.[62] The reactivity ratios describe the propensity of the propagating species to add a homo-monomer or the other monomer. In other words, considering a growing copolymer of generic monomers A and B, terminating with a A unit, then the reactivity ratio r_A can be defined as the ratio between k_A and k_B according to the following reactions:

$$\text{copol-A}^{\cdot} + \text{A} \xrightarrow{k_A} \text{copol-A-A}^{\cdot} \quad (10)$$

$$\text{copol-A}^{\cdot} + \text{B} \xrightarrow{k_B} \text{copol-A-B}^{\cdot} \quad (11)$$

Analogously, the reactivity ratio r_B for the growing copolymer terminating with a B unit can be identified. The copolymer composition is determined by the Fineman-Ross equation[63] in the form:

$$\frac{f}{F}(F-1) = r_A \frac{f^2}{F} - r_B \quad (12)$$

where f is the monomer fraction in the gas feed, and F the monomer fraction at the surface.

3.2 Retention of Organic functional groups

Many thin film applications benefit from a rationally designed chemistry for controlling the properties and molecular interactions at the surface. For instance, in the biomedical field, the chemistry of the surface, as quantified by density of functional groups, is essential for controlling protein bonding or the attachment and growth of cells.[12, 64, 65] Additionally, the dynamic response of stimuli-responsive materials, i.e. materials that change their properties following an external stimulus, also depends strongly on the density of functional groups on the surface.[66-68]

For these reasons, it is very important to chemically design the deposition process, choosing the right monomer with the desired functional groups. Retaining these organic functional groups is not trivial task for most CVD processes. In general, it has been observed that in order to retain the functional groups of the monomer, the deposition rate drops down to only a few nm/min. This is especially true when the monomer is the species that is fragmented to create active sites for polymerization, as in plasma enhanced CVD (PECVD), where labile functional groups are easily cleaved off.[69] In contrast, the monomer remains intact during iCVD, and thus, fully retains the organic moieties desired for surface design.

The iCVD method is a platform technology for yielding functional polymers at high deposition rates (>200 nm/min). Successful examples of polymers deposited by iCVD are poly(aminostyrene) (PAS) which displays a high density of functionalizable $–NH_2$ groups,[4] poly(*N*-isopropylacrylamide) (PNIPAAm) whose temperature-sensitive hydrophobicity is due to the presence of amide and isopropyl groups,[70] poly(glycidyl methacrylate) (PGMA) with reactive epoxy groups[50, 71] or poly(hydroxyethyl methacrylate) (PHEMA) hydrogels, with hydrophilic hydroxyl moieties[64, 72, 73]. PGMA has been deposited also at extraordinary high deposition rates (600 nm/min) by iCVD from supersaturated monomer vapor ($P_M/P_{sat} > 1$).[74] The possibility of obtaining polymer thin films spectroscopically identical to their bulk counterpart, makes iCVD a competitor with conventional wet processes (e.g. spin coating, dip casting, etc.) for thin-film applications. The iCVD approach couples the versatility of organic chemistry for the synthesis of polymers with the advantages of dry processing, which is highly beneficial for thin film technologies and device fabrication.

High functional group retention by iCVD has been demonstrated with tens of monomers, including iCVD p(1-vinyl-2-pyrrollidone) (PVP).[75] The retention of the pyrrolidone functionality is important to achieve the hydrophilicity, biocompatibility, and antifouling properties, characteristic of this polymer. **Figure 7c** compares iCVD PVP to a conventionally polymerized PVP standard (PVP360), dissolved in water and cast onto a Si substrate. The Fourier transform infrared spectroscopy (FTIR), carbon 1s x-ray photoelectron spectroscopy (XPS), and ^1H nuclear magnetic resonance (NMR, not shown), all confirm the similar chemical structure of the films produced by both methods. Vinyl bonds are not detected in the FTIR spectra, confirming that the iCVD polymerization indeed occurs through the saturation of all the vinyl bonds of the monomer.

The functional group retention has also been very beneficial to create nanoadhesive trenches.[4] Prototype microfluidic structures were fabricated by reacting one side of the device coated with PAS, containing $–NH_2$ groups and the other side with PGMA, with epoxy

groups. The high amine density of the iCVD films enabled the formation of a robust nanoadhesive, which was orders of magnitude more robust than the counterpart obtained by depositing the polymers by PECVD with a lower density of functional groups at the surface.

High densities of functional groups are also important for creating a platform for further post-deposition reactions. Zwitterionic coatings were obtained by reacting the fully retained tertiary amine groups of the polymer deposited by iCVD with 1,3-propane sultone.[76] A high density of zwitterionic moieties was demonstrated by both depth profiling and angle-resolved XPS measurements in the top ~3 nm of the film. Such a high density of zwitterionic groups is difficult to obtain with other techniques with comparable processing time. The zwitterionic functionalized surfaces exhibited excellent anti-fouling properties against protein, carbohydrate, and bacterial adhesion.

The fragmentation of the initiator instead of the monomer molecule is the key for functional group retention. The same principle has been used in the iPECVD process.[54] During iPECVD, the chamber was fed also with TBPO, contrarily to conventional PECVD processes where any initiator is used. The presence of the initiator allowed a sufficient density of reactive radicals to be obtained at very low plasma power density. Under these conditions the monomer fragmentation was minimal and therefore the monomer structure retention was enhanced compared to other PECVD processes, without compromising the deposition rate.

3.3 Surface Design through iCVD

3.3.1 Robust Crosslinked Networks

Highly crosslinked and robust polymer networks are desirable for applications where durable, smooth, adhesive, and flexible coatings are required, like biological implantations or thin film electronics.[77] Inorganic films generally show high durability and robustness but they are fragile and do not have the same versatility of the polymers. Very often the inorganic coatings cannot be deposited on soft substrates because the stress mismatch create wrinkles and cracks and the methods to deposit inorganic thin films are generally not compatible with soft

substrates. Frequently, this type of polymer network is sandwiched between very thin inorganic films, in multilayer structures, to enhance the overall mechanical properties.[78-80] For these reasons, the deposition of a polymer network which shows properties comparable to inorganic material, keeping tunability and flexibility is of high technological interest.

The rigidity of a crosslinked network is related to the connectivity number[81, 82], i.e. the average number of possible network forming bonds per atom:

$$< r >= \frac{\sum_r r n_r}{\sum_r n_r} \qquad (13)$$

with n_r being the number of atoms having r network forming bonds. When the connectivity number is > 2.4, the percolation of rigidity occurs. This is the case of many inorganic materials. With iCVD it is possible to design the polymerization in order to keep the connectivity number in the range 2.3-2.4 which is typical of hard but flexible networks.

The crosslinking degree (and hence the connectivity number) can be tuned during the iCVD depositions by using monomers or comonomers (called crosslinker) with two or more vinyl bonds.[73, 83-85] Polymers of trivinyltrimethylcyclotrisiloxane (V_3D_3) have been investigated as biopassivating and insulating coating for neural implant.[77, 86, 87] **Figure 8a** shows the electrical resistance of poly(V_3D_3) samples under simulated bioimplanted conditions and constant electrical bias. The electrical resistance remains constant over a period greater than two-and-a-half years, demonstrating the high durability of these coatings. At the same time, the material showed also mechanical flexibility and good adhesion to the lead wires so that the probe could be bent without losing device reliability.

Another example of hard and impermeable, but still flexible, organic network was obtained through the copolymerization of maleic anhydride and aminostyrene.[88] The anhydride and the amino functionalities reacted in a post-deposition annealing step iCVD and resulted in a massively cross-linked network (**Figure 8b**) with elastic moduli exceeding 20 GPa. Typical

polymer moduli are between 0.5 and ~ 5 GPa, sensibly lower than the moduli of the cross-linked iCVD coating. The high crosslinking resulted in much lower oxygen permeability than observed for the commercial permeation barrier coatings.

3.3.2 Functional Hydrogels: Graded Film Composition

Hydrogels are materials that can reversibly absorb water and swell, increasing their volume. This creates changes in the mechanical properties, protein adsorption capabilities and hydrophilicity of the material. This dynamic property is useful for many applications, i.e. biotechnology[64, 84, 89], stimuli-responsive coatings,[90, 91] sensors[92-94] etc. Some hydrogels have similar water content to human tissue and exhibit excellent biocompatibility. Modifying the surface of the hydrogel keeping intact the swelling properties is a powerful tool to extend the hydrogels applicability and to target their action to specific drugs in drug-delivery systems or specific cell adhesion. The swelling hinders the use of solvents; therefore a dry method for the surface functionalization of hydrogel is more convenient.

Hydrogels have been deposited by iCVD (e.g. PHEMA) and they have been demonstrated to retain high swelling capability.[13, 64, 72, 73, 84, 89, 90, 92-97] In addition, iCVD allowed in one-step synthesis of a functionalized hydrogel with pentafluorophenyl functional groups nano-confined on the top surface of the material (**Figure 8c**).[95, 97] The deposition process was designed in order to obtain a graded composition from pure PHEMA to a copolymer of PHEMA and pentafluorophenylmethacrylate (PFM). Figure 8c shows the profile of the PFM group signal (m/z=253.1) as a function of film depth for both the homogeneous and graded copolymer and it can be easily observed that the PFM groups are confined in the top 10-15 nm. The pentafluorophenyl groups on the surface were used for further functionalization with peptides to enhance the cell growth. The homogeneous incorporation of the PFM limited the swelling ability of the hydrogel, therefore the cells did not attach on the surface. The graded copolymer instead retained the swelling ability of the pure PHEMA yielding successful cell growth.

3.3.3 Antifouling Surfaces

The iCVD copolymerization of hydrophobic perfluorodecylacrylate (PFDA) and hydrophilic hydroxyethylmethacrylate (HEMA) (**Figure 9a**) resulted in a smooth surface that disrupts protein-surface interactions.[98] The comonomers have highly contrasting solubility hence avoiding solvents enabled the random copolymerization. These surfaces bear compositional and surface energy heterogeneities on a molecular level, namely amphiphilicity, which leads to reduced surface protein adsorption than either of the respective homopolymers. The protein adsorption data was fitted to an analytical model (Figure 9a); a local heterogeneous site that interferes with adsorption events was estimated to encompass 4-5 repeat units of the polymer. Both piCVD and iCVD have been used to fabricate such surfaces.[98, 99]

Zwitterionic surfaces have been a subject to in-depth investigation due to its outstanding fouling resistance. These surfaces are composed of positively- and negatively-charged moieties, which mix homogeneously to create neutral charges at a molecular-length scale. The fouling resistance in aqueous environment originates from the strong hydration induced by the charges: the replacement of adsorbed water by foulant results in greater interface energy and in the case of polymer brushes, loss of entropy, and is thus not thermodynamically favorable. Poly(2-(dimethylamino)ethyl methacrylate) (pDMAEMA) and the cross-linker Poly(ethylene glycol dimethacrylate) p(EGDMA) were recently copolymerized via iCVD, and functionalized in situ with 1,3-propane sultone vapors to create poly(sulfobetaine) at the surface (**Figure 9b**).[100, 101] Cross-linking is necessary to render the coating insoluble after functionalization as zwitterionic surfaces are extremely hydrophilic. In contrast to films formed by bulk solution polymerization, the highest concentration of zwitterion was found to be at the uppermost surface of the iCVD layer (Figure 9b), where the fouling resistance of the zwitterionic moiety can be exploited.[101] Therefore, the fouling resistance of iCVD zwitterionic coatings is comparable to that of the zwitterionic brushes fabricated by self

assembled monolayers (SAMs) or atom-transfer radical-polymerization (ATRP). The benign and solvent-free reaction conditions enabled the coating of various delicate substrates, as discussed in section 2.4.

Antifouling polyethylene oxide (PEO) surfaces have also been fabricated with iCVD via a ring-opening cationic polymerization mechanism.[102] The resulted surface effectively resisted the adsorption of bovine serum albumin (**Figure 9c**).

3.3.4 Thermally responsive surfaces

PNIPAAm belongs to a general class of thermo-responsive polymers that has been extensively investigated because of its lower critical solution temperature (LCST).[103-105] Specifically, the LCST for PNIPAAm ~32°C. Below the LCST, PNIPAAm adopts a random coil configuration, which enables the exposure of hydrophilic amide moieties that interact favorably with water molecules; therefore, the polymer chains are hydrophilic. Above LCST, PNIPAAm chains collapse into a globular configuration via discontinuous phase change, which renders the amide moieties inter- or intra-chain bonded thus leaving the hydrophobic isopropyl groups exposed; therefore PNIPAAm becomes hydrophobic. Both homopolymer and cross-linked copolymers containing NIPAAm repeat units have been successfully deposited by iCVD. Cross-linkers are necessary to render the coatings insoluble in water. Novel graded film architectures with a NIPAAm-rich surface and cross-linked bulk film were utilized to create faster temperature response than that can be obtained with homogeneous copolymer films.[103] Drastic change in water contact angle was obtained by depositing cross-linked iCVD PNIPAAm conformally on multi-walled carbon nanotubes (**Figure 9d**).[106] The static water contact angle jumps from 50° to 135° by changing the system temperature of 15°C as a result of the change in chain configuration.[105] The configuration change near LCST has been found to affect the mechanism of protein attachment as well. Below the LCST,

the swollen hydrogel absorbs protein molecules; while above LCST, simple monolayer adsorption was observed.[104]

3.4 Grafting and Interfacial adhesion

3.4.1 Trichlorovinyl silane (TCVS) grafting

Poor polymer-substrate adhesion is a common reason for coating failure in materials exposed to mechanical bending, thermal stress or the effect of solvents.[107] Formation of covalent bonds between the polymer thin film and the underlying substrate provides the highest adhesion possible to prevent delamination or detachment of the coating.[108] Surface grafting and interfacial chemical reaction are two approaches to form covalent bonds that can be readily implemented in iCVD. One means of realizing grafted iCVD interfaces is covalently bonding TCVS to a plasma-treated silicon wafer or polydimethyldisiloxane (PDMS) surfaces via reaction of the chlorine moieties with the plasma generated hydroxyl groups. In the next step, radical initiators react with the vinyl group of the silane coupling agent to yield alkyl radicals that are the starting point for the grafted polymer chains. Grafting was used to create nanopatterns on silicon wafers by colloidal lithography.[109] TCVS was attached in the interstices within a template of monodisperse polystyrene nanoparticles cast on the silicon wafer. After iCVD polymerization, the nanoparticles were removed by sonication in THF leaving the polymer attached to the surface with a honeycomb structure (Figure 3e). A specific example of this technique to patterning of CVD hydrogel films will be discussed in Section 3.5. This bottom-up process offers an inexpensive and simple alternative to conventional lithography to design surface-functionalizable polymer patterns.

On elastomeric PDMS substrates, covalent adhesion promotion by TCVS resulted in robustly adhered iCVD films of poly(ethylene glycol diacrylate) pEGDA.[110] The high modulus of this highly crosslinked vapor synthesized polymer relative to the PDMS substrates was critical for maintaining adhesion of the bilayer structure during buckling deformation. Systematic and

deterministic fabrication of highly ordered herringbone patterns through sequential wrinkling strategy was demonstrated with the grafted iCVD pEGDA. This system presents a reversible behavior, switching back and forth from the initial flat surface to the ordered herringbone pattern by applying cyclic mechanical strains (**Figure 10**).

3.4.2 Maleic anhydride (MA) grafting

Vapors of maleic anhydride (MA) react directly with surface amine groups, converting them to vinyl functionalities. The subsequent reaction of the surface vinyl bonds with monomer units to form grafted polymer chains then proceeds in the same manner as for the TCVS produced surface vinyl moieties. The MA pretreatment is performed in the same vacuum chamber used for the subsequent iCVD polymer growth. Copolymers containing MA were deposited and grafted to amine-functionalized silicon nitride cantilever in a single step by iCVD.[111] A sensor was fabricated by this simple scheme, which will be discussed in greater details in section 4.2. Using MA pretreatment, the amine groups present in the polyamide salt rejection layer of reverse osmosis (RO) membranes were turned into vinyl groups to facilitate covalent grafting of the iCVD zwitterionic polymer coating (**Figure 11a** right).[100] Without MA grafting, the vapor grown films delaminated when the treated membranes where placed in water (Figure 11a left). The grafted iCVD (Figure 11a right) zwitterionic coating exhibited anti-fouling properties with respect to protein adsorption and microbial attachment.[101] By utilizing ultrathin (~30 nm) iCVD antifouling layers, the water permeation rate and salt rejection of the underlying membranes was unimpaired.

3.4.3 Tert-butyl peroxide (TBPO) grafting

iCVD utilizes heated filament to break down initiator TBPO and generate free radicals. When the filament temperature is below 250^{o}C, the labile peroxide bond is cleaved (14), which creates *tert*-butyl oxide radicals; when the filament temperature is above 250^{o}C, *tert*-butyl

oxide radials start to undergo β-scission, generating methyl radicals (15), which have greater reactivity than the tert-butoxy radicals.[112]

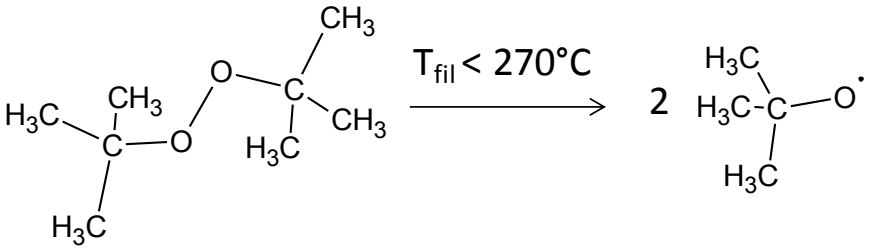

(14),

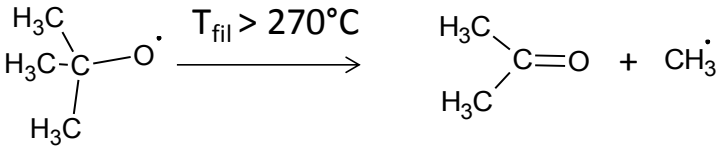

(15),

Methyl radicals are found to facilitate the grafting of vinyl monomers to silicon hydride surfaces, namely passivating silicon surfaces.[113] This treatment was performed in the common iCVD chamber and subsequent polymer growth can be performed *in situ* following the surface treatment. Without this treatment, deposited films delaminated from silicon substrate during sample trimming and handling (**Figure 11b** right), and did not stand up to nanoscratching tests, where spalling of films was observed (**Fig 11c** right). The treated silicon surfaces demonstrated the lowest surface recombination velocity for organic air-stable passivation methods reported to date, indicating the exceptional grafting quality and stability in air. The grafted iCVD coating (Figure 11b and c) can serve as anti-reflective coating in solar cell fabrication.

3.4.4 Nanoadhesive for interfacial bonding

The ring-opening reaction between amine and epoxy groups can take place at temperatures as low as 70^{o}C, and no gaseous by-products are produced. This avoids potential post-reaction defects resulted from outgassing and thus enables an effective nanoadhesive for interfacial

bonding. This has been applied to both PDMS- and non-PDMS-based devices.[114, 115] In these applications, iCVD PGMA is usually deposited on one of the interfaces to be bonded; the other surface is coated with iCVD PAS[115] (see also section 3.3) or polyallylamine (PAAm) by plasma polymerization.[114] The two surfaces are then brought into contact with each other and cured under vacuum at 70-90^{o}C for 24 hours. The exceptional conformality and pinhole-free nature of iCVD method enables the fabrication of oxygen-free flow lithography devices with complex internal 3-D structures.[115]

The amine-epoxy reaction has also been used to graft PEO coatings to amine-functionalized surfaces. The PEO coatings were grafted and deposited simultaneously from ethylene oxide via ring-opening cationic polymerization mechanism.

3.5 Patterning

The ability to pattern functional iCVD polymer is necessary to enable their incorporation in applications such as sensors, optical devices, and tools for biological research. Several patterning techniques have been demonstrated to date, including methods based on photo- and electron beam-lithography, imprinting, and colloidal lithography. Mao and Gleason demonstrated high-resolution, positive-tone patterning of annealed iCVD poly(methyl α-chloroacrylate-*co*-methacrylic acid) via electron beam irradiation (**Figure 12a**).[116] iCVD PGMA has also been used as a positive deep-UV resist and negative electron-beam lithography resist;[117, 118] the ability to conformally coat non-planar surfaces[118] and use an all-dry, supercritical CO_2 developing process[117] make this resist applicable for a range of applications.

Photochemical patterning of 3-D surfaces has recently been demonstrated with various iCVD polymers. Haller *et al.*[96] achieved positive-tone patterning of porous substrates with iCVD poly(*o*-nitrobenzyl methacrylate) (P*o*NBMA), a photosensitive polymer that can be developed

in a biologically-compatible buffer. High-curvature surfaces were patterned using a resist comprised of conformal iCVD poly(4-vinylpyridine) (P4VP) functionalized with a photoactive diacetylene.[119] Coated substrates were covered with flexible masks and exposed at 254 nm, which photopolymerized the diacetylene and rendered the exposed regions insoluble in the developing solvent (**Figure 12b**). Bifunctional organic surfaces were also patterned; additionally, the iCVD-based resist was used to create metal microstructures via pattern transfer.

Other successful patterning strategies have been based on masking and imprinting techniques. Functional polymer features were obtained by depositing a conformal iCVD film on resist templates defined using electron-beam lithography; the templates were then selectively removed using a non-solvent for the iCVD polymer (**Figure 12c**).[9] This method is independent on the chemical functionality of the iCVD film, allowing for easy exchange of responsive iCVD polymers for device applications. Fabrication of bifunctional surfaces has been demonstrated using a self-aligned, dual-purpose lithographic mask.[120] The resulting surfaces exhibited chemical and topological contrast and were used to achieve confinement of water droplets during microcondensation (**Figure 12d**). Capillary force lithography has also been used to pattern iCVD films.[121] By pressing a heated PDMS mold onto a bilayer of highly crosslinked PECVD poly(allylamine) and iCVD polypoly(propargyl methacrylate), Im and coworkers were able to achieve segregation of orthogonal amine and acetylene functionalities with spatial resolution approaching 100 nm (**Figure 12e**).

Self-assembly interactions were utilized to facilitate controllable adhesion of iCVD-coated surfaces. Chen *et al.* coated elastomeric pillars with hydrophilic iCVD polymers, which self-assembled into clusters upon submersion in water (**Figure 12f, g**).[122] Solvent bonds formed by interpenetration of polymer chains overcome the elastic restoring force, rendering the clusters stable upon drying. By patterning some of the pillars with hydrophobic P*o*NBMA,

the authors were able to direct self-assembly and control the location of pillar collapse (**Figure 12h**).

Functional, patterned iCVD polymers have been incorporated in a variety of applications. Kwong and Gupta integrated multiple unit operations into a single, paper-based microfluidic device.[123] Acidic iCVD poly(methacrylic acid) and basic poly(dimethylaminoethyl methacrylate) were deposited on chromatography paper and used as ion-exchange coatings for analyte separation. Patterned iCVD P*o*NBMA was used as a UV-responsive switch that changed hydrophobicity upon exposure, allowing passage of the analytes into the separation zone (**Figure 13a**). The device was successfully used to separate mixtures of model anionic and cationic compounds (**Figures 13b-d**). Haller *et al.* patterned microfluidic channels on paper using hydrophobic, photoresponsive P*o*NBMA (**Figure 13e**).[96]

Patterned iCVD surfaces also form excellent substrates for attachment of molecules and nanoparticles. Im and coworkers used surfaces patterned with orthogonal amine and acetylene nanodomains (Figure 12e) to selectively self-sort fluorescent dyes via a one-pot, biocompatible click/N-hydroxysuccinimide functionalization step (**Figure 13f**).[121] Tenhaeff and Gleason synthesized a highly swellable, pH-responsive hydrogel, poly[maleic anhydride-co-dimethylacrylamide-co-di(ethylene glycol) di(vinyl ether)] (PMaDD), for use in composite separation membranes.[124] The retention of functional moieties and extreme swelling response of the films were confirmed by covalently attaching CdSe/ZnS quantum dots to patterned PMaDD and imaging the films upon exposure to a pH 8 buffer solution (**Figure 13g,h**).

iCVD films can also be used to inhibit molecular attachment—for example, in the case of anti-fouling coatings. As discussed in section 3.3.3, iCVD PEO films were prepared via a

ring-opening cationic polymerization mechanism.[102] PEO features were easily patterned using microcontact printing; in addition, grafted and patterned PEO regions illustrated excellent resistance to non-specific protein adsorption, in contrast to control surfaces (Figure 9c).

3.6 Conformality

In the surface modifications of non-planar substrates, the term conformality describes the ability to encapsulate the entire surface topography with a coating of uniform thickness and composition. Conformal coating is desirable since it brings novel surface functionality to substrates without changing their original morphology. The conformal nature of iCVD is quite valuable for producing functional organic coatings over surfaces having complex geometrical features. With rapid development over the past few years, iCVD has been used on many complex substrates. Even the inner surfaces of porous and fibrous substrates can be modified with functional organic materials by iCVD.[125-128]

For solution phase processing, undesirable variations in coating thickness can result from de-wetting, liquid thinning, and surface tension effects. In contrast, the conformality of CVD polymers results from the arrival of reactants to the surface by non-line-of-sight vapor phase diffusion under the modest vacuum conditions (typically, 0.1 to 1.0 torr), combined with the limited probability of the reactants "sticking" to the surface during a single collision. Step coverage, S, the ratio of film thickness at the bottom of the feature to that at the top, is one measure of conformality. An analytic solution for iCVD film growth in a trench feature gives:

$$\ln(S) = -0.48(\Gamma)\left(\frac{L}{w}\right)^2 \qquad (16)$$

where (L/w) is the aspect ratio of the feature and Γ is the sticking coefficient[61] This profile is experimentally observed when gas phase diffusion to supply additional monomer to the surface is rapid compared to the rate at which monomer is depleted by the film formation reaction. Since the step coverage is governed mainly by the chemisorption of the radicals onto the adsorbed monomer sites, depositions at low fractional saturation partial pressure ratios (P_M/P_{sat}), leads to improved conformality due to lower sticking coefficients. Sticking coefficients in the range of ~0.001 to ~0.01 have been observed for iCVD.

The conformality of iCVD has been demonstrated on trench features etched into silicon, with aspect ratios up to 20:1 and on pores in various types of membranes, with aspect ratios up to 400:1. The primary variables that control the conformality of iCVD films, monomer partial pressure and substrate temperature, also control film deposition rate. At the highest deposition rates, >100 nm/min, the step coverage decreases and the thicker coating near the entrance to a cylindrical pore results in a bottleneck profile, i.e. higher film thickness at the pore entrance. However, a high degree of conformality is still achieved at iCVD growth rates of up to 100 nm/min. This rate is quite fast compared to conformal methods for other materials and is also quite reasonable since the electrolyte film thickness of <100 nm are desired.

The limit up to which conformal coverage can be achieved has been determined by analogy to the reaction-diffusion problem commonly encountered for catalysts on porous supports.[129] The analytic solution for the dimensionless monomer concentration, ψ, as a function of λ, the dimensionless distance down the pore, depends on the dimensional parameter known as the Thiele modulus, Φ:

$$\psi = \frac{e^{\phi\lambda} + e^{2\phi - \phi\lambda}}{1 + e^{2\phi}} \qquad (17)$$

The Thiele modulus can be readily calculated from the dimensions of the pore, the diffusivity of the monomer, and the reaction rate. Depending on the deposition conditions, different profiles over 3D-substrates can be obtained.[130] This analysis will guide the development of conformal iCVD coating on nanostructured electrodes having different architectures, which give rise to pores of different aspect ratio.

Figure 14 a shows the micrograph of a poly(caprolactone) (PCL) nanofiber mat before and after being iCVD coated with poly(perfluoroalkyl ethyl methacrylate) (PPFEMA).[3] The conformal coating by the iCVD process maintains the hierarchical nature of the electrospun mat morphology except for a slight increase in the diameter of fibers. The comparison of the XPS survey scans before and after coating (**Figure 14b**) demonstrates that the fibers were actually coated. **Figure 14c** displays a poly vinyl alcohol (PVA) mold coated by iCVD PGMA, as the supporting layer, and poly(1H,1H,2H,2H-perfluorodecyl acrylate) p(PFDA), on top of PGMA layer.[131] SEM comparison between substrates with and without iCVD coating shows the conformal nature of iCVD process on the inner surfaces of the polymeric mold. The nano-scale inner surfaces features of the PVA mold are exactly repeated by the iCVD deposited films. Additionally, the all-dry nature of the iCVD process avoids the possibility of the solvent swelling or damaging to the substrate, hence ruining the surface topography.

Figure 14d shows a conformal poly(cyclohexyl methacrylate) (pCHMA) thin films deposited by the iCVD process on a trench wafer.[126] This work exhibits the potential for utilizing conformal iCVD coating on microfluidic channels. PDMS-based microfluidic channels provide superior control over mixing than traditional batch reactions.[132] These microchannels need to be impermeable to liquids, but PDMS may swell in solutions. Conformal fluoropolymer coatings by iCVD processes can serve as excellent liquid barriers of PDMS to prevent swelling and hydrophobic recovery caused by the low glass transition temperature of

PDMS.[4, 85, 115, 123, 133-135] Riche et al. demonstrated that conformal fluorocarbon films deposited by iCVD prevent absorption of small molecules and swelling of PDMS in organic solvents.[85] This achievement provides a way to synthesize nanomaterials that are difficult to synthesize with conventional batch reactions. Lazarus et al. showed that devices coated in such way were used for more than 24 hours without degradation or delamination.[133] Jeong et al. deposited p(PDFA) via iCVD on the PDMS micromold, which substantially reduced the diffusion of oxygen and the swelling caused by organic solvents.[134]

Conformal iCVD coatings also display excellent pore-filling properties, which is useful for dye-sensitized solar cells (DSSC).[136, 137] iCVD polymers can replace the liquid electrolyte used in the cell and enhance its operability and durability. **Figure 14 e** shows pore-filling of a 4 μm thick TiO_2 electrode coated with poly(2-hydroxyethyl methacrylate) (PHEMA).[136] In this work, Nejati et al. were able to achieve 92~100% pore filling for electrodes as thick as 12 μm.[136] Their research also indicated the solid state PHEMA electrolyte has higher efficiency than the liquid electrolyte, and results an enhanced performance of the DSSC.

As a dry mechanism without liquid phase or excipient to produce a conformal polymerization, iCVD also provides the ability to encapsulate fine particles down to nanoscale without challenges of particle agglomeration, toxic solvents, and poor quality control in conventional coatings.[138]

3.7 Templating

The substrate-independent and conformal nature of iCVD allows the coating of complex 3D surfaces to be used as a template to engineer novel and functional materials. The ability and ease to design these new-shaped materials opens the door to unexplored possibilities in materials development. Fabrication of responsive polymers with customized 3D structure or encapsulation procedures for drug delivery are some examples of potential applications using

the iCVD technology. Ozaydin-Ince et al.[94] conformally coated the inner walls of an anodic aluminum oxide membrane (AAO) (pore size 200 nm and 60 μm in length) with a 50 nm layer of p(HEMA-*co*-EGDA) hydrogel. The hollow left in the membrane was filled in with an optode solution; afterwards, both sides of the membrane were coated with the same hydrogel and finally the AAO membrane was etched away resulting in the release of microworms structures (**Figure 15 a-b**). Due to their cylindrical shape, these biocompatible microworms are retained in the same location after subcutaneous injection more effectively than nanoparticles with equivalent diameter. Thus, microworms show potential application as fluorescent sensors for *in-vivo* detection and monitoring of analytes. Further studies utilized the same AAO membrane template to synthesize responsive coaxial nanotubes.[90] The coaxial deposition consisted of, first, coating the AAO membranes walls with tert-butylacrylate copolymerized with diethylene glycol divinyl ether (p(TBA-*co*-DEGDVE)), a memory shape polymer, and next the hydrogel copolymer p(HEMA-*co*-EGDA) (**Figure 15 d**). Immersing the nanotubes in a heated dye solution causes the hydrogel to swell; thus, widening the aperture of the nanotube, through which the dye diffuses and gets adsorbed (**Figure 15 e**). Lowering the temperature under the glass transition of the p(TBA-*co*-DEGDVE) fixes the shape of the nanotube. Raising the temperature again leads to shrinkage of the memory shape polymer returning to its initial diameter. As a consequence, the dye absorbed inside is released due to the mechanical stress of the coaxial polymer. Also microtextured PDMS surfaces have successfully been used as templates. Conformal coating of thermosensitive PNIPAAm polymer over PDMS microgrooves was used to fabricate tissue constructs.[65] Once the polymer was deposited on the PDMS surface, the microgrooves were seeded with NIH-3T3 fibroblasts at a temperature of 24 ºC. Conversely, for an optimal cell culture the temperature was increased to 37 ºC, in which PNIPAAm is above the LCST and adopts its collapsed and hydrophobic form. After growth of the tissue, the PDMS mold is placed in contact with a glass slide at 24 ºC. Temperature variation drives PNIPAAm undergo transition

from above to below its LCST. Therefore, the polymer swells resulting in the retrieving of the tissue construct shaped with the size of the microgroove (**Figure 15 c**). Besides solid substrates, Gupta and co-workers have shown that iCVD is able to coat liquids with low vapor pressure, *e.g.* ionic liquids (ILs).[139] Surfaces patterned with IL and silicone oil resulted in the selective encapsulation of IL, given that continuous iCVD films can only be deposited on ILs but not on silicone oil.[140] In addition, marbles of IL were fully encapsulated within a polymer shell of p(PFDA-*co*-EGDA).[141] Rolling the marbles over a bed of loose polytetrafluoroethylene (PTFE) particles creates a textured surface around the IL that facilitates the conformal coating of the polymer to form a shell. The structure of the encapsulated marbles is stable after removal from the substrate and shows no evidence of leaking.

4. Responsive iCVD Surfaces and Devices

4.1 Responsive Surfaces

The ability to dynamically alter surface properties is useful in a wide range of applications including biosensors, cell culture, microfluidics, and tissue engineering. The response of the surface can depend on externally applied stimuli, such light[142-144], temperature[84], or pH[145-147]. The high degree of organic functional group retention by the iCVD synthesis method is essential for achieving the responsiveness.

With biocompatibility and well-known hydrogel properties, PHEMA is widely used in biological and biomedical applications.[148-150] Ozaydin-Ince et al.[84] fabricated pHEMA-based hydrogel nanotubes within the pores of AAO templates. Crosslinking prevented dissolution of the iCVD layer when exposed to aqueous solution. As shown in **Figure 16 a**, the well-ordered nanotube arrays exhibit responsive behavior, diagram schematically in **Figure 16 b**.[84] The swelling ratio achieved depends on the crosslinking ratio. Because swelling of the iCVD fabricated hydrogel nanoforest is not limited by the substrate, a larger

degree of swelling is achieved than for a thin film hydrogels. Moreover, switchable hydrophilicity nanotubes can provide a novel approach to control protein adsorption and drug release. **Figure 16 c** shows a conformal PHEMA layer coated by iCVD on a silica microsphere.[92] The PHEMA layer brings an enhancement of the surface resistance to adhesion of nonspecific protein. This work suggests iCVD provides an ideal route to coat particle sensors, which can be as small as 5 μm.[92]

iCVD has also been used to micropattern bifunctional surfaces (see also section 3.5). Baxamusa et al.[151] used iCVD process combined with physical masks (TEM grid) to synthesize all-polymer patterned surfaces with identical control over chemical and topographic features. **Figure 16 d** shows an AFM image of hydrophobic depressions in a hydrophilic matrix, where the height of the hydrophilic walls changes due to swelling.[151] Dynamic microcondensation experiments indicate water preferentially condensing on the hydrophilic region of the bifunctional surface, as shown in **Figure 16 e**.

iCVD represents a room temperature encapsulation method, which is important for thermally sensitive materials. Lau et al.[146] use a methacrylic acid (MAA) and ethyl acrylate (EA) copolymer as encapsulating layer to provide enteric release properties with pH-responsive swelling behavior of the copolymer. **Figure 16 f** shows the pH-dependent swelling of the copolymer, which enables active materials to be encapsulated for enteric release.[146] Karaman et al.[152] deposited poly(2-(diisopropylamino) ethyl methacrylate) (PDPAEMA) via iCVD on a rough substrate, which generate a surface that can switch between superhydrophobic and superhydrophilic state. Especially, the surface amino groups can be protonated at high pH and then react with anionic biological materials. McInnes et al.[153] developed a controlled drug delivery system with iCVD deposited pH-responsive polymers. The drug was loaded in porous Si (pSi), then capped with a pH-responsive copolymer film via iCVD (**Figure 16g**). Their results show the drug release rate in the system increased more than 4 times from pH

1.8 to pH 7.4. Remarkably, this approach does not affect or degrade the drug, and the iCVD process was independent of both pore and surface chemistry.

iCVD can also be used along with colloidal lithography to provide simple and inexpensive technique for creating various polymeric nanostructures with functional patterns up to 500 nm high without harmful solvents (see also section 3.5).[109] **Figure 16 h** shows grafted hydrophilic hydrogel patterns of well-ordered PHEMA arrays deposited by iCVD.[109]

iCVD can also be used to create wrinkling surface patterns, which are important in a wide range of applications (see section 3.4.1). In **Figure 16 i**, wrinkling surface patterns of poly(2-hydroxyethyl methacrylate-ethylene glycol diacrylate) [p(HEMA-EGDA)] were deposited via iCVD process on PDMS substrates.[110] The wrinkling patterns provide an approach to create ordered herringbone patterns, and more important, the ability to probe the surface topologies via simplified theoretical model, and a way to measure the elastic modulus of the film.

4.2 Responsive Devices

Exact control over the composition, thickness, and conformality of polymer thin films can be achieved by controlling the deposition conditions in iCVD. This, as well as the easiness of integrating iCVD with standard semiconductor manufacturing practices, makes it an ideal technique for fabricating responsive polymer device components. iCVD films have been incorporated into a variety of such applications, including biosensors, enteric coatings, and sensing platforms for vapor-phase analytes. Ozaydin-Ince and coworkers used an iCVD templating technique to create "microworm" optode sensors for *in vivo* measurement of sodium concentration (Figure 15 a, b).[8] iCVD PHEMA coatings have also been used to increase device response in impedance biosensors.[93] The hydrogel coatings protect the electrodes, enhance their surface resistance, and improve the quality of the electrode-electrolyte interface. Analyte diffusion is unaffected due to the increased pore size resulting from swelling of the film in aqueous solution.

pH-responsive iCVD films have been incorporated into a variety of controlled release applications. Methacrylic acid (MAA)-containing iCVD copolymers have been used as enteric coatings for pharmaceuticals.[145] The benign reaction conditions inherent to the iCVD process make it an ideal method for coating thermally-sensitive drugs. Encapsulation of fine drug particles, including microcrystals, is facilitated by the use of a rotary iCVD reactor.[154, 155] Additionally, iCVD MAA films have been used to cap the pores of biodegradable, nanoporous Si matrices loaded with a model drug compound.[156] Release of the drug from the coated matrices is four times faster at pH 7.4 than at pH 1.8, in contrast to uncoated matrices, which show similar rates at both pH values. Synthesis of the iCVD coating is facilitated by the fact that the process is independent of both the surface chemistry and pore size of the Si. iCVD has also been used to achieve controlled release of a water-soluble crop protection compound (CPC). [157] Microcapsules of the CPC were encapsulated with iCVD poly(glycidyl methacrylate) and poly(cyclohexyl methacrylate), and the impact of monomer hydrophilicity, coating thickness, and cross-linking density on CPC release profiles was evaluated.

Responsive iCVD thin films have proven useful for a diverse range of sensing applications. Karaman *et al.* fabricated Bragg mirrors by using a single reaction chamber to deposit alternating layers of iCVD PHEMA and hot wire CVD (HWCVD) titania with high refractive index contrast (**Figure 17a**). [158] Exposure to water vapor induces a rapid and reversible swelling response in the PHEMA, altering the periodicity of the layers and the color of the mirror (**Figure 17b**). The excellent performance of these devices is attributed to layer thickness uniformity and the sharp interfaces achievable using the all-dry CVD processes. Use of CVD also enables device fabrication on a variety of unique surfaces, including glass, flexible polycarbonate, and paper (**Figure 17c**). iCVD polymers have also been used as responsive components in micro-scale resistive sensors. Arora *et al.* created a low-power electromechanical switch consisting of a silicon nitride cantilever suspended over a series of interdigitated electrodes.[111] The top surface of the cantilever was coated with a

highly cross-linked iCVD maleic anhydride copolymer, and the underside was coated with metal. Reaction of maleic anhydride moieties with parts-per-million concentrations of hexylamine analyte causes stress generation in the polymer film; the resulting cantilever deflection enables the metal-coated portions of the device to connect, completing a circuit (**Figure 17d**). The iCVD mechanism has also been exploited to create microcantilever-based peroxide sensors. Peroxide radicals are formed when contaminated air is passed through heated filaments; these radicals adsorb onto a cantilever previously coated with a monolayer of surface-tethered monomers. Polymerization then occurs, resulting in optically detectable deflection of the cantilever.[159] More recent work has focused on developing inexpensive, portable sensors for detecting nitroaromatic explosives. Tenhaeff *et al*.[10] created a low-power resistive sensor by coating a micro-scale silicon trench with a conformal film of iCVD P4VP and a non-conformal Au/Pd layer. The P4VP film expands upon exposure to nitroaromatic compounds, causing the metal-coated surfaces to contact and decreasing the resistance measured across the device (**Figure 17e**). The Flory-Huggins equation described the swelling of the iCVD P4VP.[10]

$$\frac{P_M}{P_{sat}} = (1-\varphi_P)\exp\left[\left(1-\frac{1}{N}\right)\varphi_P + \chi\varphi_P^2\right] \qquad (18)$$

where φ_P is the volume fraction of polymer at the equilibrium (swollen state), χ is the Flory-Huggins interaction parameter for the analyte-polymer system and N is the degree of polymerization.

An additional nitroaromatic sensor was also fabricated, consisting of patterned iCVD P4VP features (Figure 12a) overlaid with a nano-scale metal line (**Figure 17f**).[9] Analyte exposure causes the P4VP to expand, deforming the metal line and increasing its measured resistance. The responses of both sensors are rapid and selective for nitroaromatic compounds. Calculated limits of detection for 2,4,6-trinitrotoluene are in the parts-per-billion range; in addition, the versatility of the polymer deposition and patterning processes ensure that the

sensor designs are interchangeable and can readily be altered by substituting different iCVD polymers (**Figure 17 g**).[9, 10]

5. Fluoropolymers

5.1 Acrylates with perfluoro side chains

Low-surface-energy surfaces have a wide range of applicability, having utility as biocompatible surfaces, antifouling coatings,[12] and low dielectric constant material for microelectronics. The CVD method is very attractive because solvents and surfactants for fluoropolymers tend to be difficult to find, expensive, and/or persistent in the environment. Furthermore, CVD fluorocarbon coatings can be directly deposited on a large range of substrates, including those with limited thermal stability, and those have surface features such as microchannels or nanostructures, thus simplifying the fabrication and widening the applicability of fluoropolymer coatings.

Recently, perfluoroacrylates have received much attention due to their exceptional properties, including fast polymerization of the unsaturated acrylate group and hydrophobicity for the fluorinated pendant chain. As a result of the $–CF_3$ terminated side groups and comb-like structure, the typical range of surface energies for fluorinated acrylic polymers is very low (5.6 to 7.8 mN/m).

The iCVD p(PFDA) has been widely studied either pure[139, 160, 161] and copolymerized[95, 145, 162] with other monomers. The side chains with eight perfluorinated carbons, so called “C8”, was completely retained during the polymerization[161] giving interesting properties to the iCVD polymer such as hydrophobicity, oleophobicity, crystallinity.

The iCVD p(PFDA) can be deposited to yield high conformality in high-aspect-ratio pores. This properties has been used to coat commercially available membranes[163] and enhanced their selectivity[129] achieving hydrophobicity-based separation (**Figure 18 c**). Electron microprobe analysis on the membrane cross-section confirmed the presence of coating through the whole length of the pore. Superhydrophobic fabrics were obtained by conformal

coverage of iCVD p(PFDA) on electrospun mats. [3, 164] Hierarchical morphology, in the form of coating roughness overimposed on the fiber networks, resulted in grade 8 oleophobicity. The p(PFDA) was used to encapsulate paper solar cells, which could then operate even when totally submerged in water (**Figure 18b**).

Free-standing p(PFDA) polymer films have been obtained by depositing the iCVD polymer over droplets of ionic liquid.[140] The low surface energy of the p(PFDA) coatings have been applied on PDMS-based micromold[165] and microfluidic[85] devices in order to create a barrier coating towards organic solvents. Uni-directional liquid spreading without lateral diffusion of the chemicals (Figure 13e) was demonstrated inside the microfluidic device, while the micromold was used to synthesize monodisperse polymeric particles of sizes down to 3 μm. **Figure 18a** shows the conformal p(PFDA) coating inside the micromold.

Another powerful capability of the iCVD method is that the fluorocarbon monomers can easily be copolymerized with other monomers in a one-step process and without the need of finding a common solvent for both monomers. With this strategy bifunctional surfaces with hydrophobic p(PFDA) chains and hydrophilic groups were deposited. PFDA was copolymerized with HEMA[151], MAA [162], DVB[166]. The copolymer of PFDA and MAA showed proton conductivity similar to the one of the commercial available Nafion membranes. The PFDA units were responsible of creating a hydrophobic backbone to ensure membrane stability, while the acid units with ionizable groups created the ionic channels for proton passage.

5.1.1 Crystallinity

The C8 fluorinated chains of the p(PFDA) pending from the polymer backbone have a natural tendency to reorient toward themselves and form a crystalline bilayer structure, termed the smectic B phase. Semicrystalline polymers give stable surface properties, without hydrophobic recovery and create generally rough surfaces (root mean square roughness higher than 30 nm), which can be useful for enhancing cell growth or enhancing the hydrophobicity

of the surface. By tuning the iCVD parameters (filament temperature, initiator over monomer ratio and substrate temperature), it is possible to tune also the degree of crystallinity in the film and the orientation of the crystallites (perpendicular or parallel to the surface).[160] **Figure 18f** shows the x-ray diffraction (XRD) pattern of the iCVD p(PFDA). This is the same crystal structure observed in conventionally synthesized p(PFDA). At high filament temperature, 300 °C, the diffraction peaks sharpen when the x-ray beam is oriented perpendicularly to the substrate while they are absent when x-ray beam is parallel to the substrate, indicating vertical alignment of the perfluoro side-chains. At low filament temperature, 240 °C, instead, the diffraction peaks are sharp at 90° and broad at 0° indicating a change to a horizontal alignment. The difference in orientation influenced the roughness and the wettability of the film. The lowest degree of hysteresis in the water contact angle is observed in films with the highest degree of crystallinity.

Grafting the polymeric p(PFDA) chains to the surface, using the trichlorovinyl silane as coupling agent resulted in even higher advancing water contact angle of 160°, with a hysteresis of only 5°.[167] The grafted film showed enhanced crystalline fiber-like structures with high roughness. **Figure 18d** shows the contact angles of the grafted and ungrafted surface wetted with different hydrocarbon oils with increasing number of carbon atoms and **Figure 18e** the cosine of the contact angle (CA) as a function of the liquid-surface energies of the hydrocarbon oils. The grafted polymer exhibits oleophobicity in contrast to the ungrafted one, which displays much lower CAs.

5.2 Hot-wire CVD and iCVD Polytetrafluoroethylene

Of high technological interest is the deposition of thin fluorocarbon films, which are spectroscopically indistinguishable from bulk polytetrafluoroethylene (PTFE, Teflon®). PTFE in its defect-free, true linear form (-$(CF_2)_x$-) has excellent chemical resistance, high hydrophobicity, low refractive index and dielectric constant, low coefficient of friction, and high thermal stability.

Due to its extremely low solubility in common solvents, it is very difficult to process the PTFE in thin film form and therefore in-situ polymerization techniques, i.e. CVD polymerizations, have been investigated. PECVD of teflon-like coatings resulted in structure containing high concentrations of dangling bonds and a variety of bonding environments (i.e. CF_3 and CF, in addition to CF_2). The CF_2 content was just 38% when the PTFE was deposited by PECVD and with growth rate ~140 nm min^{-1}. Films containing high percentages of CF_2 were obtained by using pulsed plasmas, but deposition rates are substantially lower.

On the contrary a structure exclusively made of CF_2 repeating units was successfully obtained by HWCVD[168] and iCVD[47] at much higher growth rates. HWCVD can be considered as the ancestor of iCVD: it takes place in a similar reactor configuration and the chemical species are thermally broken by a filament. Unlike iCVD, the initiator is not involved in the process and the monomer is the species that is thermally decomposed. HWCVD has been used to create high quality fluorocarbon and organosilicon films and has attracted significant attention due to the scalability of the process.[125, 169] The monomer, which has been used to create PTFE films, is the hexafluoropropylene oxide (HFPO). HFPO pyrolysis results in difluorocarbene (CF_2:) radicals.[170] CF_2 production has been observed in the gas phase by UV absorption spectroscopy[171]. PTFE chain growth proceeds by the addition of singlet CF_2 to unterminated C_nF_{2n} chains, following the pathway identified by density functional theory.[172] Chain termination most likely occurs by reaction with the primary initiating radical or with another propagating chain.

PTFE films produced by HWCVD technique can reach essential 100% CF_2 groups. Measurements of x-ray photoelectron spectroscopy (XPS) and Fourier transform infrared (FTIR) spectra demonstrate the predominance of the $–CF_2-$ bonding environment, similarly to what also observed for conventionally synthesized bulk PTFE. Same results were obtained by solid-state magic angle spinning ^{19}F nuclear magnetic resonance (NMR) as shown in **Figure 19e**.[173] The PTFE obtained by HWCVD showed also some crystalline organization as

observed by x-ray diffraction (XRD), which was enhanced by an annealing step to the point that spherulites were visible to the naked eye.[5]

Typical surface energy for PTFE is ~20 mN/m, higher than the surface energy of the acrylate-based fluorocarbon coating, due to the low density of terminal CF_3 groups. In spite of this, superhydrophobic coatings were obtained by depositing conformal PTFE by HWCVD over vertically aligned multiwalled carbon nanotube forests (mean diameter ~50 nm, mean height ~2 μm) (**Figure 19a**).[174] **Figure 19b** shows an essentially spherical water droplet suspended on the PTFE-coated forest. PTFE coated nanotube forest displayed advancing and receding contact angles with water of 170° and 160°, respectively. The super-hydrophobicity was explained as an effect of the higher roughness due to the deposition on nanotubes of different height.

Also in HWCVD the substrate remains at ambient temperature. This enables the coating of nearly any object, including paper. **Figure 19c** shows, in fact, a PTFE-coated tissue paper.[125] The paper substrate survived the HWCVD step, demonstrating the gentle nature of the process, and the water did not wet it after depositing the hydrophobic coating. In contrast, substrates need to withstand a temperature of 400°C in order to survive the conventional spray and bake process for PTFE coatings used for relative thick coatings (~25 μm), such as those applied to non-stick cookware.

HWCVD has been used to coat substrates with complex 3D shape and morphology (**Figure 19d, f**). A conformal coating 16 μm thick PTFE, was deposited on a 25 μm diameter stainless steel wire.[175] The coating is visible all around the circumference of the wire.[168] The uniformity of coating thickness can be also observed over all the surfaces of a MEMS test structure.[2]

PTFE has been also obtained through iCVD, using the initiator perfluorooctane sulfonyl fluoride (PFOS).[47] Thermal decomposition of the PFOS over the heated nichrome filament, produced $\cdot(CF_2)_7CF_3$ initiating radicals. For iCVD PTFE, the filament not only was useful to

create radical species from the initiator, but also, to decompose the precursor gas (HFPO) to form the polymerizing species. The addition of PFOS, as initiator, accelerated the deposition rates, < 1 μm/min. Furthermore, PFOS initiating radicals contained terminal CF_3 groups which were included in the PTFE polymer chains, lowering the surface energy of the polymer. iCVD synthesis of CF_3 terminated PTFE chains was confirmed by solid-state magic angle spinning ^{19}F nuclear magnetic resonance (NMR).

Laird et al.[48] have recently investigated the use of another initiator: the perfluorobutane sulfonyl fluoride ($CF_3(CF_2)_3SO_2F$, PBFS). It has a shorter C4 perfluorinated chain, which is preferable to avoid bioaccumulating C8 species. They have investigated the nanoscale roughness and chain orientation of the ultrathin iCVD PTFE conformal coatings on single wall carbon nanotubes (SWCNT). The SWCNT induced PTFE crystallization in situ. **Figure 19g** shows the SEM image of SWCNT buckypaper with a thin coating of PTFE. The PTFE shows lamellar structures, with a disk shape, spaced on average 13 nm apart and kept strung together by a one-dimensional template, presumably SWCNT bundles. This type of structure (reported for the first time by this research group) has been assembled to "nanohybrid shish kebabs" in which the shishes are the nucleation templates onto which crystalline polymers crystallize with lamellar orientation. A schematic of the disks arrangement on the SWCNT bundle has been given in **Figure 19i**. Detailed size analysis showed that the mean diameter of the disks was ~40 nm (**Figure 19h**). The achieved control not only over the surface chemistry of the PTFE films but also on their topology is expected to have major implications in applications as antifouling and wear-resistant surfaces.

6. Scale-up and Commercialization

The industrial viability of iCVD PTFE has been demonstrated by Pryce Lewis et al.[169] Computer control of the reactant flow rates, the temperatures of various parts of the system, pressure, and the safety interlocks, reduces the training and knowledge required by the operator of a commercial iCVD reactor system (**Figure 20**) and improves the reproducibility

of the process. The same reactor designs provide a unified platform for the growth of any iCVD functional polymer or copolymer.

A benchtop system with a 200 mm diameter vacuum chamber (Figure 20a) is designed to facilitate academic and industrial research and development. Reactor chambers with large deposition areas improve the economics of the process, increase process throughput, and allow for the surface modification of large objects. Computational fluid dynamic modeling and non-dimensional analysis of convective and diffusive heat and mass transport[71] allow processes developed in bench scale systems to be translated with equivalent performance into large reactors. The design of the reaction chamber and the process conditions employed (temperatures, pressures, and reactant flow rates) determines the deposition rate achieved and the efficiency of reactant utilization. The latter two factors are among the most critical for determining the overall process cost. Utilizing reactants commercially available in bulk quantities, as opposed to custom synthesized molecules, is highly desirable for achieving favorable process economics for CVD polymers.

Two production size iCVD reaction chambers are shown in Figure 20b and 20c, a batch deposition reactor with an integrated touch screen control panel and a coating width of 1.2 m, and a 0.5 m wide roll-to-roll web system for coating of flexible media, respectively. The roll-to-roll system can achieve a higher percentage of active coating time by eliminating the down periods associated with pumping up and pumping down each time the door is opened and closed. Semi-continuous roll-to-roll systems are typically designed to run for ~0.5 day or ~ 1 day without operator intervention, requiring greater process stability and control than for batch operation. Rolling the media averages any gradients present along the direction of travel, but excellent uniformity of composition and thickness is required in the perpendicular direction across the roll. The economic benefit of roll-to-roll operation, for example, is utilized for metallization of food packages such as on the internal surfaces of potato chip bags.

While the initial investment in bench scale CVD equipment exceeds that required for typical solution processing, at the manufacturing scale CVD can have a lower cost of ownership. For example, for the growth of low dielectric constant layers for the semiconductor industry, the purchase and operation of both automated, controlled vapor ambient, spin-coating tracks and post bake furnaces for removing residual solvent, combined with high consumable cost of the spin-on resins, made solution-based approaches more costly than CVD. The CVD materials also had superior properties and thus now dominate the market for low dielectric constant films, despite significant investment from many major chemical suppliers offering solution applied low dielectric materials. Commercialization of solvent-free CVD processes can also be favored by the absence of environmental, health, and, safety issues associated with solvent usage and the elimination of solvent disposal costs.

It should be noted that an older CVD process for poly-para-xylylene (PPX) and its variants, has been successfully commercialized since the 1960's.[176] These coatings, as known as parylenes, are desired for their conformal coverage and are widely used as protective encapsulation over the complex features of printed circuit boards and medical devices. An excellent review of the synthesis and applications of functionalized forms of PPX has been recently been authored by Lahann et al.[177]

7. Historical Development

The first HWCVD polymer deposition in 1996[175] was actually a negative result! At that time, our MIT group had been carrying out traditional plasma enhanced CVD of polymer-like thin films. In the literature for this field, it was widely hypothesized that the ions produced by the plasma were essential for the growth of organic films.[7] We were using a monomer, hexafluoropropylene oxide (HFPO), which we subsequently learned was also thermally cracked for use in molecular beam experiments to produce the neutral species, difluorocarbene (CF_2). Since we were also carrying our research on HWCVD of

polycrystalline diamond thin films, we decided to test the long-standing hypothesis by thermally decomposing HFPO in a HWCVD reactor, to produce a high concentration of neutrals in the absence ions. The expectation was that no film would form. The wire temperatures needed for pyrolysis of the HFPO were only ~450°C rather the ~2000°C used in the diamond deposition work. Surprisingly, in first HWCVD from HFPO, doctoral student Scott Limb rapidly deposited film with essentially 100% functional group retention.

Since this initial unanticipated result, the conceptual development of iCVD and oCVD has been guided by the work of the many researchers who established the fundamental mechanisms of solution phase polymerization. Several generations of graduate students and postdoctoral researchers contributed to the development of these technologies for CVD polymerization and only a few highlights will be mentioned. A separate intentional initiation species was first introduced by doctoral student Hilton Pryce Lewis in 2001[47], yielding a dramatic increase in deposition rate. As CEO of GVD Corporation (gvdcorp.com), Dr. Pryce Lewis has led the scale up, automation, and commercialization of HWCVD and iCVD polymers. The utilization of a separate initiator was extended by doctoral student Yu (Jessie) Mao to the first successful polymerization vinyl monomers in 2004.[50] She also demonstrated the first iCVD copolymerization and extended the use of reactivity ratios developed for solution synthesis to the vapor deposited films. Fundamental knowledge of the iCVD process was significantly advanced by doctoral student Kenneth K.S. Lau.[51, 57] Thus, the iCVD method could be rapidly extended to the free radical polymerization of many new monomers. Also in 2006, the first demonstration of oxidative step growth polymerization to form oCVD electrical conductive films was achieved by doctoral candidate John Lock.[24] The *in situ* grafting of oCVD film to create robust adhesion to surfaces with aromatic groups was achieved by doctoral student Sung Gap Im.[19] In 2012, as a professor at Drexel, Dr. Lau has shown that iCVD can be extended to cationic polymerization.[102]

The polymeric compositions achievable and their applications are anticipated to blossom as more research groups adopt this technology.

8. Conclusions and Future Prospects

New CVD polymer methods augment the capabilities of traditional methods for polymeric surface modification and are an enabling technology for multiple applications. CVD polymerization brings the precision of the vacuum deposition methods developed for inorganic films to the realm of functional and responsive organic materials. Vapor methods enable the direct chemical synthesis and thin film formation of organic polymer layers in a single step. The platform technologies of oCVD and iCVD are analogous to traditional oxidative step growth and free radical chain growth mechanisms, respectively.

The full degree organic functional group retention is highly desirable for designing surfaces, which display controlled wettability, antifouling behavior, or respond to external stimuli. Additionally, the chemical and biological specificity, which can be imparted by the organic functional groups, is a characteristic that clearly differentiates CVD polymers from their inorganic CVD counter parts. This specificity of chemical and biological interaction is only beginning to be exploited for applications from chemical sensing to tissue engineering.

A wide range of homopolymers and copolymer compositions have been demonstrated by both iCVD and oCVD methods. A unique feature of CVD is that the monomers used for the copolymerization do not require a common solvent.

Dielectrics, semiconductors, and electronic conductors have all been demonstrated by CVD polymerization. Contiguous films can be obtained with thickness as low as 10 nm, while high growth rate conditions, in some cases > 1 μm/min, can be utilized to deposit films which are tens of microns thick.

The easy tunablity of the film and surface properties has allowed the successful integration of CVD polymers into prototypes for applications including, but not limited to, membranes, microfluidics, sensors, controlled release, and flexible optoelectronics. As passivation of

neural probes, dielectric iCVD layers have measure stability over > 9 years in 37°C saline solution under continuous cycling between +/- 5 V. The diversity of applications for CVD polymers is anticipated to expand with increasing codification of the processing knowledge and ready availability of automated reactor systems.

By eliminating the need to dissolve macromolecules, the CVD approach is particularly advantageous for the synthesis of linear polymers or crosslinked networks of limited solubility. Additionally, vapor processing avoids the potential for the substrate to disintegrate, dissolve, swell, shrink, fade, or wrinkle as a result of solvent exposure. Solvent-free and surfactant-free processing eliminates the environmental, safety, and health considerations associated with these components and can reduce waste disposal. Process simplification can result by eliminating post-deposition steps, such as annealing for removing residual solvent from solution-applied film. Undesirable dewetting effects, which lead to pinhole and void formation, are also avoided by utilizing CVD.

Unlike typical solution processing, CVD polymerization produces conformal coatings, which precisely follow the geometry of the underlying substrate. The conformal nature of CVD polymers allows the uniform modification of objects having complex shapes and surface features, including the interior surfaces of porous or fiber-based media. This conformal behavior has been achieved at high rates (~100 nm/min). The high deposition rate and the specific chemical composition of the resulting polymers differentiate iCVD and oCVD conformal coatings from those achieved by either atomic layer deposition (ALD) or layer-by-layer (LBL) deposition.

By building the films from the interface up, in situ interfacial grafting strategies have resulted in robust interfaces. To date, these grafted interfaces have been shown to prevent delamination failures, which is essential for most applications. The adhesion allows patterning the functional layers to submicron resolution and this patterning is essential for the successful integration of CVD polymer into device structures. In addition, grafted iCVD interfaces have

enabled the stable electronic passivation of silicon at room temperature. Future efforts are expected to produce hybrid organic/inorganic interfaces with novel thermal and electronic properties.

The modest substrate temperature, often near room temperature, allows the CVD polymers to be directly grown on thermal sensitive materials, such as plastics and textiles. In contrast, materials synthesized at high temperature must be first grown on thermal stable substrate and then transferred onto the substrate of lower thermal stability, through a complex and costly process. Since flexible substrates are essential for economical roll-to-roll manufacturing, the ability to grow flexible layers of insoluble materials, including electrical conductors and semiconductors, directly on flexible substrates, is an enabling capability for low-cost processing. Additionally, the controlled vacuum deposition environment and the high purity of commercially available small molecule reactants enable high quality film, making CVD polymers desirable for biomedical and optoelectronic applications. Precise control and quantitative modeling of the delivery of reactants, vapor flow patterns, and reaction temperatures, couples with real-time monitoring of the deposited thickness allow for reproducible of processing and scale up of reactor size. These two latter factors have been the key to the commercial success demonstrated to date, and will remain essential to further expansion of the many practical benefits of CVD polymer technology.

Acknowledgments

The authors acknowledge financial support from the MIT Institute for Soldier Nanotechnologies (ISN) under Contract DAAD-19-02D-0002 with the U.S. Army Research Office, the King Fahd University of Petroleum and Minerals (KFUPM) in Dhahran, Saudi Arabia, for funding support through the Center for Clean Water and Clean Energy at MIT and KFUPM, and the Masdar Institute. D. C. Borrelli and C.D. Petruczok gratefully acknowledge support from the National Science Foundation Graduate Research Fellowship Program. R.M. Howden acknowledges support from Department of Energy Office of Science Graduate

Fellowship Program (DOESCGF), made possible in part by the American Recovery and Reinvestment Act of 2009, administered by ORISE-ORAU under Contract No. DE-AC05-06OR23100.

[1] G. Ozaydin-Ince, A. M. Coclite, K. K. Gleason. *Rep Prog Phys* **2012**, *75*, 1-40.
[2] M. E. Alf, A. Asatekin, M. C. Barr, S. H. Baxamusa, H. Chelawat, G. Ozaydin-Ince, C. D. Petruczok, R. Sreenivasan, W. E. Tenhaeff, N. J. Trujillo, S. Vaddiraju, J. J. Xu, K. K. Gleason. *Advanced Materials* **2010**, *22*, 1993-2027.
[3] M. L. Ma, Y. Mao, M. Gupta, K. K. Gleason, G. C. Rutledge. *Macromolecules* **2005**, *38*, 9742-9748.
[4] J. J. Xu, K. K. Gleason. *Chem Mater* **2010**, *22*, 1732-1738.
[5] K. K. S. Lau, K. K. Gleason. *J Phys Chem B* **2001**, *105*, 2303-2307.
[6] J. Lahann, D. Klee, W. Pluester, H. Hoecker. *Biomaterials* **2001**, *22*, 817-826.
[7] R. Dagostino, F. Cramarossa, F. Illuzzi. *Journal of Applied Physics* **1987**, *61*, 2754-2762.
[8] Kazuhiko Endo, Toru Tatsumi. *J Appl Phys* **1995**, *78*, 1370-1372.
[9] Nancy H. Lee, Lisa M. Christensen, Curtis W. Frank. *Langmuir* **2003**, *19*, 3525-3530.
[10] P. Simon, S. Mang, A. Hasenhindl, W. Gronski, A. Greiner. *Macromolecules* **1998**, *31*, 8775-8780.
[11] S. Seidel, C. T. Riche, M. Gupta. Chemical Vapor Deposition of Polymer Films. In: *Encyclopedia of Polymer Science and Technology*: John Wiley & Sons, Inc.; 2002.
[12] R. Yang, A. Asatekin, K. K. Gleason. *Soft Matter* **2012**, *8*, 31-43.
[13] S. G. Im, K. K. Gleason. *Aiche J* **2011**, *57*, 276-285.
[14] Miles C. Barr, Chiara Carbonera, Riccardo Po, Vladimir Bulovic, Karen K. Gleason. *Applied Physics Letters* **2012**, *100*, 183301.
[15] M. C. Barr, J. A. Rowehl, R. R. Lunt, J. Xu, A. Wang, C. M. Boyce, S. G. Im, V. Bulovic, K. K. Gleason. *Adv. Mat.* **2011**, *23* 3500-3505.
[16] Rishabh M. Jain, Rachel Howden, Kevin Tvrdy, Steven Shimizu, Andrew J. Hilmer, Thomas P. McNicholas, Karen K. Gleason, Michael S. Strano. *Advanced Materials* **2012**, *24*, 4436-4439.
[17] D. Bhattacharyya, K. K. Gleason. *Chem. Mat.* **2011**, *23*, 2600-2605.
[18] D. Bhattacharyya, K. Senecal, P. Marek, A. Senecal, K. K. Gleason. *Adv Func. Mat.* **2011,**, *21*, 4328-4337.
[19] S. G. Im, P. J. Yoo, P. T. Hammond, K. K. Gleason. *Advanced Materials* **2007**, *19*, 2863-2867.
[20] Miles C. Barr, Jill A. Rowehl, Richard R. Lunt, Jingjing Xu, Annie Wang, Christopher M. Boyce, Sung Gap Im, Vladimir Bulović, Karen K. Gleason. *Advanced Materials* **2011**, *23*, 3500-3505.
[21] Sung Gap Im, Karen K. Gleason. *Macromolecules* **2007**, *40*, 6552-6556.
[22] Hitesh Chelawat, Sreeram Vaddiraju, Karen Gleason. *Chem Mater* **2010**, *22*, 2864-2868.
[23] Siamak Nejati, Kenneth K. S. Lau. *Langmuir* **2011**, *27*, 15223-15229.
[24] John P. Lock, Sung Gap Im, Karen K. Gleason. *Macromolecules* **2006**, *39*, 5326-5329.
[25] Dhiman Bhattacharyya, Rachel M. Howden, David C. Borrelli, Karen K. Gleason. *Journal of Polymer Science Part B: Polymer Physics* **2012**, *50*, 1329-1351.
[26] H. Park, R. M. Howden, M. C. Barr, V. Bulovic, K. Gleason, J. Kong. *Acs Nano* **2012**, *6*, 6370-6377.

[27] Rachel M. Howden, Elaine D. McVay, Karen K. Gleason. *Journal of Materials Chemistry A* **2013**, *1*, 1334-1340.
[28] Dhiman Bhattacharyya, Rong Yang, Karen K. Gleason. *Journal of Materials Chemistry* **2012**, *22*, 17147-17152.
[29] S. Vaddiraju, H. Cebeci, K. K. Gleason, B. L. Wardle. *Acs Applied Materials & Interfaces* **2009**, *1*, 2565-2572.
[30] Sreeram Vaddiraju, Kris Seneca, Karen K. Gleason. *Adv Funct Mater* **2008**, *18*, 1929-1938.
[31] Nathan J. Trujillo, Miles C. Barr, Sung Gap Im, Karen K. Gleason. *Journal of Materials Chemistry* **2010**, *20*, 3968–3972.
[32] Sung Gap Im, Karen K. Gleason, Elsa A. Olivetti. *Appl Phys Lett* **2007**, *90*.
[33] Vittorio Scardaci, Richard Coull, Jonathan N. Coleman. *Appl Phys Lett* **2010**, *97*.
[34] John P. Lock, Jodie L. Lutkenhaus, Nicole S. Zacharia, Sung Gap Im, Paula T. Hammond, Karen K. Gleason. *Synthetic Metals* **2007**, *157*, 894-898.
[35] Miles C. Barr, Rachel M. Howden, Richard R. Lunt, Vladimir Bulovic, Karen K. Gleason. *Advanced Energy Materials* **2012**, *2*, 1404-1409.
[36] Miles C. Barr, Chiara Carbonera, Riccardo Po, Vladimir Bulovic, Karen K. Gleason. *Appl Phys Lett* **2012**, *100*.
[37] Rachel M. Howden, Eletha J. Flores, Vladimir Bulović, Karen K. Gleason. *submitted*.
[38] Serap Günes, Helmut Neugebauer, Niyazi Serdar Sariciftci. *Chemical Reviews* **2007**, *107*, 1324-1338.
[39] Abhishek P. Kulkarni, Christopher J. Tonzola, Amit Babel, Samson A. Jenekhe. *Chem Mater* **2004**, *16*, 4556-4573.
[40] Jana Zaumseil, Henning Sirringhaus. *Chemical Reviews* **2007**, *107*, 1296-1323.
[41] David C. Borrelli, Miles C. Barr, Vladimir Bulović, Karen K. Gleason. *Solar Energy Materials and Solar Cells* **2012**, *99*, 190-196.
[42] David C. Borrelli, K. K. Gleason. *Manuscript submitted* **2013**.
[43] Hua Bai, Gaoquan Shi. *Sensors* **2007**, *7*, 267-307.
[44] Sreeram Vaddiraju, K. K Gleason. *Nanotechnology* **2010**, *21*, 125503.
[45] Dhiman Bhattacharyya, Karen K. Gleason. *Chem Mater* **2011**, *23*, 2600-2605.
[46] Dhiman Bhattacharyya, Kris Senecal, Patrick Marek, Andre Senecal, Karen K. Gleason. *Adv Funct Mater* **2011**, *21*, 4328-4337.
[47] H. G. P. Lewis, J. A. Caulfield, K. K. Gleason. *Langmuir* **2001**, *17*, 7652-7655.
[48] Eric D. Laird, Ranjita K. Bose, Wenda Wang, Kenneth K. S. Lau, Christopher Y. Li. *Macromolecular Rapid Communications* **2012**, n/a-n/a.
[49] K. Chan, K. K. Gleason. *Chem Vapor Depos* **2005**, *11*, 437-443.
[50] Y. Mao, K. K. Gleason. *Langmuir* **2004**, *20*, 2484-2488.
[51] K. K. S. Lau, K. K. Gleason. *Macromolecules* **2006**, *39*, 3688-3694.
[52] J. Xu, K. K. Gleason. *ACS Appl. Mat. Interf.* **2011**, *3*, 2410-2416.
[53] Jose Luis Yagüe, Anna Maria Coclite, Christy Petruczok, Karen K. Gleason. *Macromolecular Chemistry and Physics* **2013**, *214*, 302-312.
[54] A. M. Coclite, K. K. Gleason. *Plasma Process Polym* **2012**, *9*, 425-434.
[55] K. Chan, K. K. Gleason. *Langmuir* **2005**, *21*, 11773-11779.
[56] T. P. Martin, K. L. Sedransk, K. Chan, S. H. Baxamusa, K. K. Gleason. *Macromolecules* **2007**, *40*, 4586-4591.
[57] K. K. S. Lau, K. K. Gleason. *Macromolecules* **2006**, *39*, 3695-3703.
[58] G. Ozaydin-Ince, K. K. Gleason. *J Vac Sci Technol A* **2009**, *27*, 1135-1143.
[59] K. Chan, K. K. Gleason. *Macromolecules* **2006**, *39*, 3890-3894.
[60] A. M. Coclite, G. Ozaydin-Ince, R. d'Agostino, K. K. Gleason. *Macromolecules* **2009**, *42*, 8138-8145.
[61] S. H. Baxamusa, K. K. Gleason. *Chem Vapor Depos* **2008**, *14*, 313-318.

[62] G. Odian. *Principles of polymerization, 4th ed.* Hoboken, N.J.: Wiley-Interscience; 2004.
[63] M. Fineman, S. D. Ross. *Journal of Polymer Science* **1950**, *5*, 259-262.
[64] R. K. Bose, K. K. S. Lau. *Thin Solid Films* **2011**, *519*, 4415-4417.
[65] H. Tekin, G. Ozaydin-Ince, T. Tsinman, K. K. Gleason, R. Langer, A. Khademhosseini, M. C. Demirel. *Langmuir* **2011**, *27*, 5671-5679.
[66] G. Ozaydin-Ince, G. Demirel, K. K. Gleason, M. C. Demirel. *Abstr Pap Am Chem S* **2010**, *240*.
[67] G. Ozaydin-Ince, K. K. Gleason, M. C. Demirel. *Soft Matter* **2011**, *7*, 638-643.
[68] M. E. Alf, T. A. Hatton, K. K. Gleason. *Thin Solid Films* **2011**, *519*, 4412-4414.
[69] R. Forch, A. N. Chifen, A. Bousquet, H. L. Khor, M. Jungblut, L. Q. Chu, Z. Zhang, I. Osey-Mensah, E. K. Sinner, W. Knoll. *Chem Vapor Depos* **2007**, *13*, 280-294.
[70] M. E. Alf, T. A. Hatton, K. K. Gleason. *Polymer* **2011**, *52*, 4429e4434.
[71] M. Gupta, K. K. Gleason. *Thin Solid Films* **2006**, *515*, 1579-1584.
[72] R. K. Bose, K. K. S. Lau. *Biomacromolecules* **2010**, *11*, 2116-2122.
[73] K. Chan, K. K. Gleason. *Langmuir* **2005**, *21*, 8930-8939.
[74] R. Tao, M. Anthamatten. *Langmuir* **2012**, *28*, 16580-16587.
[75] K. Chan, L. E. Kostun, W. E. Tenhaeff, K. K. Gleason. *Polymer* **2006**, *47*, 6941-6947.
[76] R. Yang, J. Xu, G. Ozaydin-Ince, S. Y. Wong, K. K. Gleason. *Chem. Mat.* **2011**, *23*, 1263-1272.
[77] W. S. O'Shaughnessy, S. K. Murthy, D. J. Edell, K. K. Gleason. *Biomacromolecules* **2007**, *8*, 2564-2570.
[78] A. M. Coclite, G. Ozaydin-Ince, F. Palumbo, A. Milella, K. K. Gleason. *Plasma Process Polym* **2010**, *7*, 561-570.
[79] D. A. Spee, M. R. Schipper, C. H. M. van der Werf, J. K. Rath, R. E. I. Schropp. *Thin Solid Films* **2013**, *532*, 84-88.
[80] A. M. Coclite, F. De Luca, K. K. Gleason. *J Vac Sci Technol A* **2012**, *30*.
[81] M. F. Thorpe. *Journal of Non-Crystalline Solids* **1983**, *57*, 355-370.
[82] J. C. Phillips. *Journal of Non-Crystalline Solids* **1979**, *34*, 153-181.
[83] R. K. Bose, A. M. Heming, K. K. Lau. *Macromol Rapid Commun* **2012**, *33*, 1375-1380.
[84] G. O. Ince, G. Demirel, K. K. Gleason, M. C. Demirel. *Soft Matter* **2010**, *6*, 1635-1639.
[85] C. T. Riche, B. C. Marin, N. Malmstadt, M. Gupta. *Lab on a Chip* **2011**, *11*, 3049-3052.
[86] G. Aresta, J. Palmans, M. C. M. van de Sanden, M. Creatore. *J Vac Sci Technol A* **2012**, *30*.
[87] G. Aresta, J. Palmans, M. C. M. van de Sanden, M. Creatore. *Micropor Mesopor Mat* **2012**, *151*, 434-439.
[88] J. Xu, A. Asatekin, K. K. Gleason. *Advanced Materials* **2012**, *24*, 3692-3696.
[89] J. L. Yagüe, K. K. Gleason. *Soft Matter* **2012**, *8*, 2890-2894.
[90] G. Ozaydin-Ince, K. K. Gleason, M. C. Demirel. *Soft Matter* **2011**, *7*, 638-643.
[91] Anna Maria Coclite. Smart surfaces by initiated chemical vapor deposition. *Surface Innovations* 2013. Available at: http://www.icevirtuallibrary.com/content/article/10.1680/si.12.00019.
[92] S. H. Baxamusa, L. Montero, J. M. Dubach, H. A. Clark, S. Borros, K. K. Gleason. *Biomacromolecules* **2008**, *9*, 2857-2862.
[93] Laura Montero, Gemma Gabriel, Anton Guimerà, Rosa Villa, Karen K. Gleason, Salvador Borrós. *Vacuum* **2012**, *86*, 2102- 2104.
[94] G. Ozaydin-Ince, J. M. Dubach, K. K. Gleason, H. A. Clark. *P Natl Acad Sci USA* **2011**, *108*, 2656-2661.
[95] S. H. Baxamusa, K. K. Gleason. *Adv Funct Mater* **2009**, *19*, 3489-3496.

[96] P. D. Haller, C. A. Flowers, M. Gupta. *Soft Matter* **2011**, *7*, 2428-2432.
[97] L. Montero, S. H. Baxamusa, S. Borros, K. K. Gleason. *Chem Mater* **2009**, *21*, 399-403.
[98] Salmaan H. Baxamusa, Karen K. Gleason. *Adv. Funct. Mat.* **2009**, *19*, 3489-3496.
[99] Gozde Ozaydin-Ince, Asif Matin, Z Khan, Karen K. Gleason. *unpublished* **2010**.
[100] Rong Yang, Jingjing Xu, Gozde Ozaydin-Ince, Sze Yinn Wong, Karen K. Gleason. *Chem. Mater.* **2011**, *23*, 1263-1272.
[101] Rong Yang, Karen K. Gleason. *Langmuir* **2012**, *28*, 12266-12274.
[102] Ranjita K. Bose, Siamak Nejati, David R. Stufflet, Kenneth K. S. Lau. *Macromolecules* **2012**, *45*, 6915-6922.
[103] Mahriah E. Alf, T. Alan Hatton, Karen K. Gleason. *Polymer* **2011**, *52*, 4429-4434.
[104] Mahriah E. Alf, T. Alan Hatton, Karen K. Gleason. *Langmuir* **2011**, *27*, 10691-10698.
[105] Mahriah E. Alf, T. Alan Hatton, Karen K. Gleason. *Thin Solid Films* **2011**, *519*, 4412-4414.
[106] Mahriah E. Alf, Paul D. Godfrin, T. Alan Hatton, Karen K. Gleason. *Macromolecular Rapid Communications* **2010**, *31*, 2166-2172.
[107] Anthony J Kinloch. *Adhesion and adhesives: science and technology*: Springer; **1987**.
[108] E. M. Liston, L. Martinu, M. R. Wertheimer. *J Adhes Sci Technol* **1993**, *7*, 1091-1127.
[109] N. J. Trujillo, S. H. Baxamusa, K. K. Gleason. *Chem Mater* **2009**, *21*, 742-750.
[110] J. Yin, J. L. Yague, D. Eggenspieler, K. K. Gleason, M. C. Boyce. *Advanced Materials* **2012**, *24*, 5441-5446.
[111] William J. Arora, W. E. Tenhaeff, Karen K. Gleason, G. Barbastathis. *Microelectromechanical Systems, Journal of* **2009**, *18*, 97-102.
[112] Gozde Ozaydin-Ince, Karen K. Gleason. *J. Vac. Sci. Technol., A* **2009**, *27*, 1135-1143.
[113] Rong Yang, Tonio Buonassisi, Karen K. Gleason. *Advanced Materials* **2013**, n/a-n/a.
[114] Sung Gap Im, Ki Wan Bong, Chia-Hua Lee, Patrick S. Doyle, Karen K. Gleason. *Lab on a Chip* **2009**, *9*, 411-416.
[115] Ki Wan Bong, Jingjing Xu, Jong-Ho Kim, Stephen C. Chapin, Michael S. Strano, Karen K. Gleason, Patrick S. Doyle. *Nat. Commun,* **2012**, *3*.
[116] Y. Mao, K. K. Gleason. *Langmuir* **2006**, *22*, 1795-1799.
[117] Yu Mao, Nelson M. Felix, Peter T. Nguyen, Christopher K. Ober, Karen K. Gleason. *Journal of Vacuum Science & Technology B: Microelectronics and Nanometer Structures* **2004**, *22*, 2473-2478.
[118] Shinya Yoshida, Tatsuya Kobayashi, Masafumi Kumano, Masayoshi Esashi. *Journal of Micro/Nanolithography, MEMS, and MOEMS* **2012**, *11*, 023001-023001.
[119] Christy D. Petruczok, Karen K. Gleason. *Advanced Materials* **2012**, *24*, 6445-6450.
[120] Salmaan H. Baxamusa, Laura Montero, Salvador Borrós, Karen K. Gleason. *Macromolecular Rapid Communications* **2010**, *31*, 735-739.
[121] Sung Gap Im, Ki Wan Bong, Byeong-Su Kim, Salmaan H. Baxamusa, Paula T. Hammond, Patrick S. Doyle, Karen K. Gleason. *Journal of the American Chemical Society* **2008**, *130*, 14424-14425.
[122] Benny Chen, Scott Seidel, Hiroki Hori, Malancha Gupta. *ACS Applied Materials & Interfaces* **2011**, *3*, 4201-4205.
[123] P. Kwong, M. Gupta. *Analytical Chemistry* **2012**, *84*, 10129-10135.
[124] Wyatt E. Tenhaeff, Karen K. Gleason. *Chemistry of Materials* **2009**, *21*, 4323-4331.
[125] K. K. S. Lau, Y. Mao, H. G. P. Lewis, S. K. Murthy, B. D. Olsen, L. S. Loo, K. K. Gleason. *Thin Solid Films* **2006**, *501*, 211-215.
[126] J. J. Xu, K. K. Gleason. *Acs Applied Materials & Interfaces* **2011**, *3*, 2410-2416.
[127] C. A. Pfluger, B. J. McMahon, R. L. Carrier, D. D. Burkey. *Tissue Eng Pt A* **2013**, *19*, 649-656.

[128] M. M. Hassan, J. R. McLaughlin. *Acs Applied Materials & Interfaces* **2013**, *5*, 1548-1555.
[129] A. Asatekin, K. K. Gleason. *Nano Letters* **2011**, *11* 677-686.
[130] A. M. Coclite, K. K. Gleason. *J Appl Phys* **2012**, *111*.
[131] M. Karaman, N. Cabuk, D. Ozyurt, O. Koysuren. *Applied Surface Science* **2012**, *259*, 542-546.
[132] C. H. Choi, J. Lee, K. Yoon, A. Tripathi, H. A. Stone, D. A. Weitz, C. S. Lee. *Angewandte Chemie-International Edition* **2010**, *49*, 7748-7752.
[133] L. L. Lazarus, C. T. Riche, B. C. Marin, M. Gupta, N. Malmstadt, R. L. Brutchey. *Acs Applied Materials & Interfaces* **2012**, *4*, 3077-3083.
[134] Jae-Min Jeong, Myung Seok Oh, Bong Jun Kim, Chang-Hyung Choi, Bora Lee, Chang-Soo Lee, Sung Gap Im. *Langmuir* **2013**, *29*, 3474–3481.
[135] P. Kwong, C. A. Flowers, M. Gupta. *Langmuir* **2011**, *27*, 10634-10641.
[136] S. Nejati, K. K. S. Lau. *Nano Letters* **2011**, *11*, 419-423.
[137] S. Nejati, K. K. S. Lau. *Thin Solid Films* **2011**, *519*, 4551-4554.
[138] K. K. S. Lau, K. K. Gleason. *Advanced Materials* **2006**, *18*, 1972-1975.
[139] P. D. Haller, R. J. Frank-Finney, M. Gupta. *Macromolecules* **2011**, *44*, 2653-2659.
[140] R. J. Frank-Finney, P. D. Haller, M. Gupta. *Macromolecules* **2012**, *45*, 165-170.
[141] L. C. Bradley, M. Gupta. *Langmuir* **2012**, *28*, 10276-10280.
[142] B. Gates, Y. D. Yin, Y. N. Xia. *Chemistry of Materials* **1999**, *11*, 2827-2836.
[143] B. Lange, F. Fleischhaker, R. Zentel. *Macromolecular Rapid Communications* **2007**, *28*, 1291-1311.
[144] J. Y. Wang, Y. Cao, Y. Feng, F. Yin, J. P. Gao. *Advanced Materials* **2007**, *19*, 3865-3871.
[145] K. K. S. Lau, K. K. Gleason. *Macromol Biosci* **2007**, *7*, 429-434.
[146] K. K. S. Lau, K. K. Gleason. *Thin Solid Films* **2008**, *516*, 678-680.
[147] S. J. P. McInnes, E. J. Szili, S. A. Al-Bataineh, J. J. Xu, M. E. Alf, K. K. Gleason, R. D. Short, N. H. Voelcker. *Acs Applied Materials & Interfaces* **2012**, *4*, 3566-3574.
[148] K. S. Anseth, C. N. Bowman, L. BrannonPeppas. *Biomaterials* **1996**, *17*, 1647-1657.
[149] S. X. Lu, K. S. Anseth. *Journal of Controlled Release* **1999**, *57*, 291-300.
[150] T. T. Yu, M. S. Shoichet. *Biomaterials* **2005**, *26*, 1507-1514.
[151] S. H. Baxamusa, L. Montero, S. Borros, K. K. Gleason. *Macromolecular Rapid Communications* **2010**, *31*, 735-739.
[152] M. Karaman, N. Cabuk. *Thin Solid Films* **2012**, *520*, 6484-6488.
[153] S. J. P. McInnes, E. J. Szili, S. A. Al-Bataineh, J. Xu, M. E. Alf, K. K. Gleason, R. D. Short, N. H. Voelcker. *ACS Appl. Mater. Interfaces* **2012**, *4* 3566–3574.
[154] K. K S Lau, K. K Gleason. *Advanced Materials* **2006**, *18*, 1972-1977.
[155] Kenneth K. S. Lau, Karen K. Gleason. *Surface and Coatings Technology* **2007**, *201*, 9189-9194.
[156] Steven J. P. McInnes, Endre J. Szili, Sameer A. Al-Bataineh, Jingjing Xu, Mahriah E. Alf, Karen K. Gleason, Robert D. Short, Nicolas H. Voelcker. *ACS Applied Materials & Interfaces* **2012**, *4*, 3566-3574.
[157] Ranjita K. Bose, Alex M. Heming, Kenneth K. S. Lau. *Macromolecular Rapid Communications* **2012**, *33*, 1375-1380.
[158] Mustafa Karaman, Steven E. Kooi, Karen K. Gleason. *Chem Mater* **2008**, *20*, 2262-2267.
[159] John P. Lock, Edward Geraghty, Lawino C. Kagumba, Ken K. Mahmud. *Thin Solid Films* **2009**, *517*, 3584-3587.
[160] A. M. Coclite, Y. J. Shi, K. K. Gleason. *Adv Funct Mater* **2012**, *22*, 2167-2176.
[161] M. Gupta, K. K. Gleason. *Langmuir* **2006**, *22*, 10047-10052.

[162] Anna Maria Coclite, Peter Lund, Rosa Di Mundo, Fabio Palumbo. *Polymer* **2013**, *54*, 24-30.
[163] M. Gupta, V. Kapur, N. M. Pinkerton, K. K. Gleason. *Chem Mater* **2008**, *20*, 1646-1651.
[164] M. L. Ma, M. Gupta, Z. Li, L. Zhai, K. K. Gleason, R. E. Cohen, M. F. Rubner, G. C. Rutledge. *Advanced Materials* **2007**, *19*, 255-+.
[165] Jae-Min Jeong, Myung Seok Oh, Bong Jun Kim, Chang-Hyung Choi, Bora Lee, Chang-Soo Lee, Sung Gap Im. *Langmuir* **2013**, *29*, 3474-3481.
[166] Vivek Raghunathan, Jose Luis Yagüe, Jingjing Xu, Jurgen Michel, Karen K. Gleason, Lionel C. Kimerling. *Opt. Express* **2012**, *20*, 20808-20813.
[167] A. M. Coclite, Y. Shi, K. K. Gleason. *Adv Mater* **2012**, *24*, 4534-4539.
[168] K. K. S. Lau, H. G. P. Lewis, S. J. Limb, M. C. Kwan, K. K. Gleason. *Thin Solid Films* **2001**, *395*, 288-291.
[169] H. G. P. Lewis, N. P. Bansal, A. J. White, E. S. Handy. *Thin Solid Films* **2009**, *517*, 3551-3554.
[170] K. K. S. Lau, S. K. Murthy, H. G. P. Lewis, J. A. Caulfield, K. K. Gleason. *J Fluorine Chem* **2003**, *122*, 93-96.
[171] B. A. Cruden, K. K. Gleason, H. H. Sawin. *J Phys D Appl Phys* **2002**, *35*, 480-486.
[172] K. K. S. Lau, K. K. Gleason, B. L. Trout. *J Chem Phys* **2000**, *113*, 4103-4108.
[173] K. K. S. Lau, K. K. Gleason. *J Fluorine Chem* **2000**, *104*, 119-126.
[174] K. K. S. Lau, J. Bico, K. B. K. Teo, M. Chhowalla, G. A. J. Amaratunga, W. I. Milne, G. H. McKinley, K. K. Gleason. *Nano Letters* **2003**, *3*, 1701-1705.
[175] S. J. Limb, C. B. Labelle, K. K. Gleason, D. J. Edell, E. F. Gleason. *Appl Phys Lett* **1996**, *68*, 2810-2812.
[176] R. Sreenivasan, K. K. Gleason. *Chem Vapor Depos* **2009**, *15*, 77-90.
[177] H. Y. Chen, J. Lahann. *Langmuir* **2011**, *27*, 34-48.
[178] Sreeram Vaddiraju, Kris Seneca, Karen K. Gleason. *Adv Funct Mater* **2008**, *18*, 1929-1938.
[179] M. C. Barr, J. A. Rowehl, R. R. Lunt, J. J. Xu, A. N. Wang, C. M. Boyce, S. G. Im, V. Bulovic, K. K. Gleason. *Advanced Materials* **2010**, *23*, 3500-+.
[180] Dhiman Bhattacharyya, Karen K. Gleason. *Journal of Materials Chemistry* **2012**, *22*, 405-410.
[181] N. Mari-Buye, S. O'Shaughnessy, C. Colominas, C. E. Semino, K. K. Gleason, S. Borros. *Adv Funct Mater* **2009**, *19*, 1276-1286.
[182] Jie Yin, Jose Luis Yagüe, Damien Eggenspieler, Karen K. Gleason, Mary C. Boyce. *Advanced Materials* **2012**, *24*, 5441-5446.
[183] C. D. Petruczok, K. K. Gleason. *Adv Mater* **2012**, *24*, 6445-6450.
[184] Christy D. Petruczok, Hyungryul J. Choi, Se Young Yang, Ayse Asatekin, Karen K. Gleason, George Barbastathis. *Journal of Microelectromechanical Systems* **2012**, *PP*, 1-8.
[185] S. G. Im, K. W. Bong, B. S. Kim, S. H. Baxamusa, P. T. Hammond, P. S. Doyle, K. K. Gleason. *J Am Chem Soc* **2008**, *130*, 14424-+.
[186] G. Ozaydin-Ince, J. M. Dubach, K. K. Gleason, H. A. Clark. *PNAS* **2011**, *108*, 2656-2661.
[187] H. Tekin, G. Ozaydin-Ince, T. Tsinman, K. K. Gleason, R. Langer, A. Khademhosseini, M. C. Demirel. *Langmuir* **2011**, *27*, 5671-5679.
[188] R. Bakker, P. Weijers, C. H. M. van der Werf, J. K. Rath, R. E. I. Schropp. *Physica Status Solidi a-Applications and Materials Science* **2010**, *207*, 647-650.

Figure captions

Figure 1. (a) Reactor configuration for oxidative chemical vapor deposition (oCVD). Evaporated oxidant and vapor-phase monomer(s) adsorb onto a cooled substrate and step growth polymerization occurs. (b) Initiated chemical vapor deposition (iCVD) process. Vapor-phase vinyl monomer(s) and thermally labile initiator flow through an array of heated filaments. The initiator is decomposed into radicals; these radicals and the monomer(s) adsorb on a cooled substrate and film growth occurs via free radical polymerization.

Figure 2. Images of oCVD PEDOT along the top are compared with those of spin-cast PEDOT:PSS along the bottom. On graphene (a,b), the optical micrographs and the inset photographs, show that the dewetting defects present in PEDOT:PSS are absent in the oCVD coating. On imprinted PMMA features, the scanning electron micrographs show complete infilling of by oCVD whiles voids are left by spin-casting (c,d), and constant thickness of the conformal coating by oCVD as opposed to the variation in coating thickness observed for PEDOT:PSS (e,f). On poly (acrylonitrile) fiber mats, the conformal oCVD film, encases each fiber, while dewetting of the PEDOT:PSS forms agglomates (g,h). Photographs show the oCVD coating is uniform over rice paper, while spin-coating damages this substrate. Reproduced with permission from a- b) [26], c-f) [37], g-h) [178], i-j) [15]. a-b) Copyright 2012, American Chemical Society. c-f) Copyright 2013. g-h) Copyright 2008, John Wiley and Sons. i-j) Copyright 2011, John Wiley and Sons.

Figure 3. Patterning and grafting of oCVD PEDOT: (a) grafting to silicon enables the successful formation of interdigitated electrodes whereas delamination of the pattern's features occurs without grafting; (b) patterns achieved by lift-off and utilizing in situ grafting to PET; (c) grafted patterns on PET remain adherent with flexing; (d) grafting enables successful colloidal lithography;(e) Grafting produces a (100) x-ray diffraction peak in oCVD PEDOT grown on Si(100) (black), in addition to the (010) peak seen without grafting. Reproduced with permission from a-c) [19], d) [179], e) [31]. a,b,c) Copyright 2007, John Wiley and Sons. d) Copyright 2011, John Wiley and Sons. e) Copyright 2010, Royal Society of Chemistry.

Figure 4. (a) The tunability of work function of oCVD PEDOT as a function of deposition temperature. (b) Optical transmittance, T, at λ=550 nm, versus sheet resistance (R_{sh}) of oCVD PEDOT, showing the trade-off between these two most important characteristics for transparent electrode applications. A fit curve (red line) gives σ_{dc}/σ_{op}=9 of oCVD PEDOT and for reference, current standard metal oxide with σ_{dc}/σ_{op}=35 is provided as the black dashed line. The bottom inset shows a decrease in sheet resistance with increasing the film thickness of oCVD PEDOT. The top inset shows successful vapor printing of PEDOT at 15 point with Verdana bold on tissue paper. (c) An electrochromic device in which patterned oCVD PEDOT switches from the light/oxidized state (top) to the dark/reduced state (bottom). Reproduced with permission from a) [32], b) [179], c) [34]. a) Copyright 2007, American Institute of Physics. b) Copyright 2011, John Wiley and Sons. c) Copyright 2007, Elsevier.

Figure 5. (a) Schematic of conventional bottom-illuminated OPV structure where oCVD PEDOT anode deposition is the first step (top). The resulting devices on PET subtrates present no significant degradation in performance with repeated 5 nm-radius flexes (bottom). (b) Schematic of top-illuminated device in which deposition of the oCVD PEDOT is the final step (top). Prototype of this structure on a postage stamp, representing a rough opaque substrate. The power conversion efficiency was 2.0 % (bottom). (c) Facile monolithic integration of OPV cells for rapid production of devices independent of substrate: fabrication schematic of 250-cell arrays on paper using vapor printing oCVD PEDOT (top), the printed PEDOT anode pattern (bottom left) and a complete solar cell array on a 7 cm x 7 cm square of tracing paper capable of >50 V output (bottom right). (d) Folding of oCVD PEDOT coated subtrates into a variety of non-planar geometries (top). Increased absorption with the decreasing hinge angle of OPV half-cells fabricated using oCVD PEDOT is promising for the

improved areal output power density (bottom). Reproduced with permission from a,c)[179], b) [35], d) [37]. a) Copyright 2011, John Wiley and Sons. b) Copyright 2012, John Wiley and Sons. c) Copyright 2013, Unpublished

Figure 6. (a) oCVD unsubstituted polythiophene (PT). (left) During the oCVD process, the polymer is overoxidized which results in a doped, conductive film. Dedoping the film with some reducing agent, such as methanol, results in a neutral polymer film. (middle) The absorption spectra of the doped (blue) film shows characteristic bipolaron peaks, whereas the semiconducting (red) film shows a characteristic π- π^* transition peak. (right) Bilayer heterojunction organic photovoltaic devices fabricated with oCVD PT and C_{60} demonstrated power conversion efficiencies up to 0.8%. The inset figure shows the absorption spectra of oCVD PT and C_{60}. (b) Polyisothianaphthene films prepared by oCVD at various temperatures. Controlling the temperature of deposition is shown to control the resulting polymer properties. (c) oCVD polyselenophene films on paper substrates demonstrating the ability to easily pattern the oCVD polymer and the ability to conformally coat rough substrates. (d) Copolymers of EDOT and 3-thiopheneethanol (3TE) deposited by oCVD. (middle) Electrospun fiber mats with fluorescently labeled avidin (green) attached to –OH functional groups of conformal oCVD poly(EDOT-co-3TE). Attached to the avidin are biotin labeled with red quantum dots. (right) Response of avidin/poly(EDOT-co-3TE) on electrospun mat exposed to biotin solutions of 5 nM (blue), 50 nM (purple), 500 nM (green), and 5 μM (red) concentrations. Reproduced with permission from a) [41], b) [42], c)[180] , d) [46]. a) Copyright 2012, Elsevier. b) Copyright 2013, Unpublished. c) Copyright 2012, Royal Society of Chemistry. d) Copyright 2011, John Wiley and Sons.

Figure 7 Kinetic studies on the iCVD process. (a) Quartz microbalance measurement of the adsorbed volume and calculated areal concentration as a function of the P_M/P_{sat} (b) Arrhenius plot of the deposition rate of p(EGDA) as a function of the inverse of the gas temperature. At low filament temperature, the apparent activation energy (166 kJ/mol) has been calculated from the slope of the linear regression of the data. (c) FT-IR and C 1s XPS spectra of the PVP deposited by iCVD and the standard commercial polymer. The iCVD polymer is nearly spectroscopically identical to the commercial one. Reproduced with permission from a) [51], b) [58], c) [59]. a) Copyright 2006, American Chemical Society. b) Copyright 2009, American Vacuum Society. c) Copyright 2006, American Chemical Society.

Figure 8 Robust cross-linked networks can be easily synthesized by iCVD. (a) Electrical resistance of poly(V3D3) over 1000 days, applying constant bias. Due to the high durability of this coating, the electrical resistance remains constant. (b) Cross-linked network of maleic anhydride and aminostyrene copolymer. The latter is another example of hard and cross-linked polymer network. iCVD allows also to functionalize hydrogels with one-step polymerization. (c) pentafluorophenylmethacrylate (PFM) was copolymerized for the top 10 nm with HEMA. The resulting graded copolymer gave a platform for surface functionalization with peptides which enhanced cell attachment and growth on the surface. In the middle, HUVEC morphology at 2 h of incubation. On the left, ToF-SIMS depth profile showing the signal at m/z= 253.1, corresponding to a positively charged PFM fragment, as a function of film depth for both the homogeneous and graded copolymer. Reproduced with permission from a)[77], b)[88], c)[97, 181]. a) Copyright 2007, American Chemical Society. b) Copyright 2012, Wiley. c) Copyright 2009, American Chemical Society and Wiley.

Figure 9 iCVD surfaces for controlled interaction with protein and/or other bio-molecules and microorganisms. (a) Structure and protein adsorption of antifouling iCVD p(HEMA-co-PFDA) with various compositions. Model fitting indicates that each local heterogeneous unit that interrupts protein adsorption compasses 4-5 repeat unites. (b) iCVD PEO coatings are patterned on silicon wafer and subject to adsorption tests from fluorescently labeled bovine serum albumin (BSA); coated areas resist protein attachment effectively. (c) Structure and

XPS high resolution N(1s) scan of antifouling iCVD polysulfobetaine film at the information depth of 3 nm. The major peak near 402 eV represents quaternary ammonium, indicating high surface concentration of zwitterions. (d) Static water contact angle on multi-walled carbon nanotubes coated with iCVD PNIPAAm films below (left) and above (right) the LCST. The mass and viscoelasticity display a step change near the LCST as revealed by QCM-D; above the LCST, absorbed water is expulsed from the polymer layer, which reduces the mass and the viscoelasticity. Reproduced with permission from a)[95], b) [102], c) [101], d) [106]. a) Copyright 2009, Wiley. b) Copyright 2012, American Chemical Society. c) Copyright 2012, American Chemical Society. d) Copyright 2010, Wiley

Figure 10. (a) SEM and FEM image of a non-equi-biaxially stretched PDMS sample upon sequential release. Adjusting the pre-stretch on the *x*- and *y*-axis and carrying out a sequential release enables to obtain a herringbone pattern and tune the features (wavelength, amplitude, jog angle) of the wrinkled pattern. (b) SEM and FEM image of an equi-biaxially stretched PDMS sample upon simultaneous release. The experimental conditions carried out during the release/re-stretch process results in a disordered pattern. (c) Optical 3-D profilometer image of a herringbone pattern. Reproduced with permission from a-d) [182] Copyright 2012, Wiley.

Figure 11. iCVD enables effective *in situ* grafting of deposited polymer on various substrates (right column), which enhanced the performance and durability compared to non-grafted coatings (left column). (a) Without maleic anhydride (MA) grafting, antifouling iCVD zwitterionic coatings delaminates from the membrane substrate when placed in water; while with the MA grafting, the iCVD coating, as indicated by white dots, cannot be easily differentiated from the membrane substrate, indicating good adhesion. (b) *Tert*-butyl peroxide (TBPO) grafting enables the formation of silicon-carbon bond and the covalent attachment of polymer coatings directly to silicon substrates. The delamination events observed for non-grated coating are thus prevented. Scale bars represent 1μm. (c) Non-grafted iCVD coating on silicon substrate does not stand up to nano-scratching tests, and spalling of the films are observed under optical microscope, which does not exist for the TBPO-grafted coatings. Scale bars represent 7μm. Reproduced with permission from a)[101], b-c)[113]. a) Copyright 2012, American Chemical Society. b-c) Copyright 2013, Wiley.

Figure 12. (a) Positive-tone features patterned in a polyacrylic iCVD thin film using electron-beam lithography. (b) 4 mm-diameter glass rod patterned by exposing diacetylene-functionalized iCVD poly(4-vinylpyridine) (P4VP) through a flexible mask. (c) iCVD P4VP features patterned using a chemically non-selective lift-off technique. (d) iCVD bifunctional surface exhibiting independent chemical and topological contrast. (e) Nanodomains of iCVD and PECVD films patterned using capillary force lithography; light and dark-colored regions contain orthogonal acetylene and amine functionalities, respectively. (f) Arrays of self-assembled microstructures created by coating elastomeric pillars with hydrophilic iCVD polymer and submerging in water. (g) Close-up of a microstructure depicted in (f); solvent bonds form between the pillars, causing them to remain assembled after the system is dried. (h) By patterning the pillar-coated substrate with regions of hydrophobic polymer, the regions of self-assembly can be controlled. Reproduced with permission from a)[116], b) [183] c) [184] d) [151] e) [185] f-h) [122]. a) Copyright 2006, American Chemical Society, b) Copyright 2012, Wiley. c) Copyright 2013, IEEE, d) Copyright 2010, Wiley. e) Copyright 2008, American Vacuum Society. f-h) Copyright 2011, American Chemical Society.

Figure 13. (a) Schematic of a paper-based microfluidic device consisting of a separation zone coated with acidic or basic iCVD polymer and a UV-responsive switch consisting of a patterned region of poly(*o*-nitrobenzyl methacrylate). (b,c,d) Separation of toluidine blue O

(cationic analyte) and ponceau S (anionic analyte) on an uncoated paper microfluidic channel (b), a channel coated with acidic iCVD poly(methacrylic acid) (c), and a channel coated with basic iCVD poly(dimethylaminoethyl methacrylate) (d). (e) Microfluidic channels coated on paper using a hydrophobic, photoresponsive iCVD polymer. The channels exhibit excellent retention of aqueous dye solutions. (f) Overlaid fluorescence micrographs of iCVD and PECVD orthogonal nanodomains. The click-functionalized red dye is excited at 545 nm and the N-hydroxysuccinimide-functionalized green dye is excited at 491 nm. (g,h) Fluorescent micrographs of an iCVD hydrogel covalently functionalized with CdSe/ZnS nanoparticles in the dry state (g) and swollen upon immersion in pH 8 buffer solution (h). Reproduced with permission from a-d) [123], e) [96], f) [185], g-h) [124]. a-d) Copyright 2012, American Chemical Society. e) Copyright 2011, Royal Society of Chemistry, f) Copyright 2008, American Chemical Society, g-h) Copyright 2009, American Chemical Society

Figure 14. (a) SEM images of PCL electrospun mats before and after conformal iCVD coating of PPFEMA (scale bars = 2 μm); (b) XPS spectra for samples shown in a); (c) Top view SEM images of PVA mold before and after iCVD coating of PGMA and PPFDA (scale bar = 30 nm). The iCVD layer conformally coated inner surfaces of the polymer mold; (d) Cross-sectional SEM images of iCVD deposited pCHMA on a trench wafer substrate; (e) Cross-sectional SEM images of TiO_2 electrodes (4 μm thick) before and after iCVD coating of PHEMA (scale bar = 100 nm), which keeps the morphology of the porous network unchanged. Reproduced with permission from a-b) [3], c) [131], d) [20], e) [137]. a-b) Copyright 2005, American Chemical Society. c) Copyright 2012 Elsevier. d) Copyright 2011, American Chemical Society. e) Copyright 2010 American Chemical Society.

Figure 15. Confocal images of the microworms filled with the optode solution in brightfield (a) and fluorescence mode (b). (c) Fluorescent images of the tissue construct with the PDMS microgroove shape. (d) SEM image of the coaxial nanotubes showing a diameter of 200 nm and a wall thickness of 60 nm. (e) SEM image of the coaxial nanotubes after exposure to the dye solution at 80 ºC. Due to the swelling of the hydrogel the diameter increases to 350 nm and the wall thickness to 100 nm. Ionic liquid (IL) marbles on a liquid bath coated on a bed of loose PTFE particles (left) and a bare Petri dish (right). Left marble is fully encapsulated and the IL is retained inside the polymer shell structure showing its characteristic yellowish color. However, in the right marble the IL leaked out as a result of a crack in the shell when removing it from the Petri dish due to the bridging effect (e). Reproduced with permission from a-b)[186], c)[187]d)[67]e)[141]. a-b) Copyright 2011, PNAS. c) Copyright 2011, American Chemical Society. d) Copyright 2011, Royal Chemical Society. e) Copyright 2012, American Chemical Society.

Figure 16. (a) SEM images of crosslink pHEMA-pEGDA nanotubes in the dehydrated (left) and swollen states (right). (b) Schematics of nanotubes in the dehydrated and swollen states, respectively. (c) Cross-sectional SEM image of iCVD PHEMA coated silica microsphere at 1600X magnification (left, scale bar = 10 μm) and 5500X magnification (right, scale bar = 2 μm). The PHEMA layer is indicated by arrows. (d) AFM image of hydrophobic depressions in a hydrophilic matrix in dry state (left) and swollen state (right). (e) Water preferentially condensing on the PHEMA coated hydrophilic region (scale bar = 20 μm). (f) pH-dependent swelling property of p(MAA-EDMA) copolymers. (g) Property of drug release from the pSi drug delivery system capped with a pH responsive iCVD film. The film becomes contractive in low pH (left) and inhibits drug release, whereas the swelling film in a higher pH (right) promotes drug release. (h) Strong hydrophilic (as shown in inset) hydrogel patterns of well-ordered PHEMA arrays grafted by iCVD process (scale bar = 1 μm). i) The SEM image of wrinkled p(HEMA-EGDA) layer coated via iCVD process with a thickness of 300 ± 10 nm. Reproduced with permission from a-b) [84], c)[92], d-e)[151], f)[145], g)[153], h)[109], i)[182]. a-b) Copyright 2010, The Royal Society of Chemistry. c) Copyright 2008, American Chemical

Society. f) Copyright 2007, Elsevier. g) Copyright 2012, American Chemical Society. h) Copyright 2009, American Chemical Society.

Figure 17. (a) Transmission electron micrograph of a titania-iCVD PHEMA Bragg mirror deposited on silicon. (b) Color change of the Bragg mirror upon exposure to water vapor. The dry, as-deposited coating appears green on a quartz window (t=0 s). Exposure to 1 mol% water vapor changes the coating color to red (t=0.3 s). The green color is recovered after purging with N_2 (t=0.6 s). (c) Titania-iCVD PHEMA Bragg mirror deposited on red paper. (d) iCVD polymer-coated microcantilever switch before (top) and after (bottom) exposure to hexylamine analyte. Deflection of the cantilever upon exposure causes the metal device components to contact, completing a circuit. (e) Micro-scale silicon trench sensor before (top) and after (bottom) exposure to nitrobenzene. The responsive iCVD P4VP layer expands during analyte exposure, connecting the Au/Pd-coated regions and decreasing the resistance measured across the device. (f) Micro-scale nitroaromatic sensor consisting of a line of responsive iCVD P4VP overlaid with a nano-scale metal line. Exposure to nitroaromatic compounds results in expansion of the polymer and deformation of the metal, changing the device resistance. (g) Doped (left) and undoped (right) films of conjugated, conducting iCVD oligomers. Silver contacts are used for conductivity measurements. Reproduced with permission from a-c) [158], d) [111], e) [10], f) [9], g) [188]. a-c) Copyright 2008, American Chemical Society, d) Copyright 2009, IEEE, e) Copyright 2010 Wiley, f) Copyright 2013, IEEE, g) Copyright 2010, Wiley.

Figure 18. iCVD p(PFDA). (a) PDMS micromold bare (left image) and coated with conformal p(PFDA) coating. Superhydrophobic coating served as barrier to avoid lateral diffusion of the chemicals through the sides of the channels. (b) Paper solar cell coated with superhydrophobic p(PFDA) and soaked into a water bath. The solar cell works also after water immersion. (c) A two-layer coating of conformal p(DVB) and p(PFDA) was used to generate hydrophobicity-based selective permeation inside the pores of a AAO membrane. (d) Plot of the contact angles (CA) of the p(PFDA) surface when wetted with drops of hydrocarbon oils with different number of carbon atoms. Two types of p(PFDA) surfaces were investigated: one with the polymer chains covalently bonded to the substrate (grafted) and the ungrafted one. The grafted polymer shows higher oleophobicity than the ungrafted. (e) Cosine of the contact angles as a function of the liquid surface energy of the oils used to wet the surface of the grafted and ungrafted p(PFDA). (f) X-ray diffraction pattern of the p(PFDA) coatings deposited at different filament temperature. When the x-ray beam is oriented at 0° with respect to the normal to the surface in the diffractometer, the pattern is visible for the sample deposited at high filament temperature. The contrary applies when the x-ray beam is oriented at 90° with respect to the normal to the surface. This is an evidence of a different chain orientation, as represented in the cartoons on the right. At high T_{fil} the chains are oriented perpendicularly, while at low T_{fil} they are leaning on the substrate surface. Reproduced with permission from a)[165], b)[179], c)[129], d-e) [167], f) [160]. a) Copyright 2013, American Chemical Society. b) Copyright 2011, Wiley. c) Copyright 2011, American Chemical Society. d-e) Copyright 2012 Wiley. f) Copyright 2012, Wiley.

Figure 19. iCVD and HWCVD PFTE. (a) Nanotube coated with conformal 40-nm-thick PFTE film. (b) Perfectly rounded-shape of a water droplet deposited on PFTE-coated nanotube forest. (c) PTFE deposited by HWCVD on paper substrate. The mild deposition conditions did not damage the paper substrate. (d) PTFE deposited on a lead wire and (f) on a MEMS test structure to show the conformality that can be achieved by HWCVD. (e) Solid-state magic angle spinning ^{19}F nuclear magnetic resonance, which shows that the HWCVD PTFE is made essentially of $-CF_2$ repeating units as the bulk Teflon. (g-i) Crystalline lamellar PTFE chains were obtained on single walled carbon nanotubes (SWCNT). Such morphology was called “shish kebab” nanohybrid. (g) SEM image of SWCNT buckypaper with a thin coating of PTFE, (h) Histogram of the diameters of the shish kebab structure (i) Schematic of

the disks arrangement on the SWCNT bundle. Reproduced with permission from: a-b) [174], c)[125], d)[175], e)[173], f)[2], g-i) [48]. a-b) Copyright 2003, American Chemical Society, c) Copyright 2006, Elsevier. d) Copyright 1996, American Institute of Physics, e) Copyright 2000, Elsevier. f) Copyright 2010, Wiley. g-i) Copyright 2012, Wiley.

Figure 20. Commercial, automated iCVD reactors systems: (a) Research tool with 0.2 m diameter vacuum chamber, (b) Batch production tool with a front opening door 1.2 width, and (c) Roll-to-roll system for coating flexible media up to 0.5 m in width.

FIGURES

Figure 1

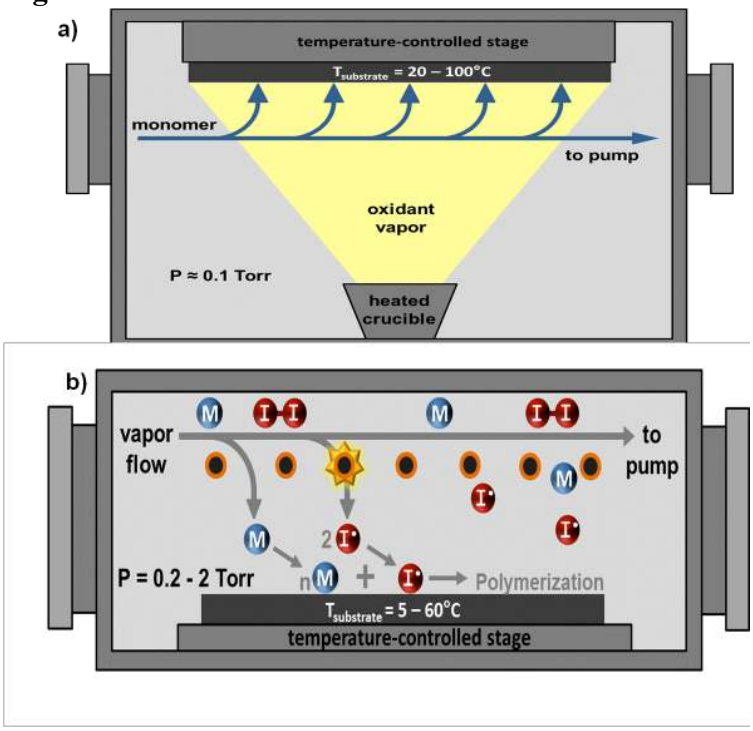

Figure 2

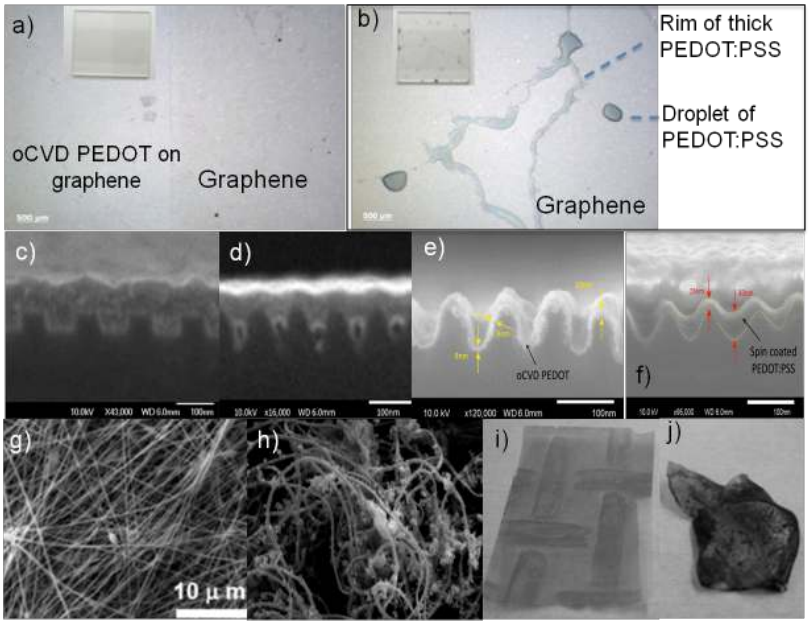
a)
oCVD PEDOT on graphene
Graphene
b)
Rim of thick PEDOT:PSS
Droplet of PEDOT:PSS
Graphene
c)
d)
e)
oCVD PEDOT
f)
Spin coated PEDOT:PSS
g)
10 µm
h)
i)
j)

Figure 3

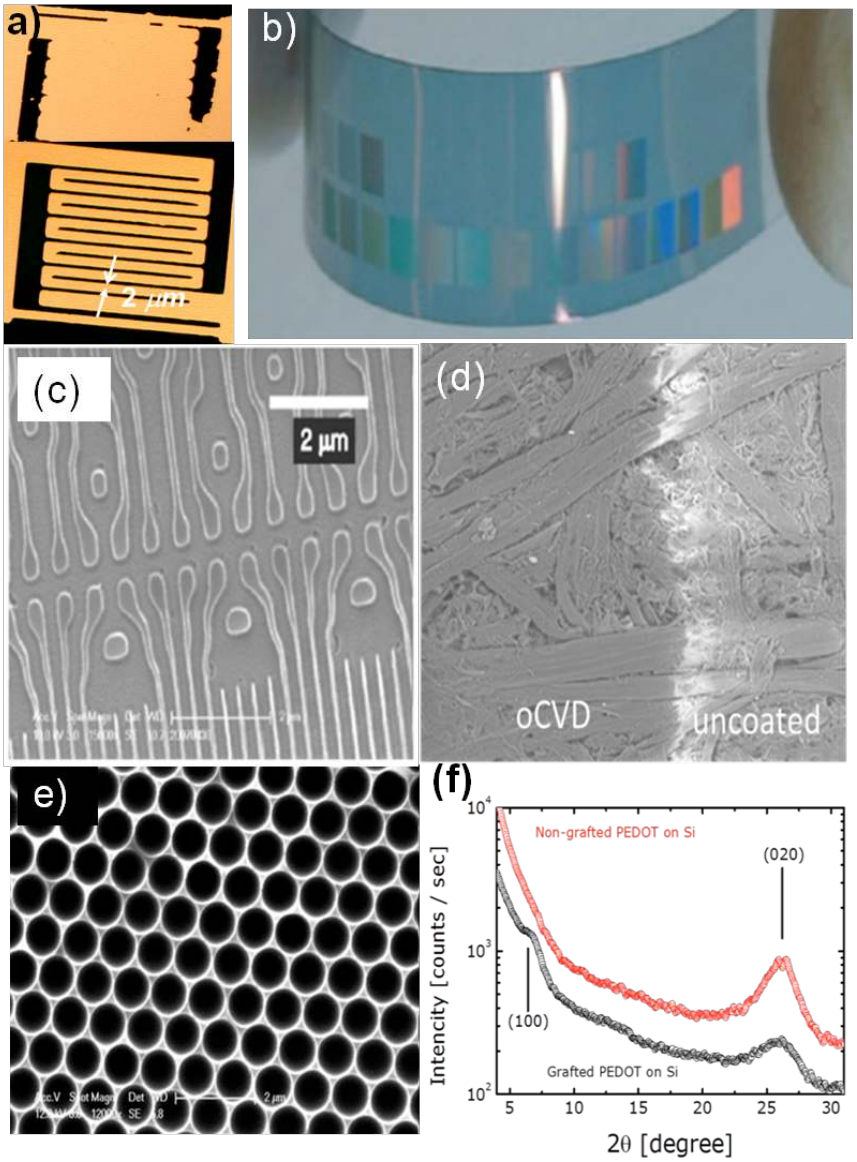
a)
2 μm
b)
(c)
2 μm
(d)
oCVD
uncoated
e)
(f)
Non-grafted PEDOT on Si
(020)
(100)
Grafted PEDOT on Si
Intencity [counts / sec]
2θ [degree]

Figure 4

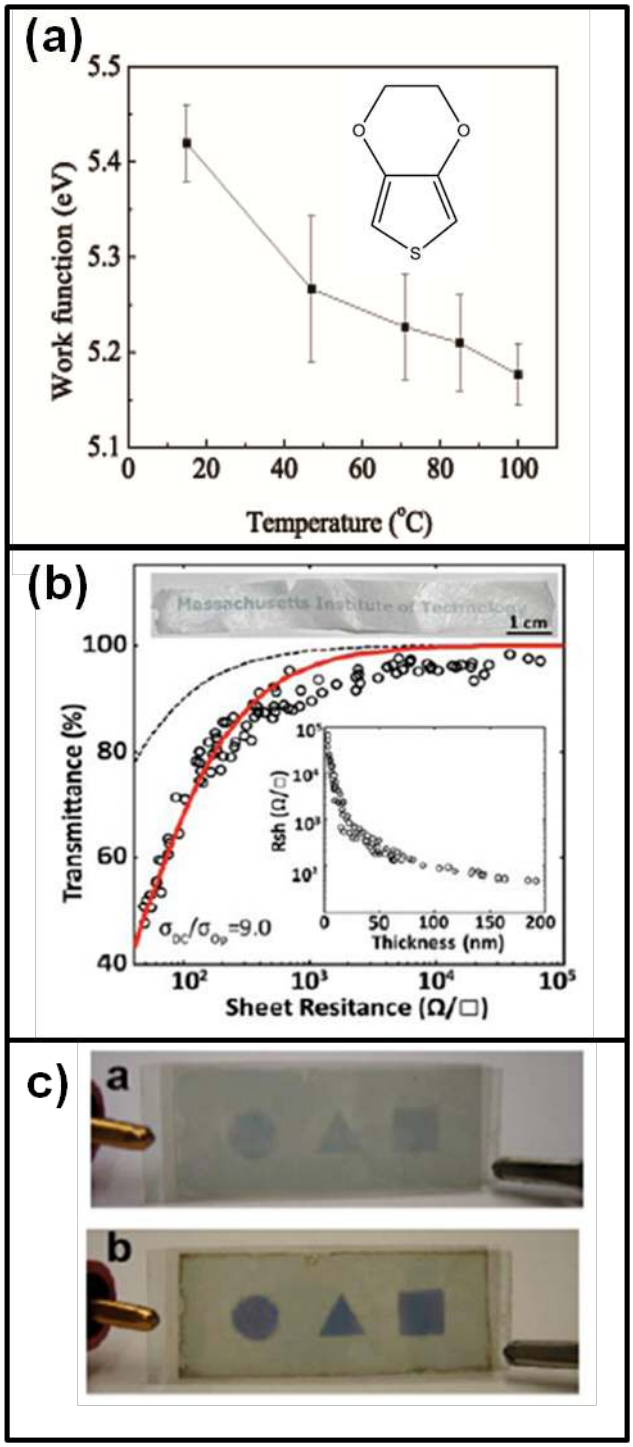
(a)
Work function (eV)
5.5
5.4
5.3
5.2
5.1
0
20
40
60
80
100
Temperature (°C)
O
O
S
(b)
Massachusetts Institute of Technology
1 cm
Transmittance (%)
100
80
60
40
10^2
10^3
10^4
10^5
Sheet Resitance (Ω/□)
σ_{DC}/σ_{Op}=9.0
Rsh (Ω/□)
10^4
10^3
10^2
0
50
100
150
200
Thickness (nm)
c)
a
b

Figure 5

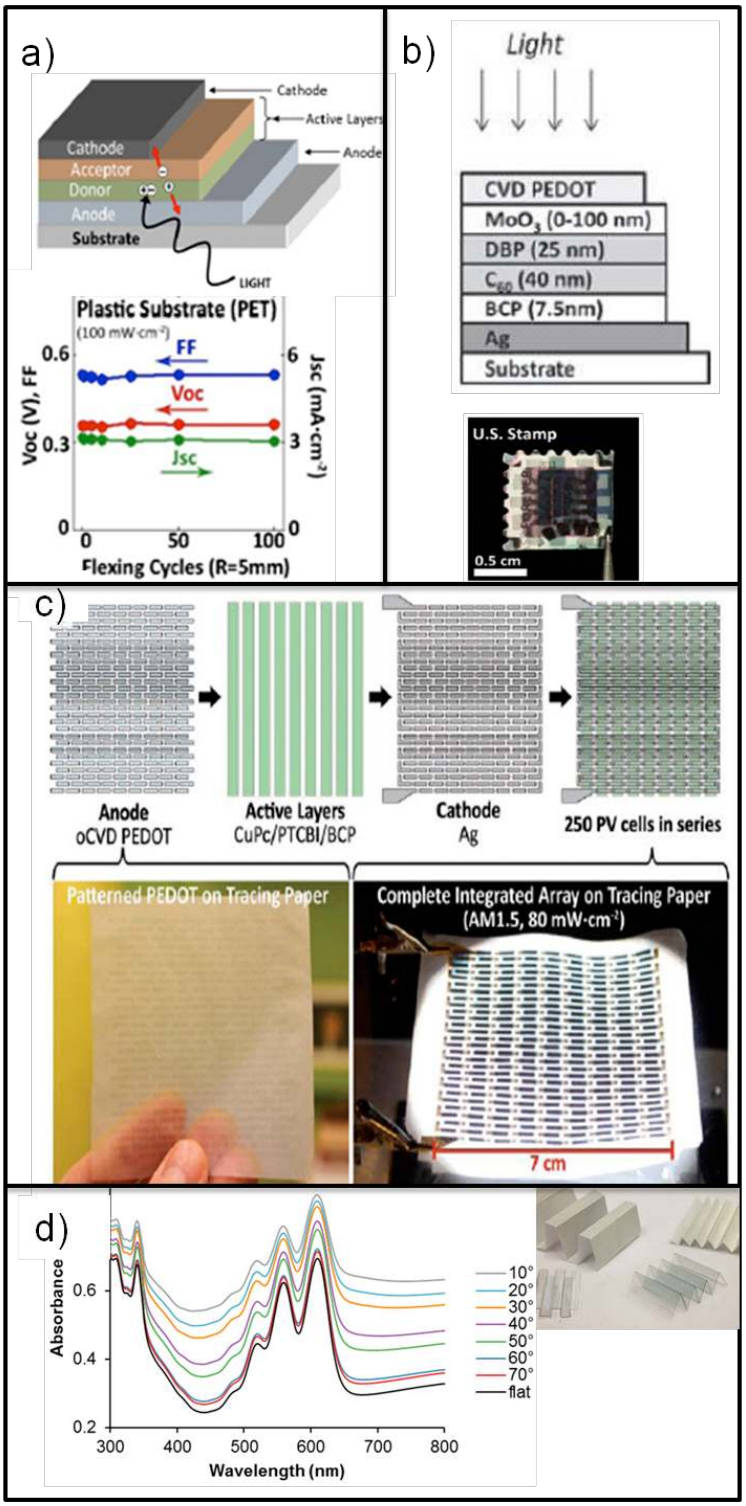
a)
Cathode
Active Layers
Anode
Cathode
Acceptor
Donor
Anode
Substrate
LIGHT
Plastic Substrate (PET)
(100 mW·cm⁻²)
FF
Voc
Jsc
Voc (V), FF
Jsc (mA·cm⁻²)
0.6
0.3
0
6
3
0
0
50
100
Flexing Cycles (R=5mm)
b)
Light
CVD PEDOT
MoO3 (0-100 nm)
DBP (25 nm)
C60 (40 nm)
BCP (7.5nm)
Ag
Substrate
U.S. Stamp
0.5 cm
c)
Anode
oCVD PEDOT
Active Layers
CuPc/PTCBI/BCP
Cathode
Ag
250 PV cells in series
Patterned PEDOT on Tracing Paper
Complete Integrated Array on Tracing Paper
(AM1.5, 80 mW·cm⁻²)
7 cm
d)
Absorbance
0.6
0.4
0.2
300
400
500
600
700
800
Wavelength (nm)
10°
20°
30°
40°
50°
60°
70°
flat

Figure 6

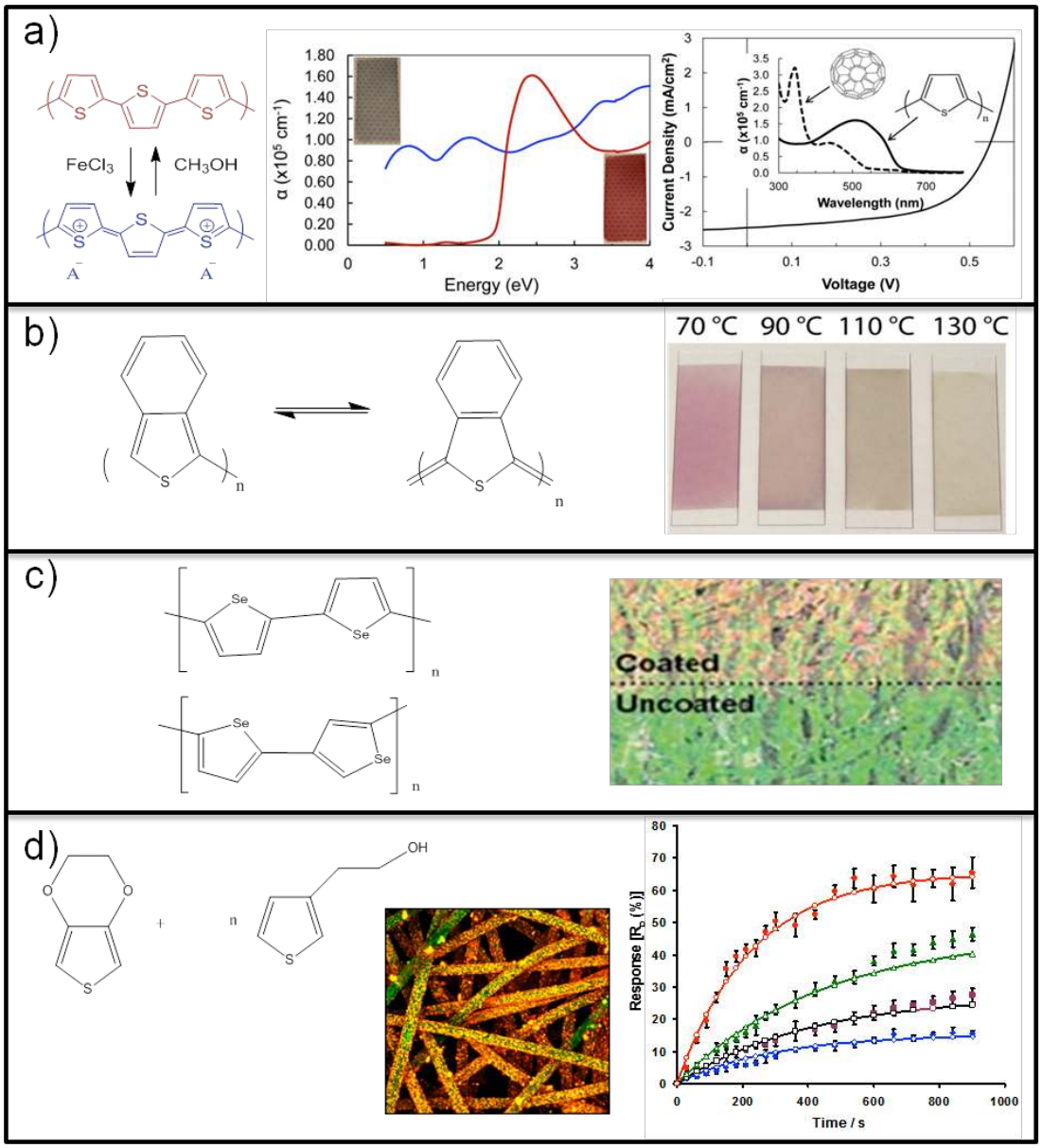
a)
FeCl3
CH3OH
A−
A−
α (x10^5 cm^-1)
Energy (eV)
Current Density (mA/cm²)
Voltage (V)
α (x10^5 cm^-1)
Wavelength (nm)
b)
70 °C
90 °C
110 °C
130 °C
c)
Coated
Uncoated
d)
OH
Response [R0 (%)]
Time / s

Figure 7

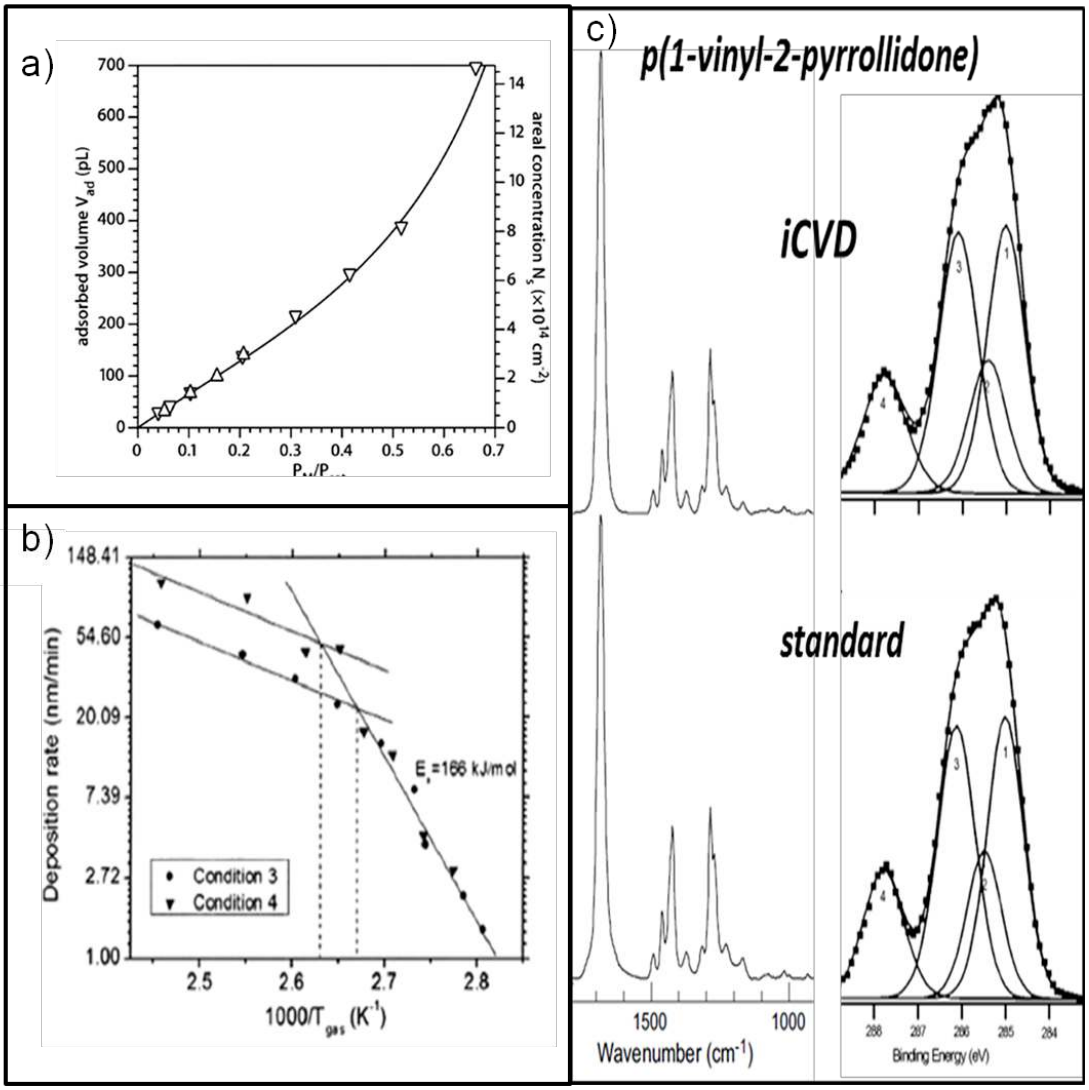
a)
adsorbed volume V_{ad} (pL)
areal concentration N_s ($\times 10^{14}$ cm^{-2})
b)
Deposition rate (nm/min)
148.41
54.60
20.09
7.39
2.72
1.00
E_a=166 kJ/mol
Condition 3
Condition 4
2.5
2.6
2.7
2.8
1000/T_{gas} (K^{-1})
c)
p(1-vinyl-2-pyrrollidone)
iCVD
standard
1500
1000
Wavenumber (cm^{-1})
288
287
286
285
284
Binding Energy (eV)

Fig 8

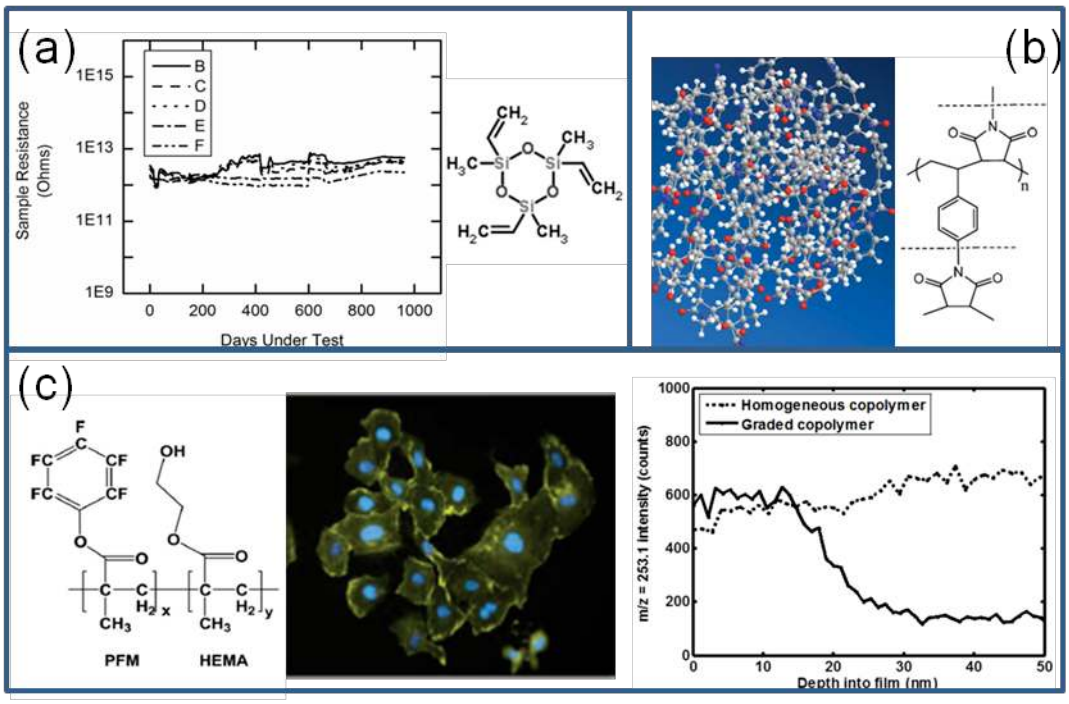

Figure 9

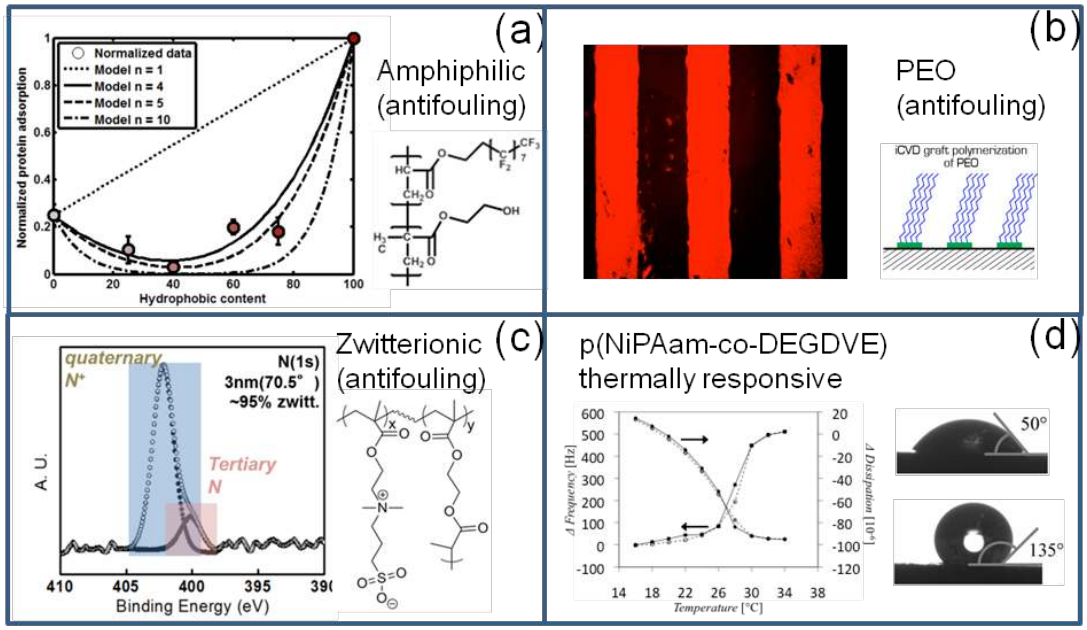

Figure 10

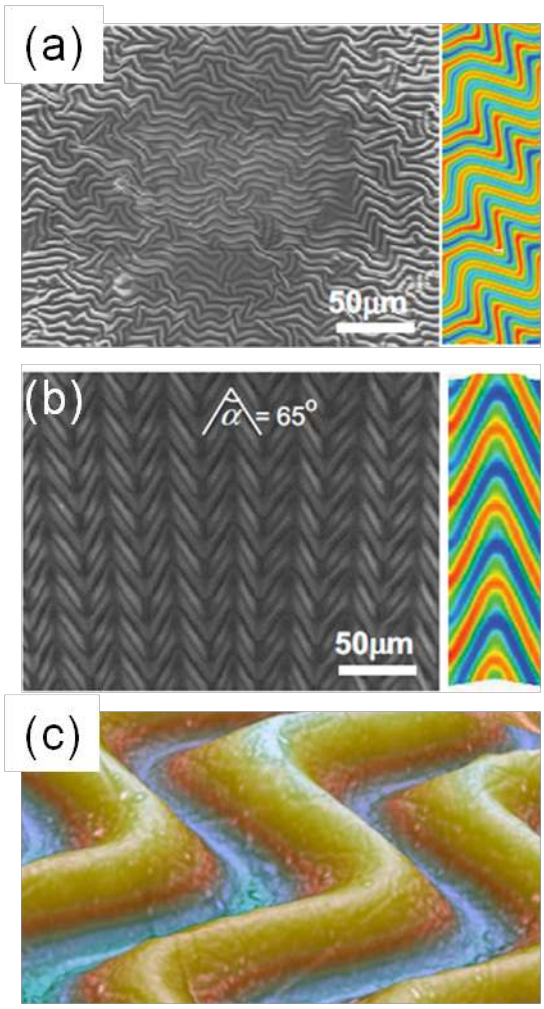

Figure 11

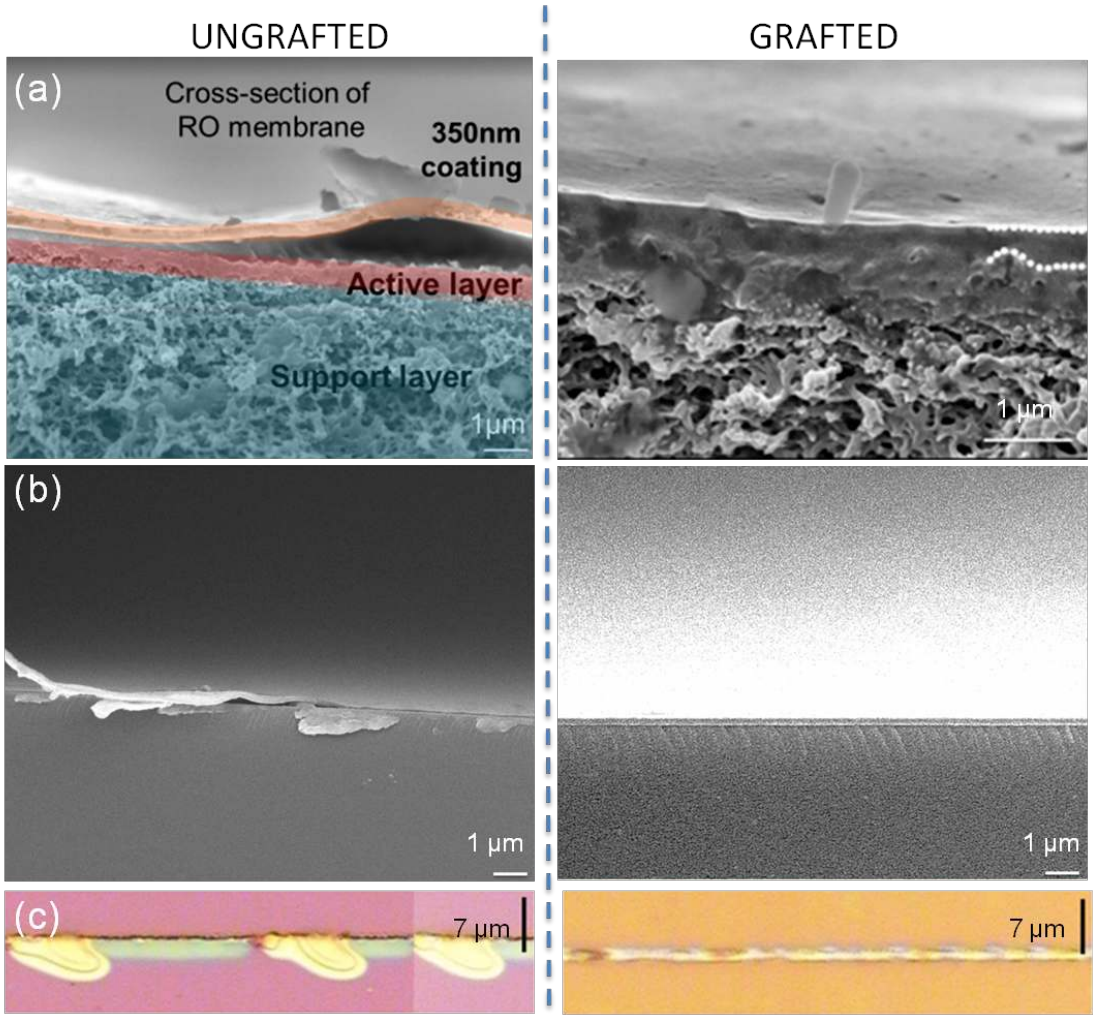
UNGRAFTED
GRAFTED
(a)
Cross-section of
RO membrane
350nm
coating
Active layer
Support layer
1μm
1 μm
(b)
1 μm
1 μm
(c)
7 μm
7 μm

Figure 12

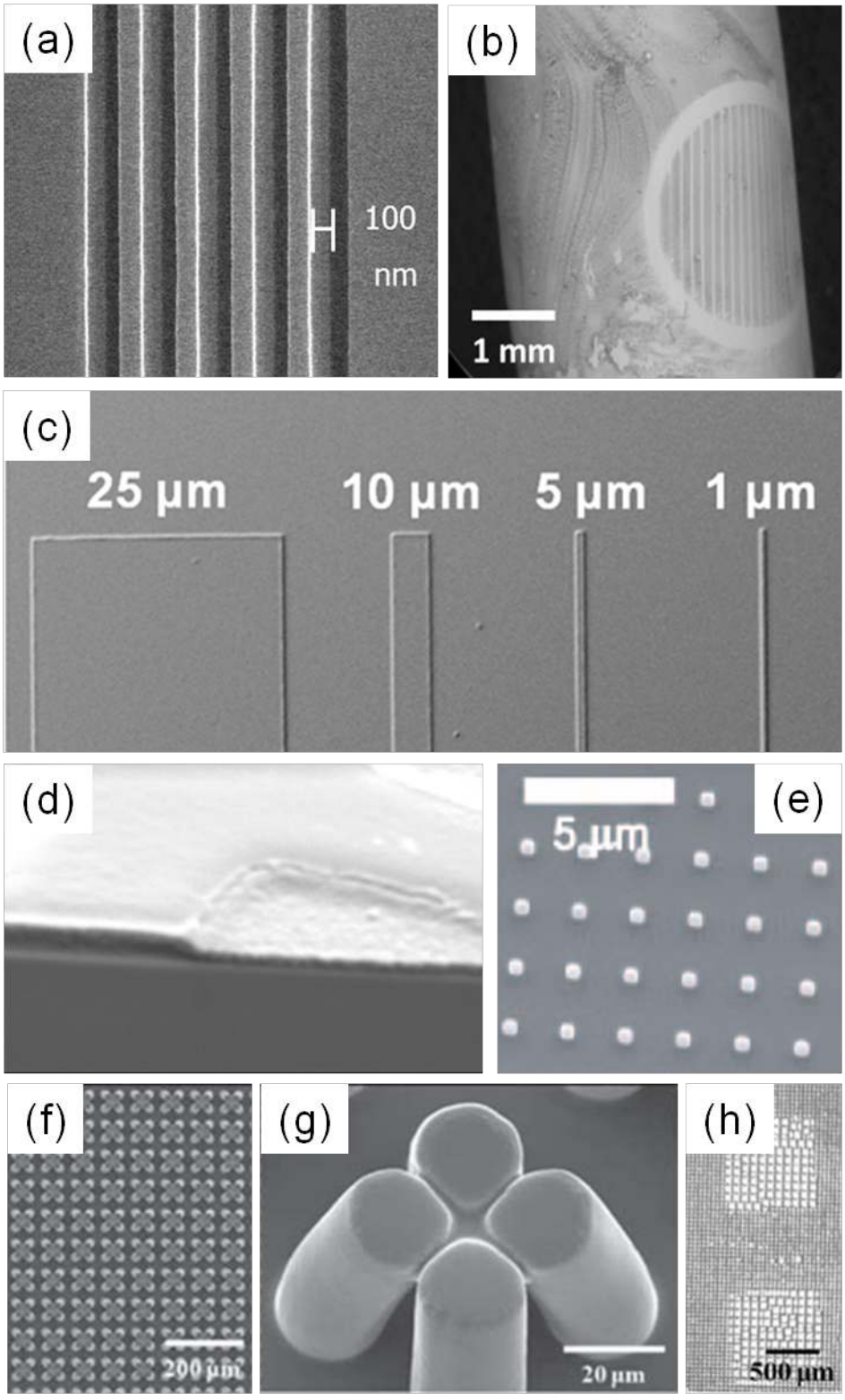

Figure 13

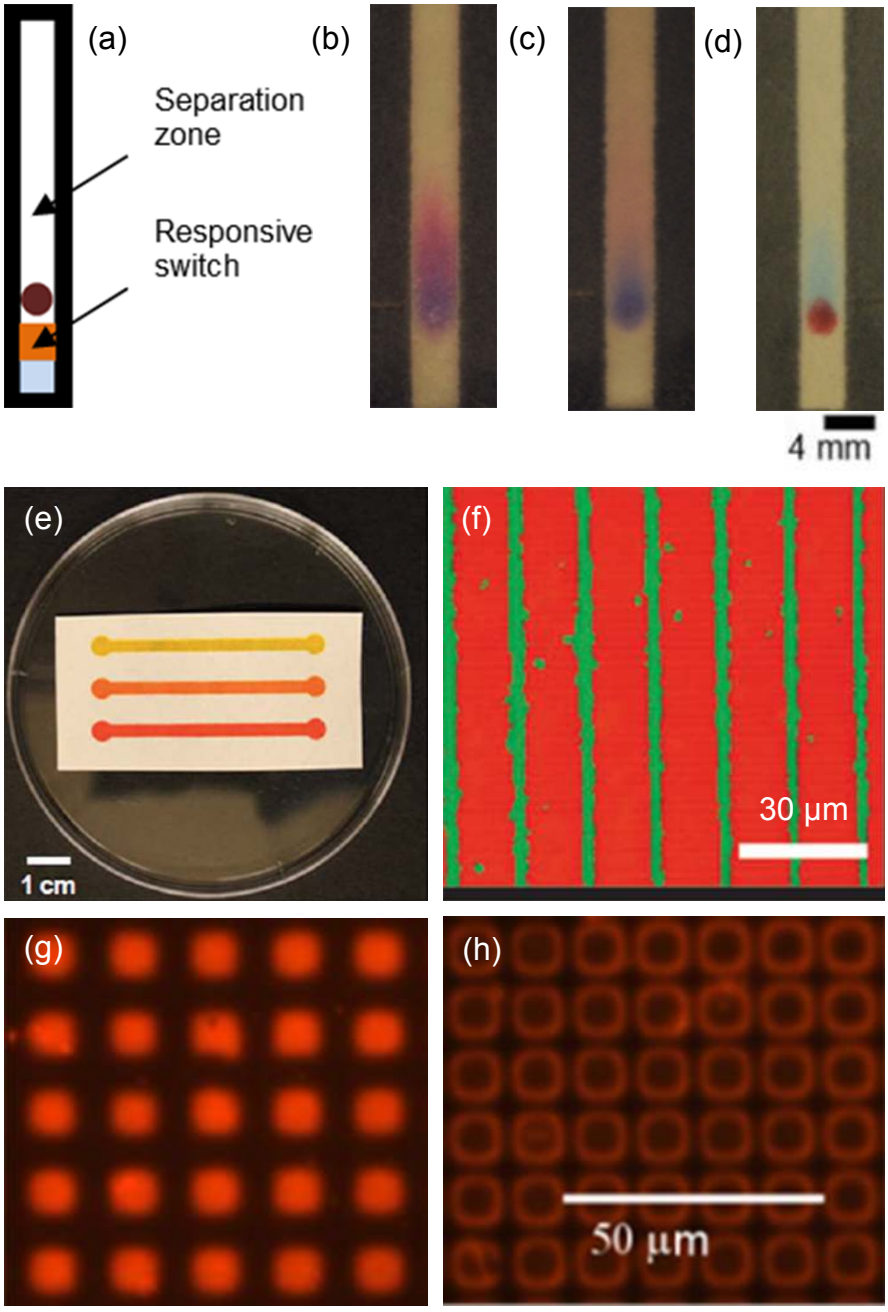
(a)
(b)
(c)
(d)
Separation zone
Responsive switch
4 mm
(e)
1 cm
(f)
30 µm
(g)
(h)
50 µm

Figure 14

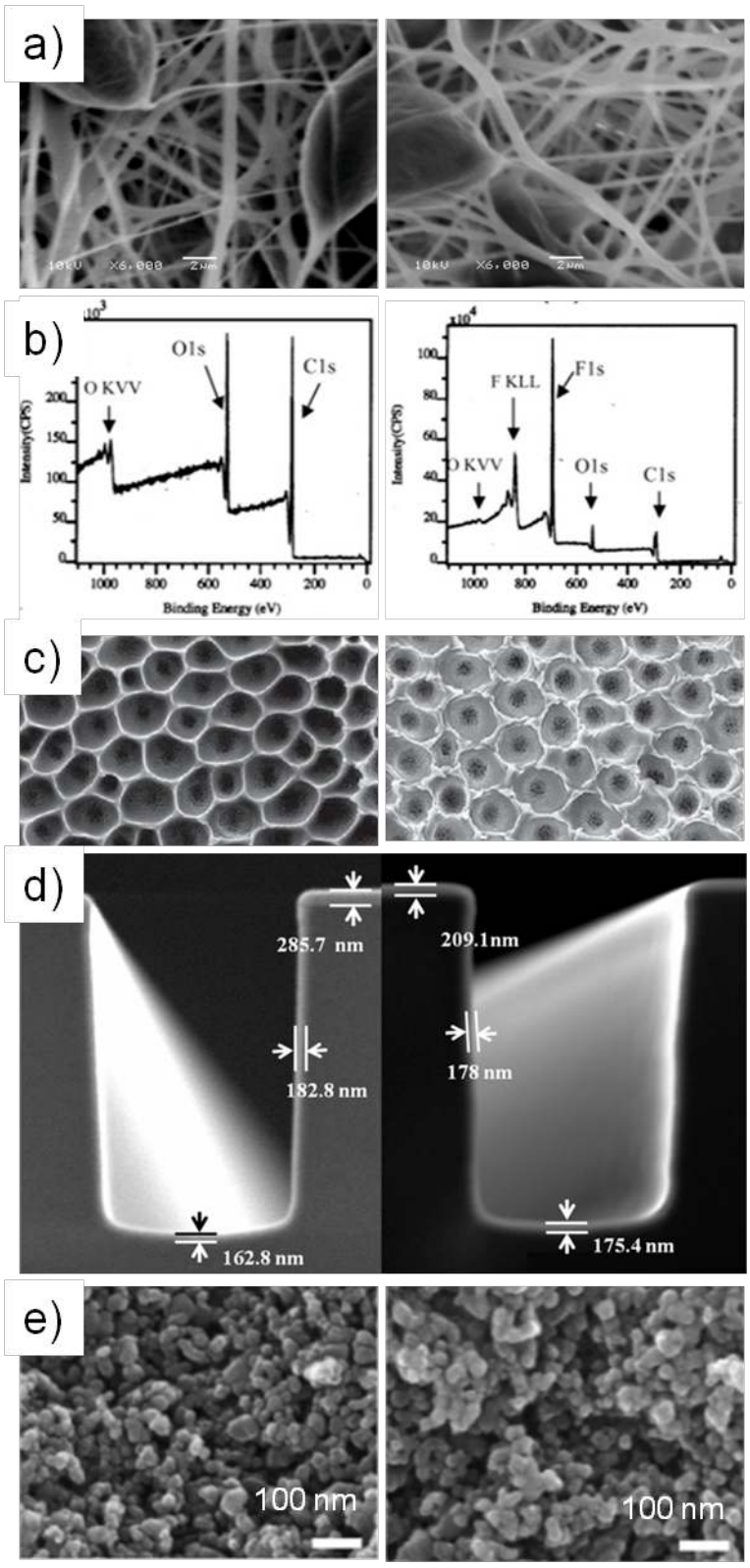
a)
b)
O KVV
O1s
C1s
F KLL
F1s
Intensity(CPS)
Binding Energy (eV)
c)
d)
285.7 nm
209.1nm
182.8 nm
178 nm
162.8 nm
175.4 nm
e)
100 nm
100 nm

Figure 15

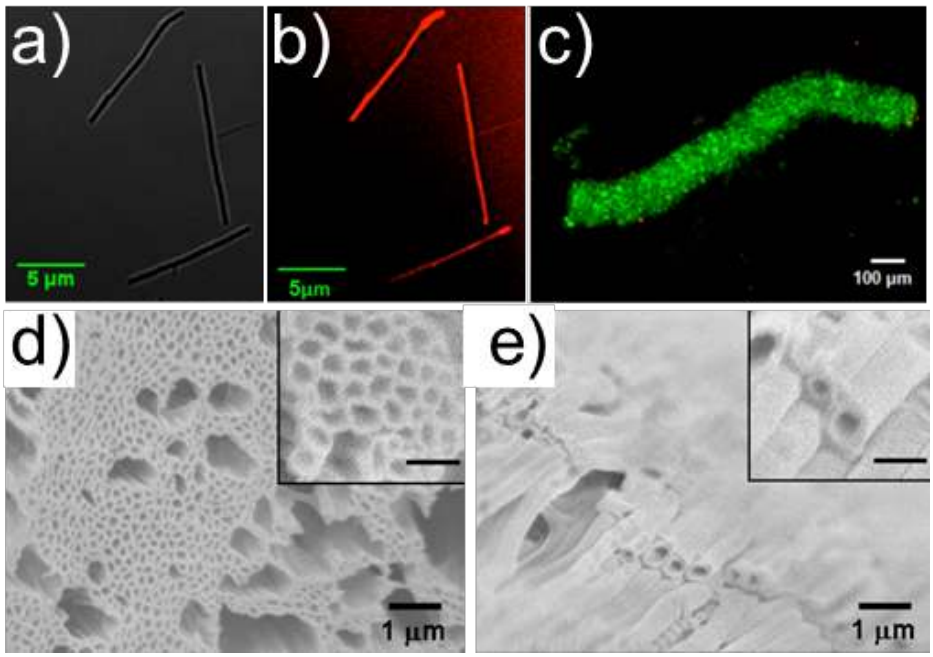

Figure 16

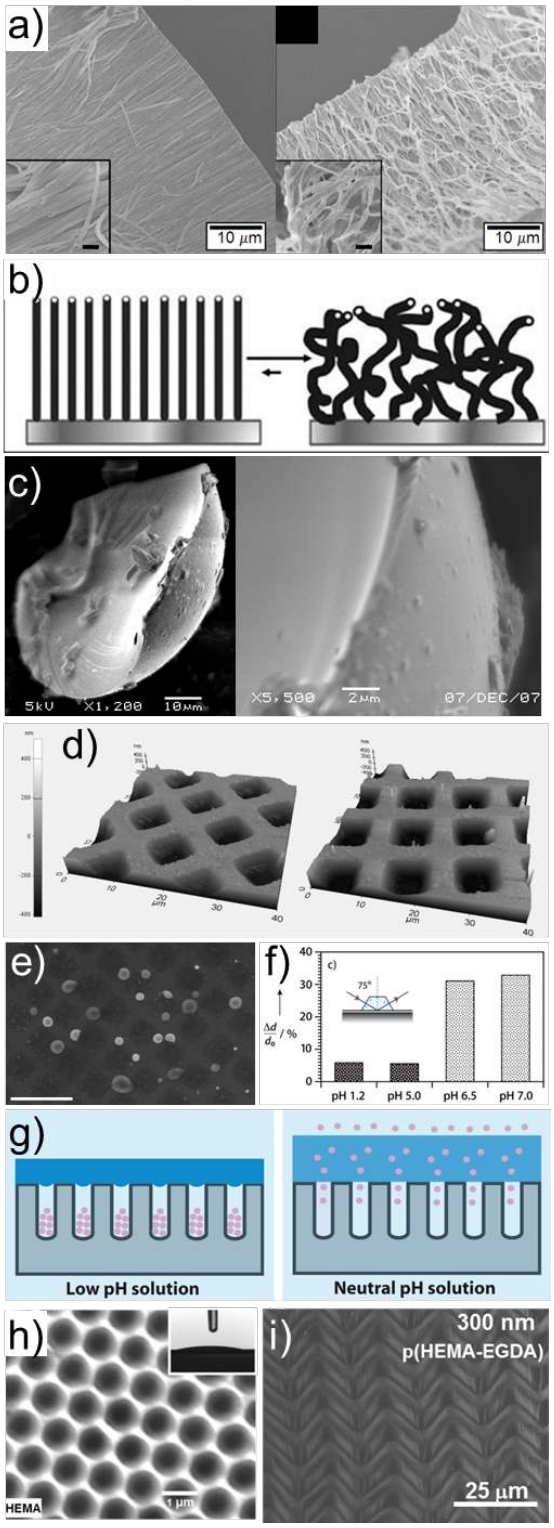
a)
10 μm
10 μm
b)
c)
5kV X1,200 10μm
X5,500 2μm 07/DEC/07
d)
e)
f)
pH 1.2
pH 5.0
pH 6.5
pH 7.0
g)
Low pH solution
Neutral pH solution
h)
HEMA
1 μm
i)
300 nm
p(HEMA-EGDA)
25 μm

Figure 17

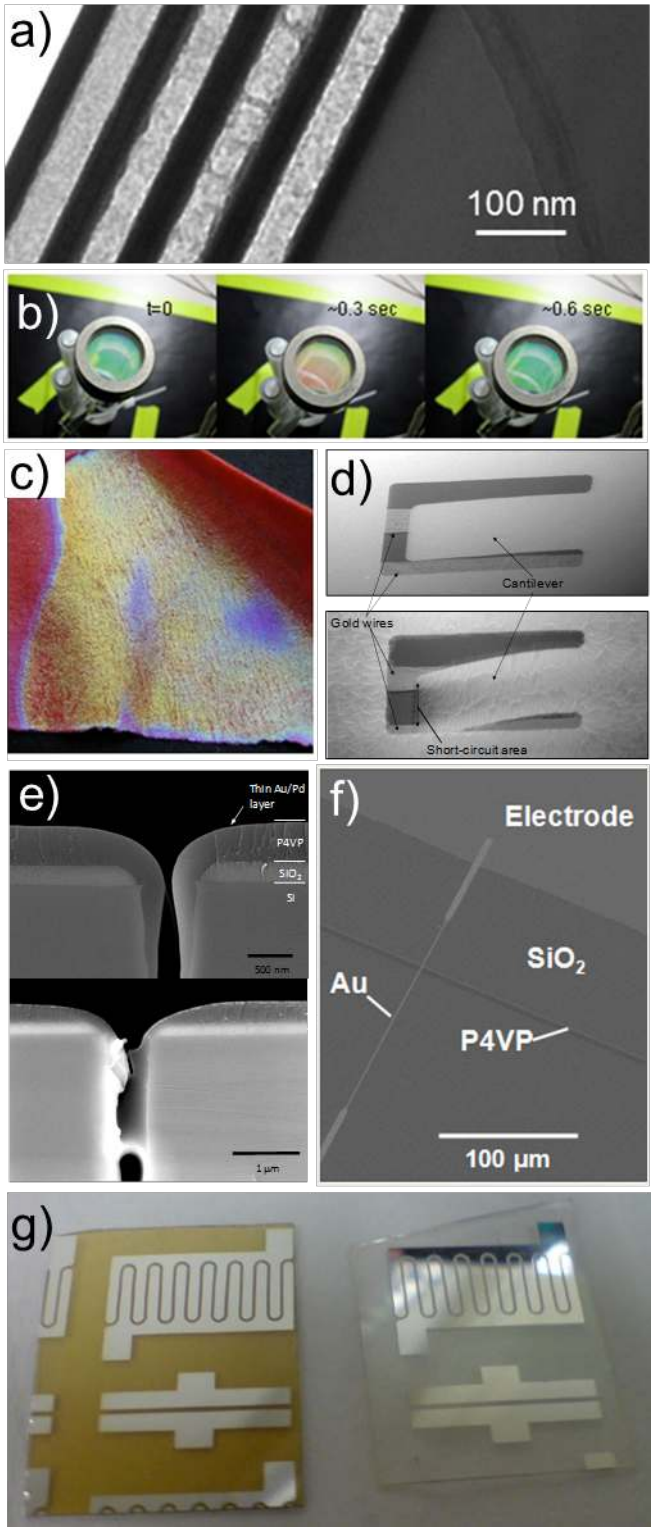
a)
100 nm
b)
t=0
~0.3 sec
~0.6 sec
c)
d)
Cantilever
Gold wires
Short-circuit area
e)
Thin Au/Pd layer
P4VP
SiO2
Si
500 nm
1 µm
f)
Electrode
SiO2
Au
P4VP
100 µm
g)

Figure 18

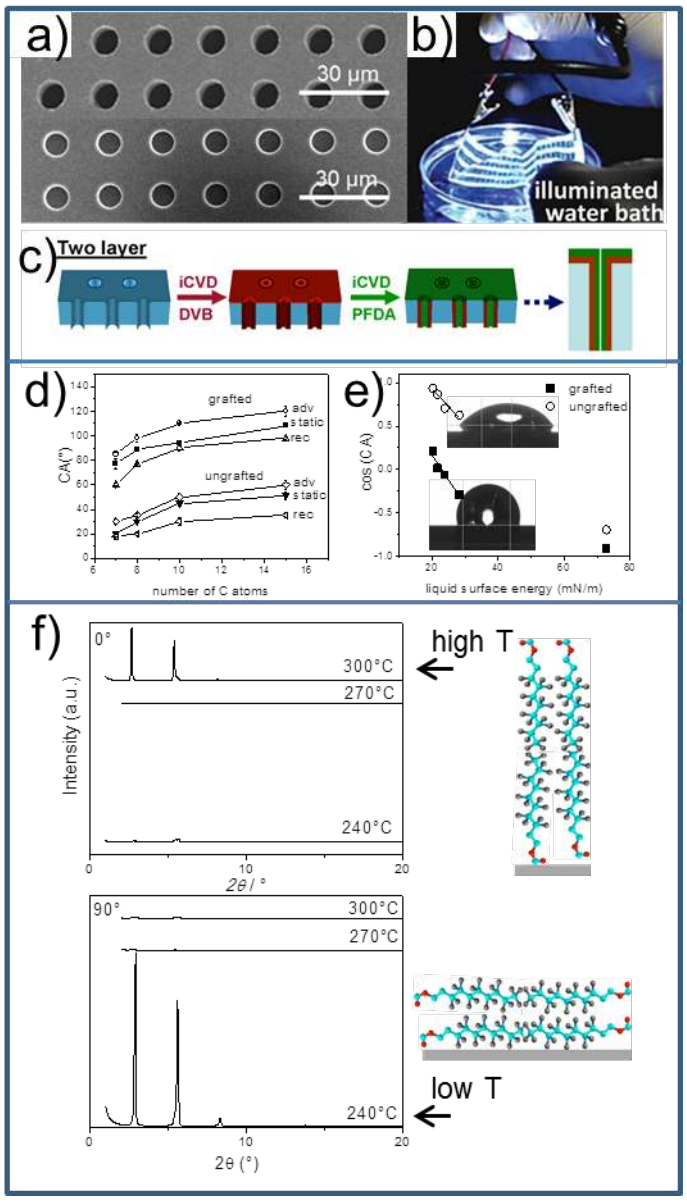
a)
30 μm
30 μm
b)
illuminated
water bath
c)
Two layer
iCVD
DVB
iCVD
PFDA
d)
grafted
adv
static
rec
ungrafted
adv
static
rec
CA(°)
number of C atoms
e)
grafted
ungrafted
cos (CA)
liquid surface energy (mN/m)
f)
0°
300°C
270°C
240°C
Intensity (a.u.)
2θ / °
high T
90°
300°C
270°C
240°C
low T
2θ (°)

Figure 19

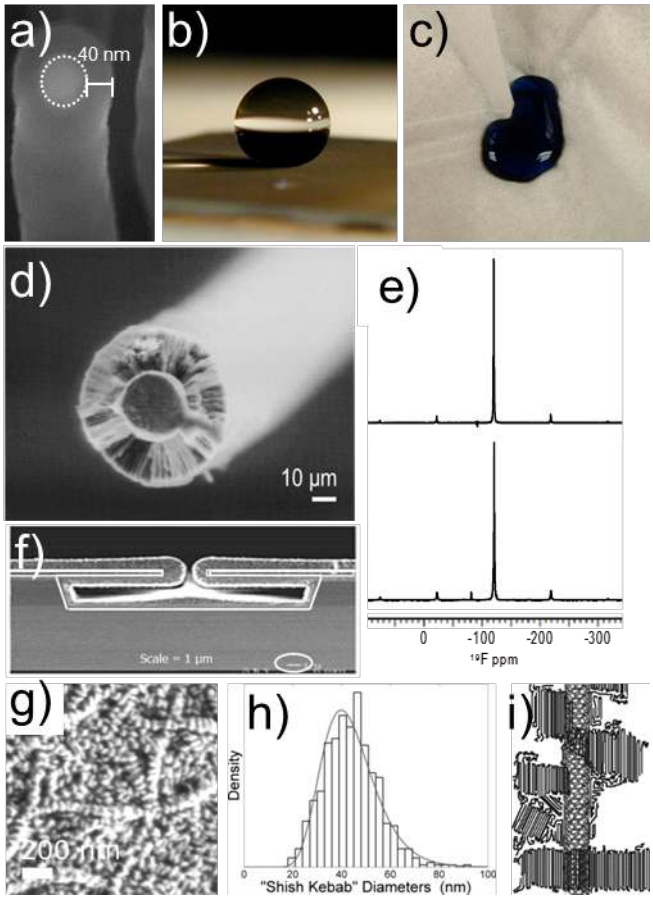
a)
40 nm
b)
c)
d)
10 μm
e)
0
-100
-200
-300
¹⁹F ppm
f)
Scale = 1 μm
g)
200 nm
h)
Density
0
20
40
60
80
100
"Shish Kebab" Diameters (nm)
i)

Figure 20

Group picture

Prof. Karen K. Gleason bio: Dr. Karen K. Gleason is the Alexander and I. Michael Kasser Professor of Chemical Engineering at MIT and has authored more than 250 publications. The coauthors are members of her lab: Drs. Anna Maria Coclite, Jose Luis Yagüe, Asli Ugur, Nan Chen, Sunghwan Lee are postdoctoral associates, David Borrelli, Christy D. Petruczok, Rong Yang, Won Jun Jo, Andong Liu, Xiaoxue Wang are currently doctoral candidates; Rachel M. Howden received her PhD in 2013. From left to right: RY, AL, CDP, NC, JLY, RMH, AU, SL, DB, WJJ, XW, KKG, YU and AMC.

Submitted to ADVANCED MATERIALS

The deposition of functional polymers from the vapor phase enables new frontiers for device fabrication and technological development. Chemical Vapor Deposition methods have a marked footprint in a wide range of applications from biotechnology to conducting polymer for solar cells. Finally, CVD processes implementation into industrial scale and commercialization are also discussed.

Keyword Chemical Vapor Deposition, Conformality, Functional polymers, Surface modification, Conjugated polymers

Anna Maria Coclite, Rachel M. Howden, David C. Borrelli, Christy D. Petruczok, Rong Yang, Jose Luis Yagüe, Asli Ugur, Nan Chen, Sunghwan Lee, Won Jun Jo, Andong Liu, Xiaoxue Wang, and Karen K Gleason *

Title **CVD Polymers: A new paradigm for surface modification and device fabrication**